HIGHLY FUNCTIONALIZED THERMOSETS FROM RENEWABLES FOR COMPOSITES AND COATINGS APPLICATIONS

A Dissertation
Submitted to the Graduate Faculty
of the
North Dakota State University
of Agriculture and Applied Science

By

Arvin Zillion Yu

In Partial Fulfillment of the Requirements
for the Degree of
DOCTOR OF PHILOSOPHY

Major Department:
Coatings and Polymeric Materials

October 2017

Fargo, North Dakota

North Dakota State University
Graduate School

Title

Highly Functionalized Thermosets from Renewables for Composites and Coatings Applications

By

Arvin Zillion Yu

The Supervisory Committee certifies that this ***disquisition*** complies with North Dakota State University's regulations and meets the accepted standards for the degree of

DOCTOR OF PHILOSOPHY

SUPERVISORY COMMITTEE:

Dean C. Webster
Chair

Bret J. Chisholm

Dante Battocchi

Amelia A. Asperin

Approved:

11-13-2017	Dean C. Webster
Date	Department Chair

ABSTRACT

Renewable sources have attracted attention due to their affordable cost and wide availability. Vegetable oils are renewable sources that have been extensively studied as potential replacement for petroleum derived chemicals. However, vegetable oils tend to produce soft materials with modest properties due to their chemical structure. Consequently, their modifications have been studied to develop high performance materials with improved properties. One of the modifications involves substituting the glycerol core with sucrose to increase the functionality per molecule. Another approach is converting the less reactive internal carbon-carbon double bonds with the more reactive epoxy groups, which permits access to a variety of crosslinking pathways.

Epoxidized sucrose soyate (ESS) is a sucrose ester fatty acid (SEFA), which was epoxidized via the Prilezhaev reaction. ESS has a rigid sucrose core and epoxy functionalized fatty acid side chains. The high functionality of ESS was exploited and it was converted to methacrylated and carbonated resins. The methacrylated resins were applied in producing themosets by free-radical polymerizations while the carbonated resins were studied in step-growth polymerizations. Several studies were done to exploit the high functionality of the methacrylated resins: reduction of the viscosity while increasing crosslinkable moieties, introduction of ductility, structure-property relationships, and investigation of resin versatility in photocurable systems. Meanwhile, the carbonated resins were used to form non-isocyanate polyurethane (NIPU) coatings via cyclic carbonate-amine reactions. Overall, the highly functionalized bio-based thermosets showed very promising properties for composites and coatings applications.

ACKNOWLEDGEMENTS

I would like to express my deepest gratitude to my advisor, Dr. Dean Webster, for always seeing the potential not only in me but in all of his students. It has been an incredible experience to work with such an inspiring mentor. Despite his busy schedule as the department chair, he never fails to make time for discussions with his students. I always feel like I am the smartest graduate student every time I leave his office after a research discussion. I have also admired his diplomatic trait, patience, and assertiveness in every situation. His scientific creativity challenges me to think outside the box and to be bold in being a pioneer in a new field.

The next group of people I need to thank is my committee, Dr. Bret Chisholm, Dr. Dante Battocchi, and Dr. Amelia Asperin, for their time, service, and advice during my Ph.D. journey.

I also would like to thank my colleagues who enjoyed initiating provocative discussions both in life and research. Shout out to the rest of "The Furious Five", Dr. Teluka Galhenage, Madhura Pade, Eric Krall, and Alison Rohly, who made graduate life both inside and outside the Webster group fun and exciting, as well as the conferences we have attended together. Make sure to pass the baton to the younger generation. I also appreciate the contributions of Alireza Rahimi, Jonas Sahouani, and Raul Setien, in carrying out tedious experiments for this dissertation.

Dr. Chunju Gu, James Bahr, and Greg Strommen also need to be thanked for tirelessly supporting the instrumentation needs of my research. Last but definitely not least are the ever-changing CPM office staff beginning with Jacinda Wollan, Carol Johnson, Katherine Backen-Anderson, Lynn Stadum, and Janice Hanson, thank you for your patience and help in reminding us students of all the administrative duties we need to accomplish.

DEDICATION

I dedicate this dissertation to my family, most especially to my parents, for always believing, encouraging, and challenging me in my academic pursuits. To my father, thank you for instilling the mentality of never settling with mediocrity, may you rest in peace.

TABLE OF CONTENTS

LIST OF TABLES

LIST OF FIGURES

LIST OF SCHEMES

CHAPTER 1. GENERAL INTRODUCTION

1.1. Sustainability

According to the Brundtland Commission Report, "Sustainable development is development that meets the needs of the present without compromising the ability of future generations to meet their own needs."[1] The World Summit on Social Development have identified the three pillars of sustainability as social development, environmental protection, and economic development.[2] These pillars are viewed as not mutually exclusive but rather interdependent with each other.[3] Sustainability happens when all three pillars intersect and the individual developmental goals are met.

1.1.1. Green chemistry

Green chemistry, synonymous with sustainable chemistry, is a scientific ideology that considers the three pillars of sustainability when designing chemical products and processes beginning from conceptualization all the way to the implementation. This philosophy encompasses all fields of chemistry as well as promotes cutting-edge and ingenious ways to minimize waste and generation of hazardous substances. The 12 Principles of Green Chemistry, developed by Anastas and Warner[4], are as follows:

1. Prevention (of waste)
2. Atom Economy
3. Less Hazardous Chemical Syntheses
4. Designing Safer Chemicals
5. Safer Solvents and Auxiliaries
6. Design for Energy Efficiency
7. Use of Renewable Feedstocks

8. Reduce Derivatives
9. Catalysis
10. Design for Degradation
11. Real-time Analysis for Pollution Prevention
12. Inherently Safer Chemistry for Accident Prevention

These principles serve as the framework for materials design and processing. Actively practicing these principles would create a paradigm shift among scientists and engineers, which would prevent depletion of the limited fossil raw materials.

By designing materials from renewable sources, the 7th principle of green chemistry is already put into practice. Additionally, materials developed from nature could potentially have built-in degradability and low toxicity, which are the 10th, 3rd, and 4th principles of green chemistry.

1.1.2. Biomass

Throughout history, mankind has been able to accomplish incredible feats such as using fire. Ever since how to make fire was discovered, burning wood has become one of the main ways of harnessing biomass into energy. Currently, chemicals obtained from biomass are categorized as new or replacement chemicals. New chemicals demand comprehensive study in order to establish their properties while replacement chemicals typically possess similar, if not identical, compositions to known petrochemicals. In polymer science, replacements are attractive due to their comparable cost and properties against commercial standards. Meanwhile, new chemicals are being developed with the intensions of broadening options for current applications or filling in the gaps in the market.

The majority of biomass comes from plant materials such as cellulose, lignin, and vegetable oils. Vegetable oils are one of the cheapest natural resources for the polymer industry. These oils are ideal biorenewable resources due to the wide availability, high production, low cost, and biodegradability.

1.1.3. Challenges

Anastas and Kirchhoff[5] foresaw the challenges that could arise from the breadth of issues of sustainability. Their article predicts challenges in the areas of research, implementation, and education. While a detailed discussion of each is impossible, some issues were enumerated with the hope to stimulate thinking and discussion. In the field of polymer research, one challenge included was designing degradation through the use of additives-free design. In terms of implementation challenge, environmentally benign technologies at the laboratory scale do not guarantee translation into industrial scale. Lastly, in order to effectively transfer green chemistry knowledge to students, educators need to have the appropriate tools, training, and materials to integrate green chemistry in teaching and research.

In addition to the aforementioned challenges, economic challenges also emerge from industry: 1) Petroleum-based raw materials are more cost effective and readily available, 2) current technology in converting raw materials into chemicals is established, well developed, and economic, and 3) markets are unwilling to compromise cost and established material properties in exchange with the exploration of unchartered territory.

Therefore, the ultimate goal in this field is to develop materials from renewable sources that are economical, produced through robust processes, and possessing properties that match, if not surpass, current standards.

1.2. Vegetable oils

The popularity of vegetable oils as alternative sources to petrochemicals has been due to the rapidly rising costs and limited sources of fossil raw materials. In addition to the competitive cost, vegetable oils have been sought as chemical commodity because they are renewable, available, abundant, have built-in functionality, and biodegradable.[6-11] They are generally made up of triglycerides containing various amounts of fatty acids (Figure 1.1). The unsaturation sites on the fatty acids can be chemically modified to produce useful functional polymers.

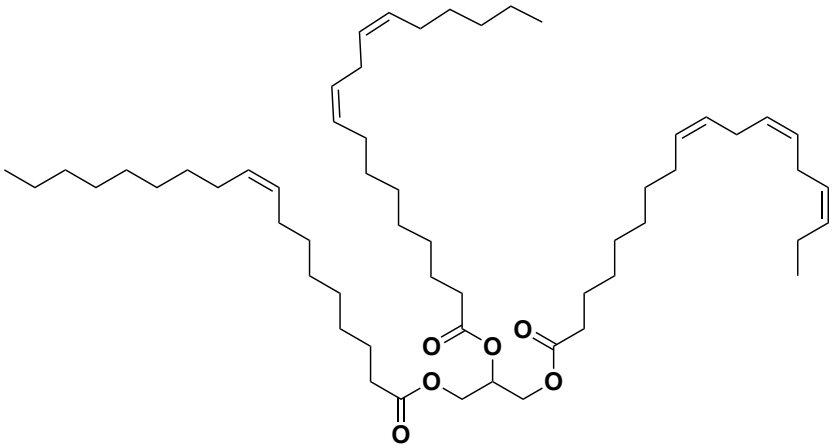

Figure 1.1. Representative structure of a triglyceride.

Vegetable oils are esters (triglycerides) formed by glycerol plus fatty acids containing 8-24 carbon atoms and ranging from saturated to unsaturated to hydroxyl-containing types (Figure 1.2), depending on the plant type and source.[12, 13] The most common fatty acids found in vegetable oils include palmitic, stearic, oleic, linoleic, and linolenic acids. The fatty acid composition, along with double bonds and iodine values, of a few vegetable oils is summarized in Table 1.[6] The iodine value (IV) is proportional to the number of double bonds in the oil and indicative of its drying behavior. Oils having IV > 140 are said to be drying oils, IV 125–140 are semi-drying oils, and IV < 125 are non-drying. Polymerization of unmodified vegetable oils usually occurs by autoxidation through the fatty acid double bonds.[14] However, these

crosslinking processes require extended periods of time to fully cure. As a result, modification of vegetable oils is carried out to access functional groups that would eventually lead to polymerizations via different mechanisms.

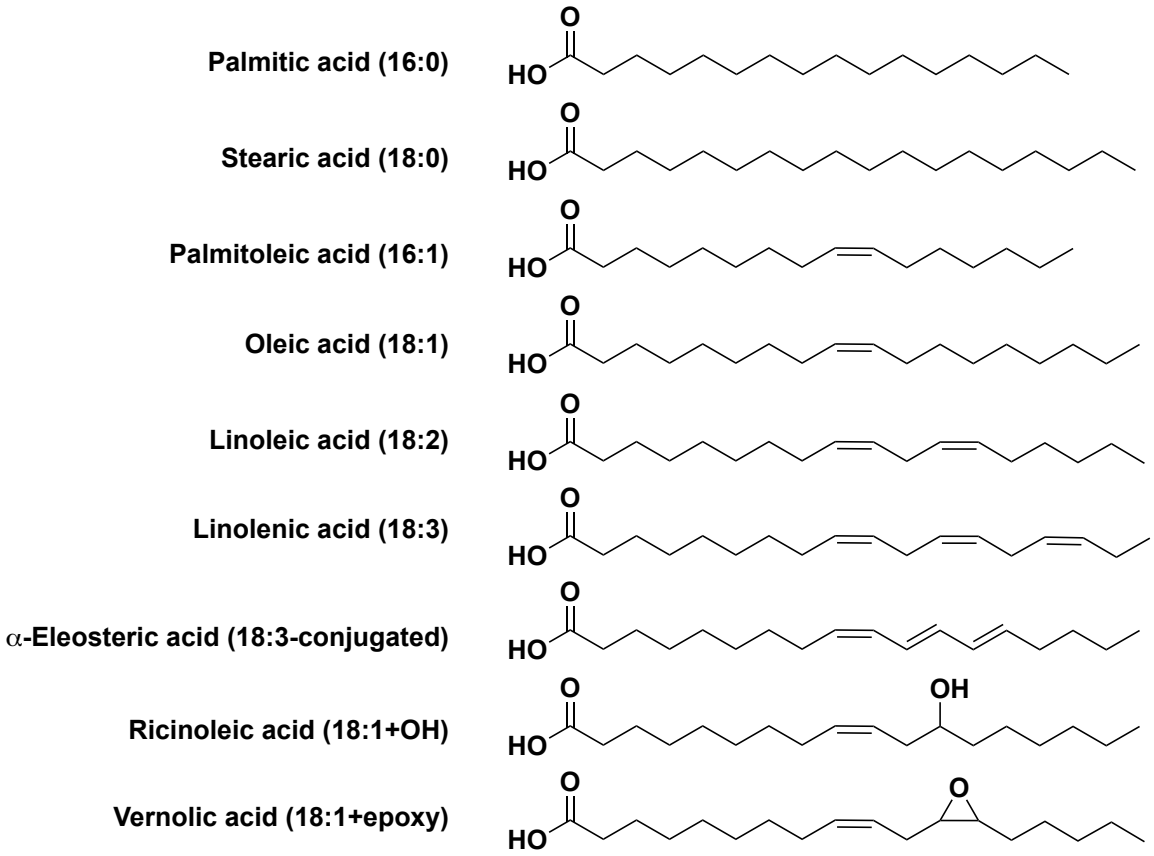

Figure 1.2. Chemical structures of common fatty acids in vegetable oils.

Table 1.1. Fatty acid composition and oil property of vegetable oils.[6]

Vegetable oil	Double bonds	Iodine value (mg/100g)	Fatty acids (%)				
			Palmitic	Stearic	Oleic	Linoleic	Linolenic
Palm	1.7	44–58	42.8	4.2	40.5	10.1	-
Olive	2.8	75–94	13.7	2.5	71.1	10.0	0.6
Corn	4.5	102–130	10.9	2.0	25.4	59.6	1.2
Soybean	4.6	117–143	11.0	4.0	23.4	53.3	7.8
Sunflower	4.7	110–143	5.2	2.7	37.2	53.8	1.0
Safflower	5.0	140–150	7.0	4.0	13.0	75.0	1.0
Linseed	6.6	168–204	5.5	3.5	19.1	15.3	56.6

1.3. Vegetable oil-based thermosets

1.3.1. Direct C=C polymerization

In the last decade, vegetable oil-based thermosets have been developed via free-radical polymerization or cationic homopolymerization of the double bonds, and copolymerization with petroleum-based monomers like styrene, divinylbenzene, and dicyclopentadiene.[15-23] However, the major drawbacks in developing high-performance thermosets from vegetable oils are the fatty acid chains that provide flexibility. In order to counteract the flexibility, petroleum-based monomers are typically used as reinforcements to improve the properties.[24, 25] Alternatively, the internal double bonds can be converted into reactive functional groups that would create avenues for different polymerizations.

1.3.2. Functionalization of C=C and polymerization

1.3.2.1. Epoxy resins

Epoxidation of double bonds (Scheme 1.1) is one of the most significant transformations for vegetable oils.[9] The highly strained structure of the oxirane ring makes it an ideal functional group for any ring-opening reaction, such as in epoxy-amine systems, and the products formed are thermodynamically favored. However, epoxidized vegetable oils contain internal epoxy groups that are less reactive, which lead to inefficient polymerizations, even with amine crosslinkers.[26-28] An ester aminolysis side reaction (Scheme 1.2) of the amine with the ester groups of the oils also results in inefficient polymerization. This inefficiency results in subpar thermoset properties. Common approaches to overcome this would be catalysis for the polymerization and addition of reinforcement or plasticizers to improve thermoset properties. A recent review by Roudsari *et al.*[29] discussed green approaches and new strategies in toughening bio-based epoxies.

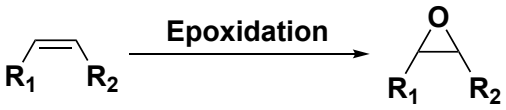

Scheme 1.1. Synthetic route of epoxy resins from double bonds.

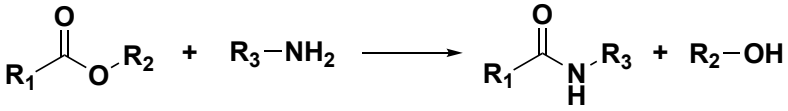

Scheme 1.2. Ester aminolysis reaction forming an amide and an alcohol.

Aside from epoxy-amine systems, epoxy resins may also be polymerized via several other crosslinking reactions. Scheme 1.3 summarizes the different crosslinking pathways epoxy resins may undergo. Reaction of epoxy with carboxylic acids generate hydroxyesters.[30] Two side reactions that may occur from the presence of the hydroxyl group are the epoxy-hydroxyl reaction and esterification of the carboxylic acid. Anhydride-epoxy reactions have proved to go through complex simultaneous mechanisms. Regardless whether catalyzed or not, the addition of epoxy and anhydride occurs alternately.[30-32] Epoxy-thiol reaction is a derivative of the epoxy-amine reaction that generates polysulfides. This approach is usually applied in designing bio-based materials by partnering these polymers with thiol-ene click chemistry.[33, 34] Activated epoxides could undergo homopolymerization to form polyethers.

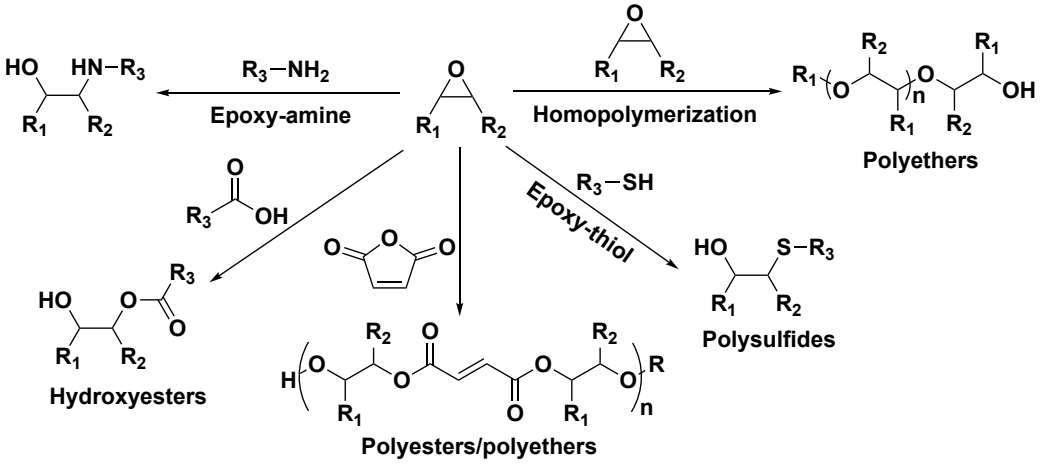

Scheme 1.3. Crosslinking reactions of epoxy resins.

1.3.2.2. Polyols

Polyols are one of the most versatile building blocks in polymer science. Aliphatic polyols are inherently flexible due to the long hydrocarbon chains and are typically used for applications that benefit from these elastomeric properties. On the other hand, aromatic polyols provide rigidity that is useful in applications that require stronger materials. Bio-based polyols could be prepared from vegetable oils[35] or lignin-derived precursors.[36] Polyols can be prepared from alkenes via epoxide/ring opening, ozonolysis/reduction, hydroformylation/amidation, thiol-ene, or transesterification/amidation reactions. Scheme 1.4 summarizes the common reactions polyols may undergo to generate different polymers. Polyols react with carboxylic acids to form polyesters. Also, polyesters containing adjacent carboxylic acid groups are generated when polyols react with cyclic anhydrides. Carbamates are prepared from polyols when reacted with urea. Polyethers are synthesized when polyols are reacted with melamine-formaldehyde (MF) resins. Polyols may also be used as a precursor to prepare acetoacetylated polymers that could be used for different crosslinking reactions. Acetoacetylated polyols are prepared from its reaction with *tert*-butyl acetoacetate (TBAA). This versatile functional group may crosslink with MF resins and amines as well as undergoes Michael addition reaction or hydrolysis. However, the largest market for the application of polyols is in the manufacture of polyurethanes (PUs).

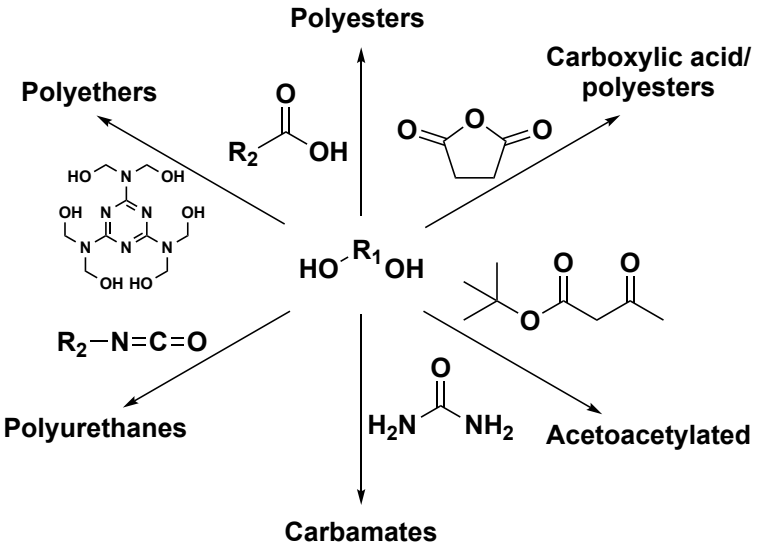

Scheme 1.4. Crosslinking reactions of polyols.

PUs are an attractive class of polymers that have garnered attention and widely used in a variety of applications due to their high elasticity, hydrolytic stability, abrasion resistance, chemical resistance, and solvent resistance.[37, 38] Their utility has extended into the biomedical applications as foams, adhesives, etc.[39, 40] Currently, synthesis of PUs employs the traditional reaction between polyols and polyisocyanates, even with PUs from renewables.[41]

1.3.2.3. Cyclic carbonates

Bio-based cyclic carbonates have attracted interest due to the wide range of possible applications such as solvents, electrolytes, and synthetic building blocks.[42-44] There are various approaches reported for the synthesis of cyclic carbonates. Commonly used approaches utilize 1,2-diols or epoxides to form cyclic carbonates (Scheme 1.5). Lang *et al.*[45] reported green catalytic processes to synthesize cyclic carbonates under mild conditions using bifunctional catalysis. Other approaches use halohydrins[46, 47]and propargyl alcohols[48, 49] as starting materials. Alkenes may also be used as precursors via epoxide/CO_2-insertion or catalyzed oxidative carboxylation reactions.[50, 51]

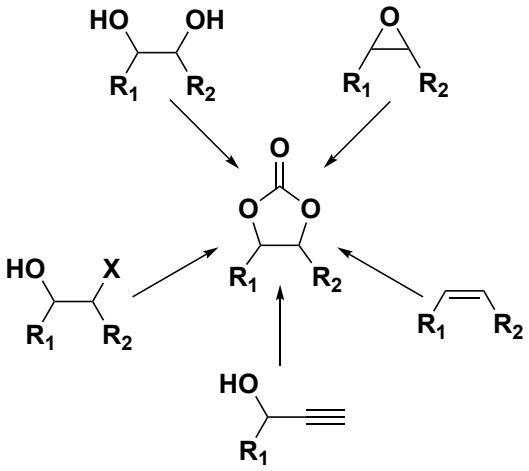

Scheme 1.5. Various synthetic routes for cyclic carbonate synthesis.

The most common crosslinking reaction for cyclic carbonates is with amines. This pathway leads to the formation of polyhydroxyurethanes (PHUs) or sometimes referred to as non-isocyanate polyurethanes (NIPUs). Carboxylic acids are also used although the reaction is accompanied by the evolution of carbon dioxide (Scheme 1.6). A comprehensive review by Rockiki *et al.*[52] discussed the synthesis, properties, and applications of NIPUs. Among the NIPU synthetic routes, the step-growth addition of cyclic carbonates with amines is the most promising.

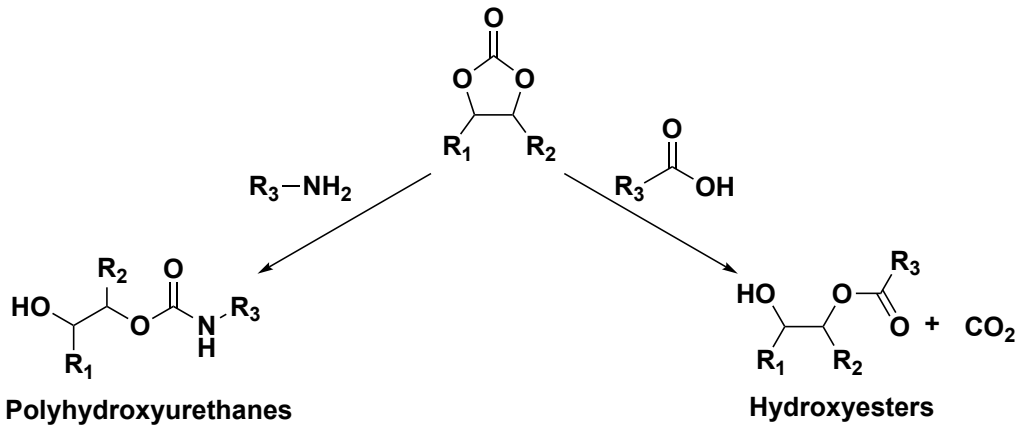

Scheme 1.6. Crosslinking reactions of cyclic carbonates.

Vegetable oil-based cyclic carbonates generate PUs that have comparable mechanical properties and better water absorption, thermal stability, and chemical resistance than conventional PUs.[53] One of the more widely studied approaches in synthesizing vegetable oil-based cyclic carbonates is via the epoxide precursors such as epoxidized soybean oil (ESBO). The high reactivity of the epoxy groups makes this transformation easily accessible to form the cyclic carbonates. Several reviews have emerged from the conversion of ESBO to carbonated soybean oil (CSBO), including the applications of the NIPUs produced.[54-56]

1.4. Star-shaped polymers

Structurally, star-shaped polymers are branched polymers consisting of a multifunctional core with at least three chains (Figure 1.3). The core is typically an atom, molecule or a macromolecule while the hydrocarbon chains can be homogeneous or heterogeneous. The unique properties of star-shaped polymers come from the chemical structure, length, and the number of the chains per molecule. The synthesis could either be a convergent (arm-first) or divergent (core-first) approach. Convergent approach utilizes monofunctional polymeric chains and reacted with a multifunctional core to create a homogeneous star-shaped polymer. The homogeneity of these polymers allows easier characterization. However, it has been found that the conversions are often incomplete and requires further purification.[57] On the other hand, the divergent approach simultaneously or sequentially[58] reacts varying types of chains to produce a heterogeneous star-shaped polymer. The difference in reactivity of the chains could effect viscosity and gelation issues.

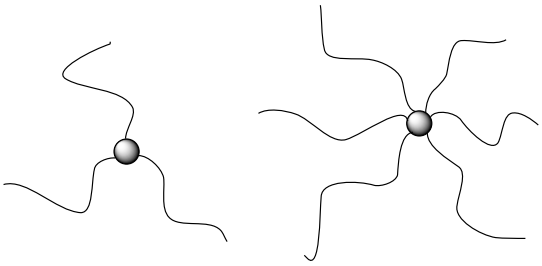

Figure 1.3. Structural representations of star-shaped polymers.

Star-shaped polymers tend to have higher compactness and exceptional rheological properties.[59] The most popular applications of this class of polymers are in the biomedical field such as diagnostic imaging, tissue engineering, and targeted drug delivery.[60, 61] The high functionality of star-shaped polymers could be exploited by modification of a portion of the functionality. Ideally, this strategy allows minimal compromise of the properties, if not retention, while gaining a new set of properties. One useful design would be immobilizing additives to the polymer structure. Additives are property modifiers and are typically non-bound in a system. Plasticizers are commonly used as additives to improve ductility of brittle materials.[62] Another potential strategy would be creating internal reinforcement into the star-shaped polymer structure.

1.5. Epoxidized sucrose soyate (ESS)

Procter and Gamble (P&G) Chemicals previously commercialized an alkyd diluent SEFOSE 1618U (sucrose soyate).[63-65] It is a sucrose ester of fatty acids (SEFAs) from soybean oil that has a rigid core and flexible side chains. In contrast to triglycerides of fatty acids, SEFAs can have up to eight fatty acid side chains attached to the sucrose core. This star-shaped polymer has minimal intermolecular interactions, which is why it has low viscosity. The fatty acid side chains contain internal unsaturation sites that are less reactive and sterically hindered. Thus,

transformation of these double bonds into more reactive groups could afford a more versatile molecule.

Epoxidized sucrose soyate (ESS, Figure 1.4) is synthesized via the Prilezhaev epoxidation reaction of SEFOSE 1618U. Webster and coworkers optimized this process and scaled up the production.[66-68] ESS contains on average 11-12 epoxy groups per molecule and has been applied in a number of crosslinking technologies.[69] This molecule has shown versatility in bio-based coatings applications such as polyurethanes[70], UV-curable[71], melamine-formaldehyde[72], acid-blocked[73], degradable[74, 75], and high performance coatings.[76-78] Without any modifications, ESS displayed exceptionally well in terms of its adhesive property when applied in fiberboards.[79]

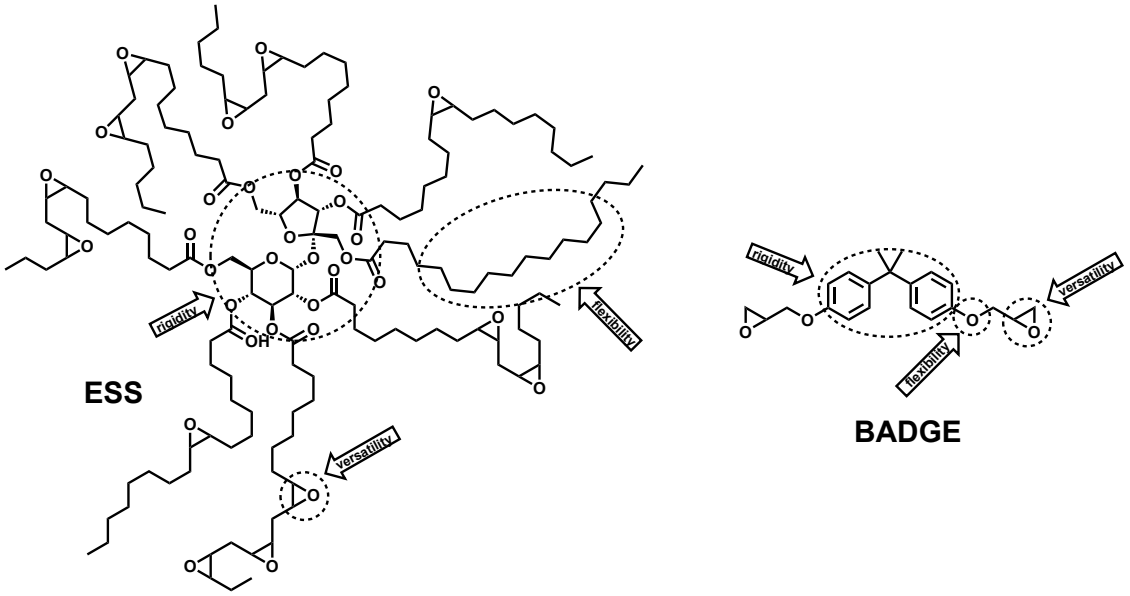

Figure 1.4. Structures and features of ESS and BADGE.

Functionally, ESS offers similar properties that are provided by conventional bisphenol A-derived monomers such as bisphenol A diglycidyl ether (BADGE, Figure 1.4). Both these molecules have rigidity, flexibility, and versatility. However, bisphenol A (BPA) has been reported to have harmful effects on humans.[80-82] ESS-derived polymers have a competitive edge

of being renewable against BPA-derived materials. The epoxy groups on both these molecules can be further functionalized (Scheme 1.3) to yield different types of polymers.

Khot *et al.*[25] further functionalized epoxidized soybean oil to acrylated epoxidized soybean oil (AESO) and accessed materials that possessed glass transition temperatures (T_g) in the range of 50° – 70°C and moduli in the 440 MPa – 1.6 GPa range, depending on composition. These resins were suitable for composites applications and set the foundation for new materials derived from renewable sources that possessed novel properties. AESO was then further functionalized via maleinization of the acrylate groups to increase the T_g and moduli.[83] Maleated AESO showed improved T_g (100°C – 115°C) and moduli (1.9 – 2.2 GPa). Both properties are comparable to commercially available unsaturated polyesters.

Webster *et al.*[84] also studied novel bio-based methacrylated epoxidized sucrose soyate (MESS) and performed thermally initiated free-radical polymerizations. The thermosets afforded improved thermomechanical properties that made them suitable fiber reinforced polymer (FRP) composite resin matrix. Further applications of MESS with flax and glass fibers showed interesting sets of properties and displayed complex behavior.[85-87] When reinforced with glass fibers, MESS resin-based composite had properties equivalent to or better than a conventional vinyl ester resin. It was also observed that MESS had better adhesion to the fibers than the vinyl ester control.[88]

1.6. Conclusions

Bio-based materials have made a comeback in the recent years due to economic and environmental reasons. Direct modifications of vegetable oils have become a well-studied field in polymer science. Despite the extensive research, vegetable oil-based materials remain soft with modest properties. Improvement was approached by structure modifications and increasing

functionalities. High functionality could lead to tunable properties that have a broad range of applications. In most cases, high functionality translates to high performance materials. This dissertation is devoted to the exploitation of the high functionality of epoxidized sucrose soyate (ESS) and its further exploration as an alternative to petrochemical feedstock in resins and thermosets for composites and coatings applications. Several principles of green chemistry were put into practice in this study such as atom economy, less hazardous chemical synthesis, designing safer chemicals, safer solvents (in some cases no solvents) and auxiliaries, use of renewable feedstocks, catalysis, and design for degradation.

1.7. References

1. Brundtland, G. H., *Report of the World Commission on environment and development:" our common future."*. United Nations: 1987.

2. Assembly, U. N. G., World summit outcome. *Resolution Adopted by the General Assembly* **2005,** *24*.

3. Adams, W. M. In *The future of sustainability: Re-thinking environment and development in the twenty-first century*, 2006; p 31.

4. Anastas, P. T.; Warner, J. C., *Green chemistry: theory and practice*. Oxford university press: 2000.

5. Anastas, P. T.; Kirchhoff, M. M., Origins, current status, and future challenges of green chemistry. *Accounts of chemical research* **2002,** *35* (9), 686-694.

6. Xia, Y.; Larock, R. C., Vegetable oil-based polymeric materials: synthesis, properties, and applications. *Green Chemistry* **2010,** *12* (11), 1893-1909.

7. Raquez, J. M.; Deléglise, M.; Lacrampe, M. F.; Krawczak, P., Thermosetting (bio) materials derived from renewable resources: a critical review. *Progress in Polymer Science* **2010,** *35* (4), 487-509.

8. de Espinosa, L. M.; Meier, M. A. R., Plant oils: the perfect renewable resource for polymer science?! *European Polymer Journal* **2011,** *47* (5), 837-852.

9. Auvergne, R.; Caillol, S.; David, G.; Boutevin, B.; Pascault, J.-P., Biobased thermosetting epoxy: present and future. *Chemical Reviews* **2013,** *114* (2), 1082-1115.

10. Liu, Z.; Kraus, G., *Green materials from plant oils*. Royal Society of Chemistry: 2014.

11. Miao, S.; Wang, P.; Su, Z.; Zhang, S., Vegetable-oil-based polymers as future polymeric biomaterials. *Acta Biomaterialia* **2014,** *10* (4), 1692-1704.

12. Belgacem, M. N.; Gandini, A., *Monomers, polymers and composites from renewable resources*. Elsevier: 2011.

13. Pfister, D. P.; Xia, Y.; Larock, R. C., Recent advances in vegetable oil‐based polyurethanes. *ChemSusChem* **2011,** *4* (6), 703-717.

14. Soucek, M. D.; Khattab, T.; Wu, J., Review of autoxidation and driers. *Progress in Organic Coatings* **2012,** *73* (4), 435-454.

15. Ma, S.; Li, T.; Liu, X.; Zhu, J., Research progress on bio‐based thermosetting resins. *Polymer International* **2016,** *65* (2), 164-173.

16. Bobade, S. K.; Paluvai, N. R.; Mohanty, S.; Nayak, S. K., Bio-Based Thermosetting Resins for Future Generation: A Review. *Polymer-Plastics Technology and Engineering* **2016,** *55* (17), 1863-1896.

17. Lu, Y.; Larock, R. C., Novel polymeric materials from vegetable oils and vinyl monomers: preparation, properties, and applications. *ChemSusChem* **2009,** *2* (2), 136-147.

18. Kundu, P. P.; Larock, R. C., Novel conjugated linseed oil-styrene-divinylbenzene copolymers prepared by thermal polymerization. 1. Effect of monomer concentration on the structure and properties. *Biomacromolecules* **2005,** *6* (2), 797-806.

19. Henna, P. H.; Andjelkovic, D. D.; Kundu, P. P.; Larock, R. C., Biobased thermosets from the free‐radical copolymerization of conjugated linseed oil. *Journal of Applied Polymer Science* **2007,** *104* (2), 979-985.

20. Valverde, M.; Andjelkovic, D.; Kundu, P. P.; Larock, R. C., Conjugated low‐saturation soybean oil thermosets: Free‐radical copolymerization with dicyclopentadiene and divinylbenzene. *Journal of Applied Polymer Science* **2008,** *107* (1), 423-430.

21. Andjelkovic, D. D.; Valverde, M.; Henna, P.; Li, F.; Larock, R. C., Novel thermosets prepared by cationic copolymerization of various vegetable oils—synthesis and their structure–property relationships. *Polymer* **2005,** *46* (23), 9674-9685.

22. Andjelkovic, D. D.; Larock, R. C., Novel rubbers from cationic copolymerization of soybean oils and dicyclopentadiene. 1. Synthesis and characterization. *Biomacromolecules* **2006,** *7* (3), 927-936.

23. Lu, Y.; Larock, R. C., Novel biobased nanocomposites from soybean oil and functionalized organoclay. *Biomacromolecules* **2006,** *7* (9), 2692-2700.

24. Li, F.; Larock, R. C., Synthesis, structure and properties of new tung oil-styrene-divinylbenzene copolymers prepared by thermal polymerization. *Biomacromolecules* **2003,** *4* (4), 1018-1025.

25. Khot, S. N.; Lascala, J. J.; Can, E.; Morye, S. S.; Williams, G. I.; Palmese, G. R.; Kusefoglu, S. H.; Wool, R. P., Development and application of triglyceride‐based polymers and composites. *Journal of Applied Polymer Science* **2001,** *82* (3), 703-723.

26. Kaplan, D. L., Introduction to biopolymers from renewable resources. In *Biopolymers from renewable resources*, Springer: 1998; pp 1-29.

27. Earls, J. D.; White, J. E.; López, L. C.; Lysenko, Z.; Dettloff, M. L.; Null, M. J., Amine-cured ω-epoxy fatty acid triglycerides: Fundamental structure–property relationships. *Polymer* **2007,** *48* (3), 712-719.

28. Park, S. J.; Jin, F. L.; Lee, J. R., Synthesis and thermal properties of epoxidized vegetable oil. *Macromolecular Rapid Communications* **2004,** *25* (6), 724-727.

29. Mashouf Roudsari, G.; Mohanty, A. K.; Misra, M., Green Approaches To Engineer Tough Biobased Epoxies: A Review. *ACS Sustainable Chemistry & Engineering* **2017**.

30. Ooka, M.; Ozawa, H., Recent developments in crosslinking technology for coating resins. *Progress in organic coatings* **1994,** *23* (4), 325-338.

31. Fischer, R. F., Polyesters from expoxides and anhydrides. *Journal of Polymer Science Part A: Polymer Chemistry* **1960,** *44* (143), 155-172.

32. Dearborn, E. C.; Fuoss, R. M.; MacKenzie, A. K.; Shepherd, R. G., Epoxy Resins from Bis–, Tris–, and Tetrakisglycidyl Ethers. *Industrial & Engineering Chemistry* **1953,** *45* (12), 2715-2721.

33. Chen, Z.; Chisholm, B. J.; Patani, R.; Wu, J. F.; Fernando, S.; Jogodzinski, K.; Webster, D. C., Soy-based UV-curable thiol–ene coatings. *Journal of coatings technology and research* **2010,** *7* (5), 603-613.

34. Guzman, D.; Ramis, X.; Fernández-Francos, X.; De la Flor, S.; Serra, A., New bio-based materials obtained by thiol-ene/thiol-epoxy dual curing click procedures from eugenol derivates. *European Polymer Journal* **2017,** *93*, 530-544.

35. Maisonneuve, L.; Chollet, G.; Grau, E.; Cramail, H., Vegetable oils: a source of polyols for polyurethane materials. *OCL* **2016,** *23* (5), D508.

36. Mahmood, N.; Yuan, Z.; Schmidt, J.; Xu, C. C., Depolymerization of lignins and their applications for the preparation of polyols and rigid polyurethane foams: A review. *Renewable and Sustainable Energy Reviews* **2016,** *60*, 317-329.

37. Demharter, A., Polyurethane rigid foam, a proven thermal insulating material for applications between+ 130 C and− 196 C. *Cryogenics* **1998,** *38* (1), 113-117.

38. Krol, P., Synthesis methods, chemical structures and phase structures of linear polyurethanes. Properties and applications of linear polyurethanes in polyurethane elastomers, copolymers and ionomers. *Progress in materials science* **2007,** *52* (6), 915-1015.

39. Santerre, J. P.; Woodhouse, K.; Laroche, G.; Labow, R. S., Understanding the biodegradation of polyurethanes: from classical implants to tissue engineering materials. *Biomaterials* **2005,** *26* (35), 7457-7470.

40. Zdrahala, R. J.; Zdrahala, I. J., Biomedical applications of polyurethanes: a review of past promises, present realities, and a vibrant future. *Journal of biomaterials applications* **1999,** *14* (1), 67-90.

41. Brenes-Granados, D.; Cubero-Sesin, J. M.; Gutiérrez, F. O.; Vega-Baudrit, J.; Gonzalez-Paz, R., Variation of Physical Properties of Rigid Polyurethane Foams Synthesized from Renewable Sources with Different Commercial Catalysts. *Journal of Renewable Materials* **2017,** *5* (3-4), 280-289.

42. Alder, C. M.; Hayler, J. D.; Henderson, R. K.; Redman, A. M.; Shukla, L.; Shuster, L. E.; Sneddon, H. F., Updating and further expanding GSK's solvent sustainability guide. *Green Chemistry* **2016,** *18* (13), 3879-3890.

43. Philipp, M.; Bhandary, R.; Groche, F. J.; Schönhoff, M.; Rieger, B., Structure-property relationship and transport properties of structurally related silyl carbonate electrolytes. *Electrochimica Acta* **2015,** *173*, 687-697.

44. Sonnati, M. O.; Amigoni, S.; de Givenchy, E. P. T.; Darmanin, T.; Choulet, O.; Guittard, F., Glycerol carbonate as a versatile building block for tomorrow: synthesis, reactivity, properties and applications. *Green Chemistry* **2013,** *15* (2), 283-306.

45. Lang, X. D.; He, L. N., Green Catalytic Process for Cyclic Carbonate Synthesis from Carbon Dioxide under Mild Conditions. *The Chemical Record* **2016,** *16* (3), 1337-1352.

46. Reithofer, M. R.; Sum, Y. N.; Zhang, Y., Synthesis of cyclic carbonates with carbon dioxide and cesium carbonate. *Green Chemistry* **2013,** *15* (8), 2086-2090.

47. Hirose, T.; Shimizu, S.; Qu, S.; Shitara, H.; Kodama, K.; Wang, L., Economical synthesis of cyclic carbonates from carbon dioxide and halohydrins using K 2 CO 3. *RSC Advances* **2016,** *6* (73), 69040-69044.

48. Chen, K.; Shi, G.; Dao, R.; Mei, K.; Zhou, X.; Li, H.; Wang, C., Tuning the basicity of ionic liquids for efficient synthesis of alkylidene carbonates from CO 2 at atmospheric pressure. *Chemical Communications* **2016,** *52* (50), 7830-7833.

49. Hu, J.; Ma, J.; Zhu, Q.; Qian, Q.; Han, H.; Mei, Q.; Han, B., Zinc (II)-catalyzed reactions of carbon dioxide and propargylic alcohols to carbonates at room temperature. *Green Chemistry* **2016,** *18* (2), 382-385.

50. Kumar, S.; Singhal, N.; Singh, R. K.; Gupta, P.; Singh, R.; Jain, S. L., Dual catalysis with magnetic chitosan: direct synthesis of cyclic carbonates from olefins with carbon dioxide using isobutyraldehyde as the sacrificial reductant. *Dalton Transactions* **2015,** *44* (26), 11860-11866.

51. Rocha, C. C.; Onfroy, T.; Launay, F., Towards a combined use of Mn (Salen) and quaternary ammonium salts as catalysts for the direct conversion of styrene to styrene carbonate in the presence of dioxygen and carbon dioxide. *Comptes Rendus Chimie* **2015,** *18* (3), 270-276.

52. Rokicki, G.; Parzuchowski, P. G.; Mazurek, M., Non‐isocyanate polyurethanes: synthesis, properties, and applications. *Polymers for Advanced Technologies* **2015,** *26* (7), 707-761.

53. Guan, J.; Song, Y.; Lin, Y.; Yin, X.; Zuo, M.; Zhao, Y.; Tao, X.; Zheng, Q., Progress in study of non-isocyanate polyurethane. *Industrial & Engineering Chemistry Research* **2011,** *50* (11), 6517-6527.

54. Poussard, L.; Mariage, J.; Grignard, B.; Detrembleur, C.; Jérôme, C.; Calberg, C.; Heinrichs, B.; De Winter, J.; Gerbaux, P.; Raquez, J. M., Non-isocyanate polyurethanes from carbonated soybean oil Using monomeric or oligomeric diamines To achieve thermosets or thermoplastics. *Macromolecules* **2016,** *49* (6), 2162-2171.

55. Javni, I.; Hong, D. P.; Petrović, Z. S., Soy-based polyurethanes by nonisocyanate route. *Journal of Applied Polymer Science* **2008,** *108* (6), 3867-3875.

56. Tamami, B.; Sohn, S.; Wilkes, G. L., Incorporation of carbon dioxide into soybean oil and subsequent preparation and studies of nonisocyanate polyurethane networks. *Journal of Applied Polymer Science* **2004,** *92* (2), 883-891.

57. Chen, Y.; Fuchise, K.; Narumi, A.; Kawaguchi, S.; Satoh, T.; Kakuchi, T., Core-first synthesis of three-, four-, and six-armed star-shaped poly (methyl methacrylate) s by group transfer polymerization using phosphazene base. *Macromolecules* **2011,** *44* (23), 9091-9098.

58. Eibel, A.; Fast, D. E.; Sattelkow, J.; Zalibera, M.; Wang, J.; Huber, A.; Müller, G.; Neshchadin, D.; Dietliker, K.; Plank, H., Star‐shaped Polymers via Simple Wavelength‐Selective Free Radical Photopolymerization. *Angewandte Chemie International Edition* **2017**.

59. Hadjichristidis, N.; Pitsikalis, M.; Iatrou, H.; Driva, P.; Sakellariou, G.; Chatzichristidi, M., 6.03-Polymers with Star-Related Structures: Synthesis, Properties, and Applications. *Polymer science: a comprehensive reference* **2012**, 29-111.

60. Yang, D. P.; Oo, M. N. N. L.; Deen, G. R.; Li, Z.; Loh, X. J., Nano‐Star‐Shaped Polymers for Drug Delivery Applications. *Macromolecular Rapid Communications* **2017**.

61. Wu, W.; Wang, W.; Li, J., Star polymers: advances in biomedical applications. *Progress in Polymer Science* **2015,** *46*, 55-85.

62. Sejidov, F. T.; Mansoori, Y.; Goodarzi, N., Esterification reaction using solid heterogeneous acid catalysts under solvent-less condition. *Journal of Molecular Catalysis A: Chemical* **2005,** *240* (1), 186-190.

63. Howie, J. K.; Schaefer, J. J.; Trout, J. E., Synthesis of polyol medium fatty acid polyesters. U.S. Patent No. 6,995,232: 7 Feb. 2006.

64. Corrigan, P. J., Synthesis of polyol fatty acid polyesters. U.S. Patent No. 6,620,952: 16 Sep. 2003.

65. Schaefer, J. J.; Trout, J. E., Synthesis of purified, partially esterified polyol polyester fatty acid compositions. U.S. Patent No. 6,887,947: 3 May 2005.

66. Monono, E. M.; Bahr, J. A.; Pryor, S. W.; Webster, D. C.; Wiesenborn, D. P., Optimizing process parameters of epoxidized sucrose soyate synthesis for industrial scale production. *Organic Process Research & Development* **2015,** *19* (11), 1683-1692.

67. Monono, E. M.; Webster, D. C.; Wiesenborn, D. P., Pilot scale (10kg) production and characterization of epoxidized sucrose soyate. *Industrial Crops and Products* **2015,** *74*, 987-997.

68. Pan, X.; Sengupta, P.; Webster, D. C., Novel biobased epoxy compounds: epoxidized sucrose esters of fatty acids. *Green Chemistry* **2011,** *13* (4), 965-975.

69. Webster, D. C.; Sengupta, P. P.; Chen, Z.; Pan, X.; Paramarta, A., Highly functional epoxidized resins and coatings. U.S. Patent No. 9,096,773: 4 Aug 2015.

70. Pan, X.; Webster, D. C., New biobased high functionality polyols and their use in polyurethane coatings. *ChemSusChem* **2012,** *5* (2), 419-429.

71. Paramarta, A.; Pan, X.; Webster, D. C., Highly Functional Acrylated Biobased Resin System. *Radtech Report* **2013,** *1*, 26-32.

72. Nelson, T. J.; Bultema, L.; Eidenschink, N.; Webster, D. C., Bio-based high functionality polyols and their use in 1K polyurethane coatings. *Journal of Renewable Materials* **2013,** *1* (2), 141-153.

73. Kovash, C. S.; Pavlacky, E.; Selvakumar, S.; Sibi, M. P.; Webster, D. C., Thermoset Coatings from Epoxidized Sucrose Soyate and Blocked, Bio‐Based Dicarboxylic Acids. *ChemSusChem* **2014,** *7* (8), 2289-2294.

74. Ma, S.; Webster, D. C.; Jabeen, F., Hard and flexible, degradable thermosets from renewable bioresources with the assistance of water and ethanol. *Macromolecules* **2016,** *49* (10), 3780-3788.

75. Ma, S.; Webster, D. C., Naturally occurring acids as cross-linkers to yield VOC-free, high-performance, fully bio-based, degradable thermosets. *Macromolecules* **2015,** *48* (19), 7127-7137.

76. Paramarta, A.; Webster, D. C., Bio-based high performance epoxy-anhydride thermosets for structural composites: The effect of composition variables. *Reactive and Functional Polymers* **2016,** *105*, 140-149.

77. Paramarta, A.; Webster, D. C., The exploration of Michael-addition reaction chemistry to create high performance, ambient cure thermoset coatings based on soybean oil. *Progress in Organic Coatings* **2017,** *108*, 59-67.

78. Paramarta, A.; Webster, D. C., Curing kinetics of bio-based epoxy-anhydride thermosets with zinc catalyst. *Journal of Thermal Analysis and Calorimetry*, 1-12.

79. Sitz, E. D.; Bajwa, D. S.; Webster, D. C.; Monono, E. M.; Wiesenborn, D. P.; Bajwa, S. G., Epoxidized sucrose soyate—A novel green resin for crop straw based low density fiberboards. *Industrial Crops and Products* **2017**.

80. Rochester, J. R., Bisphenol A and human health: a review of the literature. *Reproductive toxicology* **2013,** *42*, 132-155.

81. Pergialiotis, V.; Kotrogianni, P.; Christopoulos-Timogiannakis, E.; Koutaki, D.; Daskalakis, G.; Papantoniou, N., Bisphenol A and adverse pregnancy outcomes: a systematic review of the literature. *The Journal of Maternal-Fetal & Neonatal Medicine* **2017**, 1-8.

82. Ejaredar, M.; Lee, Y.; Roberts, D. J.; Sauve, R.; Dewey, D., Bisphenol A exposure and children's behavior: A systematic review. *Journal of Exposure Science and Environmental Epidemiology* **2017,** *27* (2), 175-183.

83. Lu, J.; Khot, S.; Wool, R. P., New sheet molding compound resins from soybean oil. I. Synthesis and characterization. *Polymer* **2005,** *46* (1), 71-80.

84. Yan, J.; Webster, D. C., Thermosets from highly functional methacrylated epoxidized sucrose soyate. *Green Materials* **2014,** *2* (3), 132-143.

85. Amiri, A.; Yu, A.; Webster, D.; Ulven, C., Bio-Based Resin Reinforced with Flax Fiber as Thermorheologically Complex Materials. *Polymers* **2016,** *8* (4), 153.

86. Taylor, C.; Amiri, A.; Paramarta, A.; Ulven, C.; Webster, D., Development and weatherability of bio-based composites of structural quality using flax fiber and epoxidized sucrose soyate. *Materials & Design* **2017,** *113*, 17-26.

87. Amiri, A.; Hosseini, N.; Ulven, C.; Webster, D. In *Advanced bio-composites made from methacrylated epoxidized sucrose soyate resin reinforced with flax fibers*, Proceedings of the 20th International Conference on Composite Materials, Copenhagen, Denmark, 2015; pp 19-24.

88. Hosseini, N.; Webster, D. C.; Ulven, C., Advanced biocomposite from highly functional methacrylated epoxidized sucrose soyate (MAESS) resin derived from vegetable oil and fiberglass fabric for composite applications. *European Polymer Journal* **2016,** *79*, 63-71.

CHAPTER 2. HIGH PERFORMANCE BIO-BASED THERMOSETS FROM DIMETHACRYLATED EPOXIDIZED SUCROSE SOYATE (DMESS)

2.1. Abstract

To tune the properties and reduce the viscosity of methacrylate functional epoxidized sucrose soyate (MESS), the use of a dual functionalization strategy was explored. Bio-based thermosets have previously been produced from free-radical curing of MESS having a large number of functional groups and have demonstrated a high glass transition temperature (T_g) and good mechanical properties. However, the resin viscosity was high. To reduce the resin viscosity, further functionalization of MESS was carried out by sequential addition of methacrylic anhydride. The synthesis was optimized and the resulting dimethacrylated epoxidized sucrose soyate resin (DMESS) was characterized using Fourier transform infrared spectroscopy (FTIR), proton nuclear magnetic resonance spectroscopy (^{1}H-NMR), gel permeation chromatography (GPC), and viscosity measurements. A series of DMESS resins with varying range of degrees of methacrylation was synthesized. The resins were mixed with varying amounts of styrene and cured using a free radical process with peroxyesters as initiators. The extent of cure was determined by gel content using Soxhlet extraction and confirmed using FTIR. The thermal and mechanical properties were evaluated using thermogravimetric analysis (TGA), differential scanning calorimetry (DSC), dynamic mechanical thermal analysis (DMTA), and tensile testing.

2.2. Introduction

Thermosetting polymers are highly desirable materials due to their low density, low cost, and good mechanical properties, and have many applications in composites, coatings, and adhesives. Typical systems used for thermosets include polyesters, epoxies, polyurethanes and

phenol-formaldehyde resins. Raw materials for the synthesis of these resins are conventionally petroleum-based chemicals. Due to the future limitations of fossil fuel sources and emergence of environmental concerns, researchers have been devoting efforts on alternative solutions such as developing polymers and composites from bio-renewable raw materials.[1-3] Uncertainties in the cost of petrochemicals and stricter environmental regulations have driven significant interest in bio-based products. Some of the possible advantages of bio-based products versus their petrochemical counterparts are sustainability, biodegradability, being environmentally friendly, and versatility.[4]

Biomass has been successfully harnessed into energy historically by humans since burning wood to make fire was discovered. Today, chemicals obtained from biomass are generally classified as either drop-in replacements or new chemicals. Drop-in replacements are chemicals derived from biomass that have an identical composition to known petrochemicals and serve as direct replacements. On the other hand, new chemicals and materials need to be investigated exhaustively due to their unknown properties. In polymer science, drop-in replacements are used due to their lower or comparable cost and/or superior properties against commercial standards. Meanwhile, new chemicals are being developed and are being investigated in a wide variety of potential applications such as resins, crosslinkers, reactive diluents, etc.

The majority of biomass is plant-based materials such as cellulose, lignin and plant oils. Plant oils are ideal biorenewable sources for the polymer industry because of the wide availability, high production, low cost, and biodegradability. Plant oil-based thermosets have been developed in the last decade via free-radical polymerization, cationic homopolymerization, and copolymerization with petroleum-based monomers like styrene and divinylbenzene.[5-11]

However, the flexible fatty acid chains of plant oils are one of the major limitations in developing high-performance thermosets. Petroleum-based monomers are typically used as reinforcements to improve these properties.[12, 13] Alternatively, incorporation of reinforcements structurally into the flexible fatty acid chains would furnish versatile materials.

Sucrose, popularly known as table sugar, is a biorenewable chemical widely produced from sugar cane or sugar beets. The fatty acid esters of sucrose have been explored for several decades and Procter & Gamble (P&G) Chemicals developed a production process to achieve a high degree of esterification.[14-16] These sucrose ester fatty acids (SEFAs) were commercialized under the brand SEFOSE 1618U for industrial uses and applied as diluents in alkyd resins, among other potential applications.

Pan *et al.* have previously established a protocol in epoxidizing various SEFAs.[17] These were cured using cyclic anhydrides.[17-19] The anhydride-cured epoxidized SEFAs had exceptional physical and mechanical properties (e.g. modulus, tensile strength, hardness) compared to thermosets made using epoxidized soybean oil. Recently, Paramarta and Webster published a study of high performance epoxy-anhydride thermosets for structural composites using epoxidized sucrose soyate (ESS).[20] ESS is synthesized by performing the Prilezhaev reaction on sucrose soyate, which is one of the SEFAs that is the most widely available. Sucrose soyate is a versatile molecule that possesses both rigid and flexible parts. Its rigidity is attributed to the sucrose core while its flexibility is attributed to the unsaturated fatty acid chains.

These epoxidized compounds could undergo further modification by ring-opening reactions using nucleophiles such as acids or alcohols.[21] Bio-based polyols can be generated for polyurethane and composite applications.[22] SEFA-based thermosets displayed much higher glass transition temperatures (T_gs) and good mechanical properties in comparison to the triglyceride

oil-based counterparts.[13, 17-19, 22-25] The improved properties are attributed to the high functionality of the SEFA-based resins as well as the rigidity of the sucrose core. Furthermore, functionalized acids such as methacrylic acid can be reacted with epoxidized sucrose soyate to generate bio-based resins containing hydroxyl groups and terminal alkenes. These methacrylated oligomers may then be polymerized to form highly crosslinked networks. These types of derivatives have been used to produce thermosets by free-radical polymerization or hydroxyl-isocyanate reactions.[26-35]

Yan and Webster studied novel bio-based methacrylated oligomers (methacylated epoxidized sucrose soyate, MESS) synthesized from ESS (Scheme 2.1).[36] Bio-based thermosets were formulated, cured using free radical initiators and afforded improved thermomechanical properties. The properties possessed by these thermosets render them good candidates for use in structural composites. Fiber reinforced polymer (FRP) composites have been extensively studied utilizing bio-based thermosets as the matrix resin in the last several years.[37-42] Similarly, MESS has been investigated, in conjunction with flax and glass fibers, and have shown interesting sets of properties and displayed complex behavior.[43-45] When used with glass fibers, it was observed that the MESS resin-based composite had properties equivalent to or better than a conventional vinyl ester resin and it was observed that MESS had better adhesion to the fibers than the vinyl ester resin.[46]

However, a drawback of the methacrylated sucrose soyate resins is their high viscosity.[47] This high viscosity is attributed to the hydrogen bonding provided by the hydroxyl groups generated from the ring-opening reaction of the epoxides. Hypothetically, substituting the hydroxyl groups with functional groups that either lower these interactions or completely remove hydrogen bonding could reduce the resin viscosity. In addition, replacing the hydroxyl groups

with crosslinkable moieties would simultaneously reduce the resin viscosity and increase the crosslink density of thermosets produced.

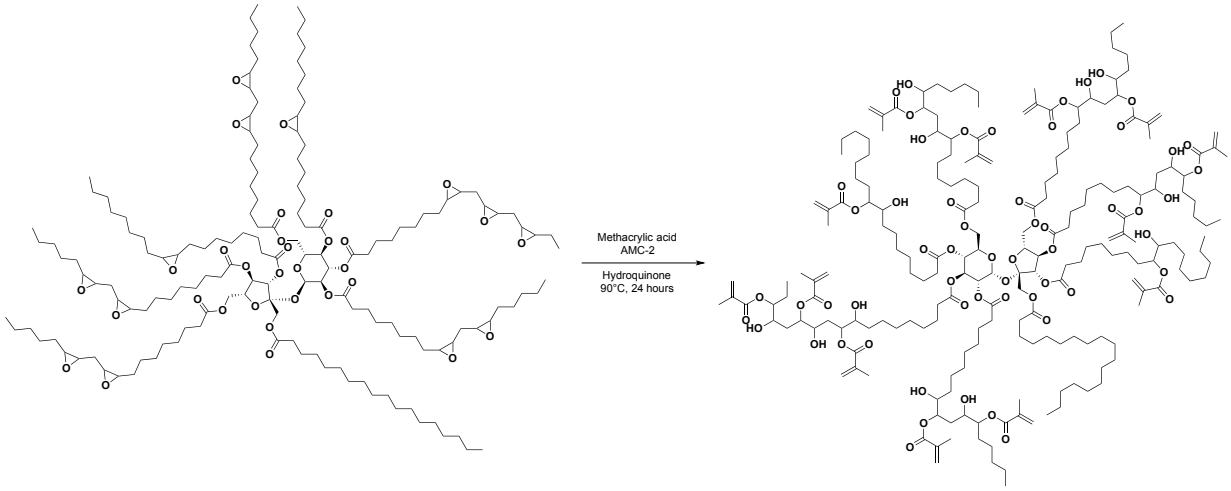

Scheme 2.1. Synthetic route to methacrylated epoxidized sucrose soyate (MESS).

Thus, the objective of this study was to explore the preparation of low viscosity and highly functional bio-based resins by methacrylating ESS on the two adjacent carbons of the epoxide groups, reducing the extent of hydrogen bonding. Furthermore, the effect of the degree of functionality on the structure-property relationships was investigated. The series of dimethacrylated epoxidized sucrose soyate (DMESS) oligomers were formulated into thermosets and cured by thermally initiated free-radical polymerization with styrene as the reactive diluent. In order to establish its set of properties, the thermomechanical properties were investigated and the structure-property relationships for the series of thermosets were elucidated.

2.3. Experimental

2.3.1. Raw materials

Procter & Gamble Chemicals (Cincinnati, OH, USA) provided sucrose soyate (SEFOSE 1618U), which was the precursor of the starting material. Methacrylic acid, methacrylic anhydride, and *N*-methylimidazole were purchased from Alfa Aesar (Ward Hill, Massachusetts,

USA). AMC-2 and ATC-3 accelerators, purchased from AMPAC Fine Chemicals (Rancho Cordova, CA, USA), are solutions of trivalent organic chromium complexes in phthalate esters. Hydroquinone and styrene were purchased from Sigma Aldrich (St. Louis, MO, USA). Free radical initiators Luperox P (*t*-butyl peroxybenzoate) and Luperox 10M75 (*t*-butyl peroxyneodecanoate) were supplied by Arkema (Philadelphia, PA, USA). All reagents were used as received. Epoxidized sucrose soyate (ESS) was synthesized from sucrose soyate following the procedure in the literature.[17, 48, 49] The epoxy equivalent weight (EEW) of ESS, which was 246, was determined by titration according to ASTM D 1652.

2.3.2. Synthesis of DMESS

The synthesis of the resin was achieved via ring-opening reaction of ESS with methacrylic acid followed by methacrylic anhydride addition. The reaction was carried out at 100°C, using ATC-3 (1.0% of total weight) as the catalyst and hydroquinone (0.1% of total weight) as the inhibitor. The degree of methacrylation was varied (90%, 80%, and 70%). The molar ratio of methacrylating agents (methacrylic acid and methacrylic anhydride) to epoxy was also varied. Changing the acid to anhydride ratio from 1:9 and 2:8 means the degree of methacrylation was decreased. A typical procedure is as follows: ESS (100.00 g), methacrylic acid (2.80 g), hydroquinone (0.15 g) and ATC-3 (1.48 g) were placed into a four-necked reaction kettle equipped with a mechanical stirrer and a thermocouple. The mixture was heated at 100°C until the most of the acid has reacted. Methacrylic anhydride (45.12 g) was added dropwise (~0.25 mL/minute). The reaction mixture was heated at 100°C until the acid number was less than 15. The final resin appeared as a dark green, viscous liquid. (The green color is due to the presence of the chromium catalyst.) A summary of the amounts used for the synthesis or each resin is shown in Table 2.1.

Table 2.1. Amounts of the reagents used for the synthesis of the various DMESS.

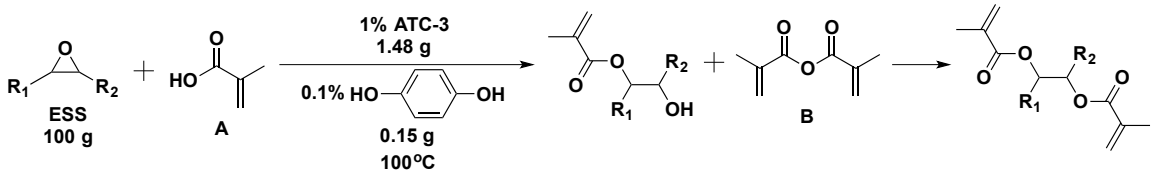

Resin	Degree of methacrylation (%)	A:B	Methacrylic acid (g) [A]	Methacrylic anhydride (g) [B]
DMESS-0.9	90	1:9	3.15	50.76
DMESS-0.8	80	1:9	2.80	45.12
DMESS-0.7	70	1:9	2.45	39.48
DMESS-0.9	90	2:8	6.30	45.12
DMESS-0.8	80	2:8	5.60	40.11

2.3.3. Characterization of oligomers

Fourier transform infrared spectroscopy (FTIR) was performed with a Thermo Scientific Nicolet 8700 with a detector type of DTGS KBr under nitrogen purge. Diluted thin films of the samples were applied on a KBr plate and the absorption spectra were taken with 32 scans at a resolution of 4 cm^{-1} in the range of 4000-400 cm^{-1}. Molecular weight of the resin was obtained using a gel permeation chromatography (GPC) system (EcoSEC HLC-8320GPC, Tosoh Bioscience, Japan) with a differential refractometer (DRI) detector. Separations were performed using two TSKgel SuperH3000 6.00 mm ID×15 cm columns. The columns and detectors were set at 40°C. Tetrahydrofuran (THF) was used as the eluent with a flow rate of 0.35 ml min^{-1}. Samples were prepared at nominally 1 mg ml^{-1} in an aliquot of the eluent and allowed to dissolve at ambient temperature for several hours and the injection volume was 20µL for each sample. Calibration was conducted using polystyrene standards (Agilent EasiVial PS-H 4ml). Proton nuclear magnetic resonance spectroscopy (^{1}H-NMR) was conducted with a Bruker system, Ascend 400 MHz magnet with an Avance III HD console (Bruker BioSpin Corporation, Billerica, Massachusetts, USA), using $CDCl_3$ as the solvent. Acid number titration was carried

out according to ASTM D664. The viscosity of the resins was measured at 25°C using an ARES Rheometer (TA Instruments) operating from 0.1 rad/s to 500 rad/s with 0.1% strain.

2.3.4. Curing of the resins

Formulations of DMESS alone and with 10, 20, and 30 percent by weight styrene as the reactive diluent were prepared. Commercially available peroxyesters Luperox P, (2% of total resin weight) and Luperox 10M75, (2% of total resin weight) were utilized as free-radical initiators. All the ingredients were mixed thoroughly using a Flacktek Speedmixer before curing. The formulations were deposited in a silicone mold and then cured. A typical procedure is as follows: DMESS (4.50 g), styrene (0.50 g), Luperox P (0.10 g), and Luperox 10M75 (0.10 g) were placed in a 15-mL plastic vial. The contents were mixed for 5 minutes at 3500 rpm using the high speed mixer. The mixture was then poured into the silicone mold, and cured at 70°C for 1 hour, 90°C for 1 hour, and 150°C for 2 hours. The mold was allowed to cool to room temperature before the cured thermosets were removed.

2.3.5. Characterization of thermosets

A Q500 thermogravimetric analysis (TGA) system (TA Instruments) with a heating rate of 20°C/min from room temperature to 600°C under a continuous nitrogen flow, was used to determine the thermal stability of the thermosets. An Instron 5542 system (Instron Corp., Norwood, MA, USA) with a strain rate of 0.2%/s was used to measure the tensile properties; ASTM D638 was followed to prepare dumbbell type V specimens. Specimen thicknesses were around 1.0 mm. At least 5 samples were measured for each thermoset and the averages and standard deviation were reported. Dynamic mechanical analysis was carried out using a Q800DMA (TA Instruments) operating at 1 Hz and a heating rate of 5°C/min from -50°C to 200°C (dual cantilever mode). The tan δ peak was identified as the T_g. The storage modulus

(E') in the rubbery plateau region was determined at 60°C above the T_g and used to calculate the crosslink density (v_e). Equation 2.1 from the rubber elasticity theory was used to calculate the crosslinking density using the storage modulus:

$$E' = 3v_eRT \qquad \text{(Equation 2.1)}$$

where E' is the thermoset storage modulus in the rubbery plateau region, R is the gas constant, and T is the absolute temperature. The gel content of the thermosets was determined via solvent extraction using dichloromethane. A 500-mL flask containing 300 mL dichloromethane and boiling stones was equipped with a Soxhlet extractor, connected to a condenser. 1 g of the samples were weighed and placed inside the thimble, and extracted for 24 h. The samples were then dried in vacuum and weighed. The gel content of the thermoset is calculated using Equation 2.2:

$$\%\ Gel\ Content = \frac{W_f}{W_i} X\ 100 \qquad \text{(Equation 2.2)}$$

where W_i is the weight of the thermoset sample prior to Soxhlet extraction, and W_f is the weight of the thermoset sample after the extraction.

2.4. Results and discussion

2.4.1. Synthesis and characterization of resins

Initial investigations of the DMESS synthesis process were initially carried out beginning with a simple modification of an established synthesis.[36] The first approach was a one-pot synthesis of DMESS using methacrylic acid (A), methacrylic anhydride (B), AMC-2, and hydroquinone (Table 2.2). A series of experiments were carried out where the ratio of the methacrylating agents (A:B) was varied. The product formation was confirmed by ^{1}H-NMR. The desired dual methacrylated product began forming when A:B ratio was 6:4 (Table 2.2, entry 4). When the amount of anhydride was increased, the ^{1}H-NMR peak (Figure 1, ~ 5.15 ppm)

corresponding to the proton of the –CH- group attached to the second methacrylate group of the product also increased. Thus, the best ratio was found to be 1:9 A:B. The resulting resin viscosities also decreased with increasing amount of methacrylic anhydride. As more of the ester replaces the hydroxyl groups, there will be less hydrogen bonding which decreases the resin viscosity, confirming our original hypothesis.

Table 2.2. One-pot synthesis of DMESS.

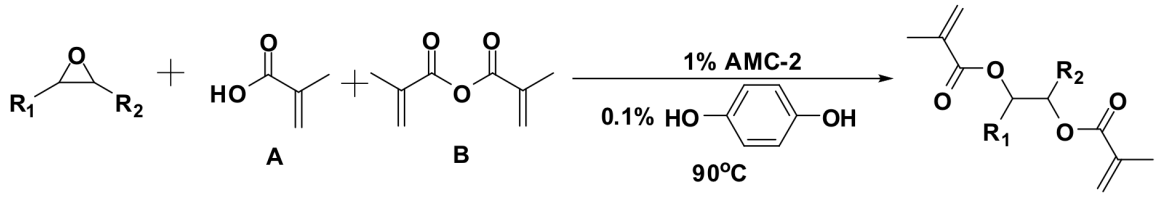

	A:B	Time (Hours)	Acid Number	M_n	$Đ$	Viscosity (Pa•s)
1	9:1	48	13	3444	1.26	634
2	8:2	49	14	3477	1.29	350
3	7:3	48	11	3555	1.26	520
4	6:4	48	8	3479	1.19	384
5	5:5	52	12	3573	1.14	316
6	4:6	58	11	3395	1.23	260
7	3:7	58	10	3366	1.20	120
8	2:8	68	13	3562	1.15	82.7
9	1:9	102	21	3441	1.24	47.6

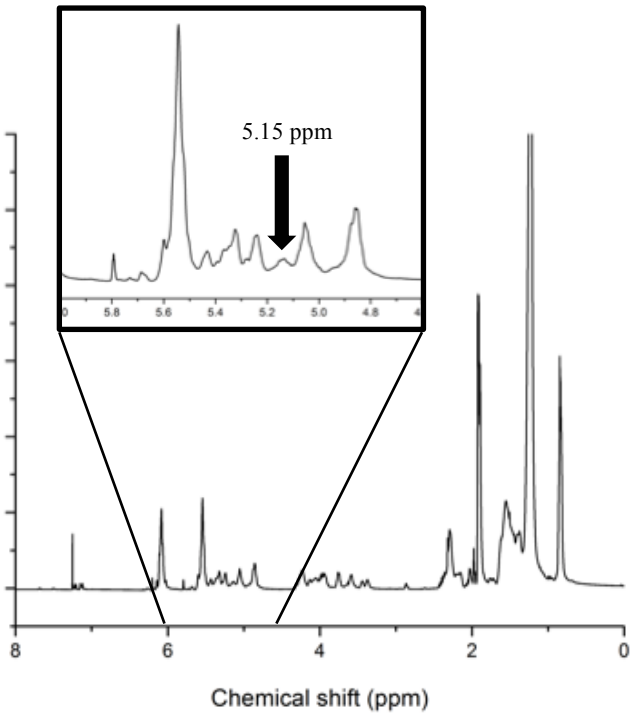

Figure 2.1. Proton NMR spectrum of DMESS.

DMESS was further characterized by FTIR. Figure 2 shows a representative FTIR spectrum of DMESS. Table 2.3 is a summary of the functional groups present in DMESS. The FTIR spectrum accounts for all the functional groups of DMESS. The presence of the hydroxyl peak at 3511 cm^{-1} is from the unreacted alcohol formed from the ring-opening step since DMESS is only partially methacrylated.

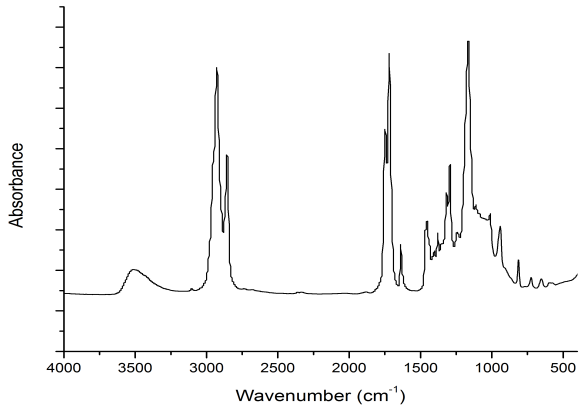

Figure 2.2. FTIR spectrum of DMESS.

Table 2.3. FTIR wavenumbers of DMESS and corresponding vibrations.

Wavenumber (cm^{-1})	Vibration type
3511	OH stretching
1750	Fatty acid C=O stretching
1720	Methacrylate C=O stretching
1635	Methacrylate C=C stretching
941	Epoxide C-O-C deformation bands
812	
654	Methacrylate =C-H out of plane bending

Next, a sequential addition approach was investigated as shown in Table 2.4. In this study, both the methacrylating agent ratios and rate of their addition were varied. *N*-Methylimidazole was used as a catalyst for the methacrylation of the alcohol group (Table 2.4, entry 3). Adekunle *et al.*[50-52] used this method in their two-step methacrylation of epoxidized soybean oil and successfully methacrylated the alcohol. DMESS formation was confirmed by ^{1}H-NMR. From this study, it was concluded that the use of an additional catalyst, *N*-Methylimidazole, proved unnecessary and dropwise addition of methacrylic anhydride was suitable to form the DMESS.

Table 2.4. Sequential addition study of methacrylic acid and methacrylic anhydride.

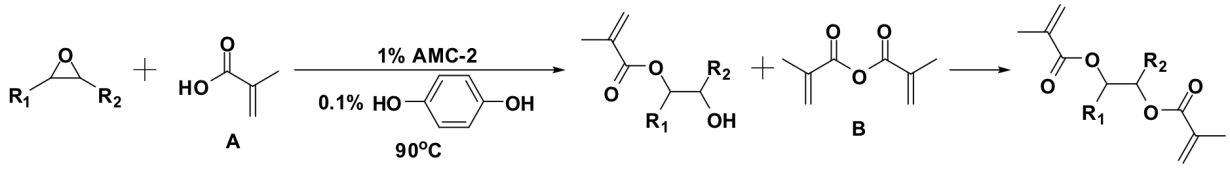

	A:B	A Addition Time (Hours)	Acid Number 1	B Addition Time (Hours)	Acid Number 2	Viscosity (Pa•s)	Time (Hours)
1	8:2	1	-	0.33	48	138	65
2	8:2	23	4	0.17	13	263	46
3[a]	8:7	7.5	37	dropwise	63	30	50
4	8:10	22	1	dropwise	85	6	96

[a] used N-Methylimidazole as second methacrylation catalyst.

Next, several catalysts were screened to determine the one most appropriate for the system. The reaction was mechanically stirred, and the amount of catalyst used and

methacrylating agent ratios were varied. The time to reach the acid number, final acid number, and the viscosity of DMESS are summarized in Table 2.5. Catalysts 1,8-diazabicycloundec-7-ene (DBU) and K-Pure® CXC-1765 both resulted in gelled products. The likely reason for this is the side reaction of the formed hydroxyl group on the ESS reacting with epoxy groups. While BV Cat 7 and ATC-3 both provided viscous liquids, it was determined that ATC-3 would be a better choice since BV Cat 7 changed the solution from colorless to a dark orange color. A much lower acid number was reached in a shorter time for the reaction catalyzed with ATC-3 compared with BV Cat 7. The literature for ATC-3 and AMC-2 states that these types of catalysts are designed to suppress the side reaction of hydroxyl-epoxy reactions, however imparts a dark green color. The number-average molecular weight (M_n) for the reaction catalyzed by ATC-3 provided the expected number-average molecular weight (M_n). As a result, ATC-3 was used as the catalyst of choice in the succeeding syntheses.

Table 2.5. Catalyst screening of the DMESS synthesis.

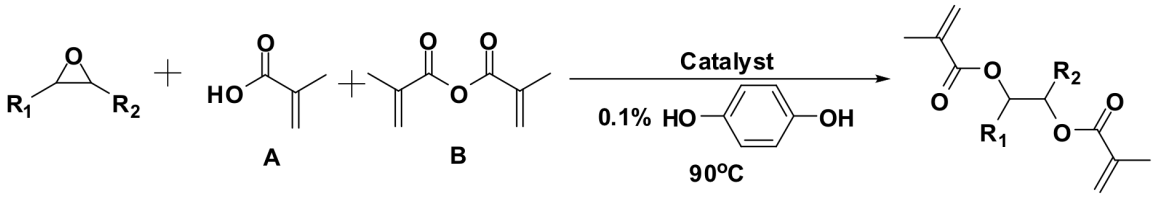

	A:B	Time (Hours)	Acid Number	Catalyst	Amount (% wt)	M_n	$Đ$	Comments
1	9:1	11	-		2			Gelled
2	1:1	10	17	DBU	2	2204	1.17	Partially gelled
3	1:9	13	13		2	1910	1.29	Dark solution
4	9:1	11	36	K-Pure®	2			Gelled (18 h)
5	1:1	14	-	CXC-	2			Gelled
6	9:1	10	52	1765	2			1% Hydroquinone
7	9:1	20	18	BV Cat 7	1			Dark solution
8	9:1	12	13	ATC-3	1	3602	1.00	

Previously, the MESS synthesis was carried out at 90°C. Table 6 shows the summary of the temperature study of the DMESS synthesis. The ratio of methacrylic acid (A): methacrylic anhydride (B) was kept constant at 1:9. The degree of methacrylation was also kept constant at 80%. At 90°C, the acid number was 20 after 53 hours. Increasing the temperature to 100°C allowed the acid number to reach 7 after 47.5 hours. When the temperature was increased further to 110°C, the reaction gelled after 18 hours. At this temperature, it seems that there is sufficient energy to encourage the homopolymerization of the epoxide groups. Upon temperature optimization, it was found that the optimum temperature was 100°C. This temperature was also employed in the synthesis of DMESS with 90% methacrylation. The acid number of 9 was reached after 52 hours (Table 2.6, entry 4). The longer reaction time compared to entry 2 is due to the higher degree of methacrylation. In all cases, the number-average molecular weight was consistently around 4000 kg/mol. The viscosities were also significantly lower than MESS.

Table 2.6. Temperature study of the DMESS synthesis.

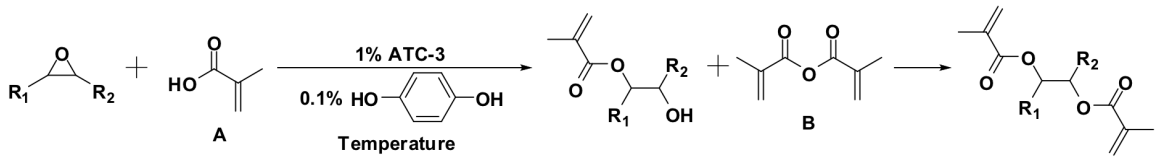

	A:B	Time (Hours)	Acid Number	Temperature (°C)	M_n	$Đ$	Viscosity (Pa•s)	Comments
1[a]	1:9	53	20	90	3986	1.01	62.6	
2[a]		47.5	7	100	3905	1.01	67.3	
3[a]		18	-	110				Gelled
4[b]		52	9	100	4140	1.01	197.6	

[a] 80% Methacrylation, [b] 90% Methacrylation

Mechanistically (Scheme 2.2), it is proposed that the reaction proceeds first when methacrylic acid activates the epoxide by protonation. Because of this, only a small amount of methacrylic acid is needed to facilitate the epoxide protonation. The methacrylate ion then

attacks this activated intermediate to form MESS. In the presence of an anhydride, the hydroxyl group of MESS reacts with the anhydride to form the dual methacrylated product, while regenerating methacrylic acid. The cycle repeats until all of the methacrylic anhydride have reacted with the hydroxyls. Every molecule of methacrylic anhydride that reacts with the hydroxyl group of MESS generates a molecule of methacrylic acid. Hence, there will be unreacted hydroxyls equivalent to the amount of the methacrylic acid used.

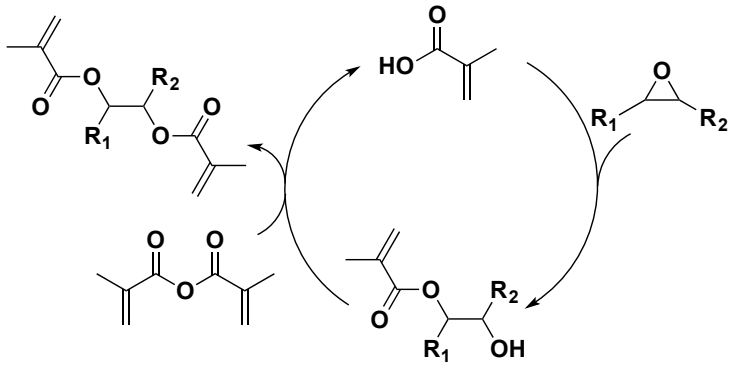

Scheme 2.2. Proposed reaction mechanism of DMESS synthesis.

Based on the preliminary studies, a series of DMESS resins was then synthesized where the total amount of methacrylation was varied, as was the ratio of methacrylic acid to methacrylic anhydride. A control resin from the previous study, MESS, was also synthesized. Table 2.7 shows the summary of the reaction parameters used in the synthesis of the resins. In all cases, the reaction was stopped as soon as the acid number was 15 or less. MESS synthesis reached the acid number of 15 after 23 hours while that of DMESS reached low acid numbers after about 48 hours. The reaction time for DMESS synthesis is about twice as long as MESS synthesis since it involves MESS as its intermediate. Once MESS is formed, it becomes sterically hindered compared with its starting material, ESS. MESS also contains hydroxyl groups that form hydrogen bonding with the other hydroxyl groups. The synthesis was also run neat, which contributes to its high viscosity. The solids contents of all the resins are over 98.97.

The resulting viscosity of the DMESS resins was dramatically lower compared to MESS. The lowered viscosity of the DMESS resins is attributed to the reduction of the hydrogen bonding that resulted from replacement of the hydroxyls with methacrylates. The M_n for MESS was 3750 g/mol while all the DMESS resins were around 4000 g/mol. The reduced viscosity and increase in M_n for DMESS, combined with the ^{1}H-NMR (Figure 2.3) and FTIR analyses (Figure 2.4), confirm the successful substitution of the hydroxyls with methacrylates.

Table 2.7. Properties of the resins.

Resin	A:B	Temperature (°C)	Time (Hours)	Acid Number	% Solid	Viscosity (Pa•s)	M_n	$Đ$
MESS-0.8		90	23	15	98.97	433.6	3748	1.01
DMESS-0.9	1:9	100	52	9	99.85	197.6	4140	1.01
DMESS-0.8	1:9	100	47.5	7	99.20	67.3	3905	1.01
DMESS-0.7	1:9	100	42	6	99.98	73.2	4014	1.01
DMESS-0.9	2:8	100	47	7	99.81	198.0	4142	1.01
DMESS-0.8	2:8	100	51	10	99.83	89.8	3976	1.01

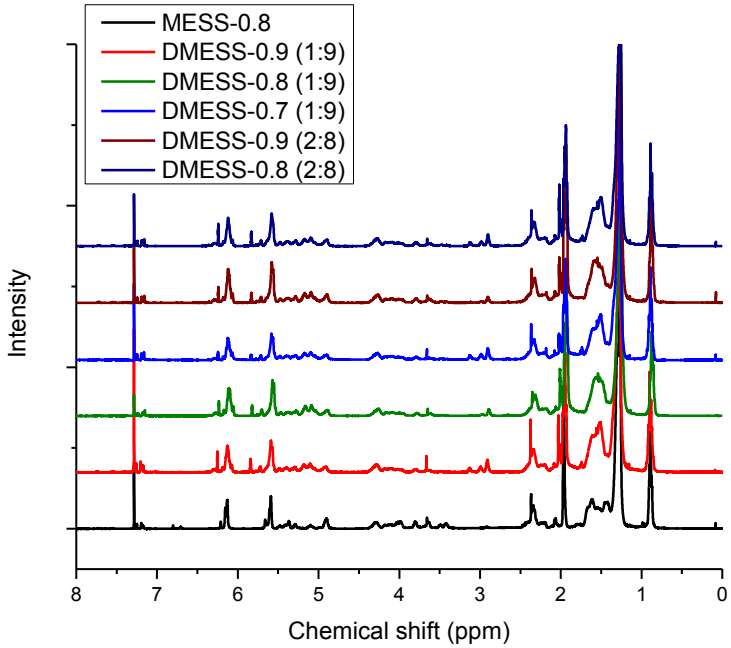

Figure 2.3. ^{1}H-NMR spectra of all the resins.

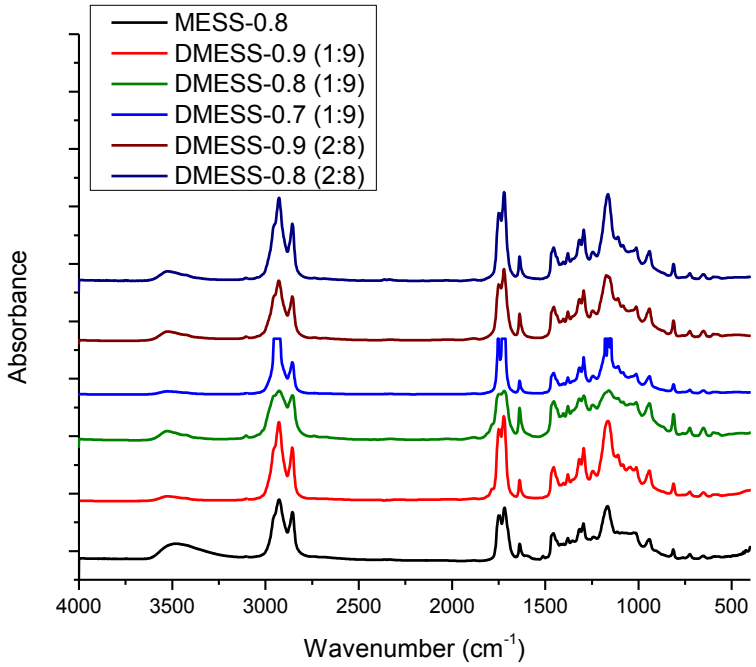

Figure 2.4. FTIR spectra of all the resins.

The viscosities of the resins with styrene as the reactive diluent were studied via rheometry. The viscosities of the resin alone and the resin containing 10, 20, and 30 percent by weight styrene were measured (Table 2.8). The viscosity of the formulations as a function of styrene content is shown in Figure 2.5. The viscosities of the neat resins are over 60 Pa•s, which are generally too viscous to be used for thermoset formulations, however, it can be observed that the dual methacrylated resins have significantly lower viscosities than the MESS resin. As expected, styrene exhibited very strong compatibility with the resins. The general trend shows that the viscosities logarithmically decreased as the amount of styrene was increased. At 30% styrene, the viscosities of the resins are in the range 207-689 mPa•s (Table 2.8). Commercial vinyl ester resins (Ashland) such as Derakane 411-350, a bisphenol-A-based epoxy vinyl ester resin, and Derakane 470-300, a novolac-based epoxy vinyl ester resin, require 45% and 33% styrene to achieve viscosities of 370 mPa•s and 325 mPa•s, respectively. DMESS resins have comparable or much lower viscosities with much lower styrene content than the Derakane resins.

The reduction or elimination of styrene is desired due to several factors. First, the Environmental Protection Agency of the United States of America classifies styrene as a volatile organic compound (VOC) and a hazardous air pollutant (HAP).[53] Styrene also shows limited evidence in humans for carcinogenicity and has been classified as potentially carcinogenic to humans.[54]

Table 2.8. Viscosities of the resins with various amounts of styrene.

Resin		Viscosity (mPa•s)			
	A:B	0% styrene	10% styrene	20% styrene	30% styrene
MESS-0.8		433572	27226	3696	713
DMESS-0.9	1:9	197618	10896	1782	689
DMESS-0.8	1:9	67331	8527	2067	657
DMESS-0.7	1:9	73157	5536	831	207
DMESS-0.9	2:8	197951	11167	1259	293
DMESS-0.8	2:8	89811	5972	963	216

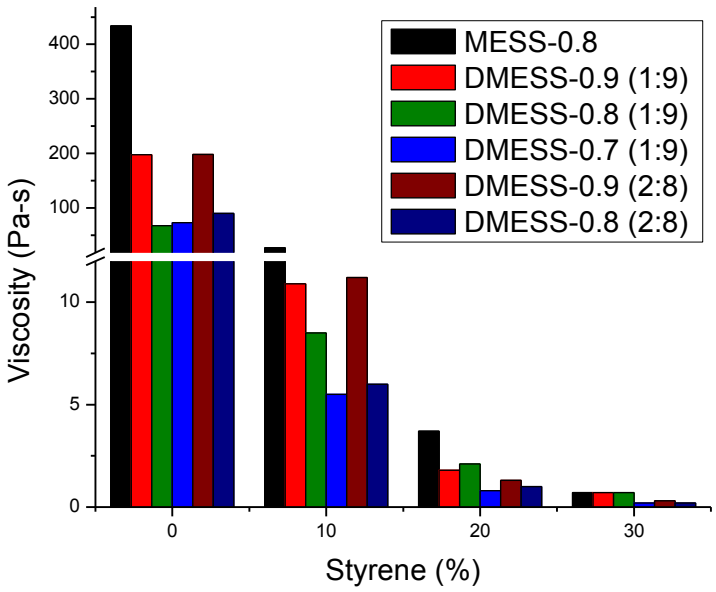

Figure 2.5. Viscosity of resins as a function of styrene content and degree of methacrylation.

2.4.2. Curing of the resins

Free radical initiators were then added to the resin systems to form curable materials. The DSC curve of an unreacted formulation shown in Figure 6 indicates the presence of two

exotherms due to the use of two initiators having different half-lives. The formulations were then cured at two different curing conditions: 1) 120°C for 2 hours and 2) 120°C for 2 hours, then 175°C for 1 hour. The DSC curves (Figure 2.6) showed the disappearance of the first exotherm after curing at 120°C (2 hours), indicating crosslinking, however, an exotherm was still observed at higher temperature indicating that further curing was taking place. The crosslinking reaction required the curing conditions to be 120°C (2 hours), then 175°C (1 hour) in order for both exotherms to disappear, indicating complete crosslinking. The onset temperatures for these curing conditions were around 70°C and 150°C, respectively. Several curing conditions were studied to ensure complete crosslinking (Table 2.9 and 2.10). Subsequently, it was determined that stepwise curing was required to produce the thermosets. Representative ATR-FTIR spectra of samples cured stepwise with 120°C and 150°C as the upper temperatures are shown in Figure 2.7. The spectra show methacrylate carbonyl peaks (~1720 cm^{-1}) and C=C peaks (~1635 cm^{-1}), indicating that 120°C was not sufficient for complete crosslinking. On the other hand, 150°C ensured crosslinking since the spectra showed an increase in the carbonyl peaks for non-conjugated esters (~1750 cm^{-1}), as well as the disappearance of the methracrylate carbonyl and C=C peaks. All other formulations displayed similar spectra (Figure 2.8). Consequently, the thermosets were cured at temperatures of 70°C for 1 hour, 90°C for 1 hour, and 150°C for 2 hours.

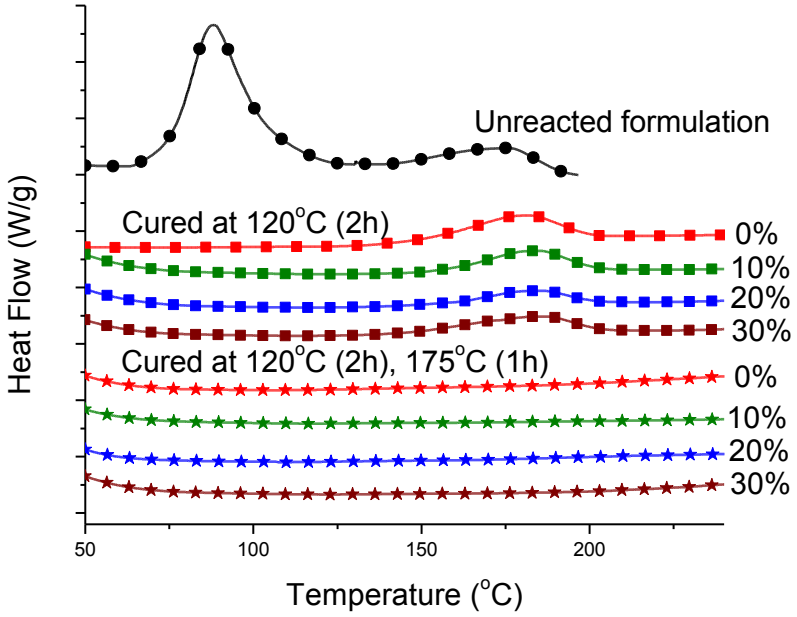

Figure 2.6. DSC curing study of DMESS-0.8 (1:9) resin with various amounts of styrene, Luperox P, and Luperox 10M75, cured at two different conditions.

Table 2.9. Thermal stability of thermosets.

		$T_{5\%}$							
	Resin (A:B)	DMESS-0.8 (1:9)				DMESS-0.9 (1:9)			
	Styrene (%)	0	10	20	30	0	10	20	30
Curing conditions	150°C-1h, 175°C-1h, 200°C-5h	331	327	331	333	316	306	324	321
	150°C-1h, 175°C-1h, 200°C-4h	336	330	337	331	342	318	332	318
	150°C-1h, 175°C-1h, 200°C-3h	335	341	335	334	330	334	332	336
	150°C-1h, 175°C-1h, 200°C-2h	335	318	334	322	333	327	326	327
	150°C-1h, 175°C-1h, 200°C-1h	328	334	318	302	333	320	317	323
	150°C-1h, 175°C-1h	325	330	323	331	337	329	322	324
	120°C-2h	313	312	309	304				
	120°C-1h	329	328	329	319				
	120°C-0.5h	311	311	313	287				
	90°C-1.5h	326	316	313	304				
	90°C-1h	309	307	298	299				
	120°C-1h, 150°C-3h	322	316	306	311				
	90°C-1h, 120°C-1h, 150°C-3h	315	312	325	311				
	70°C-1h, 90°C-1h, 120°C-1h	300	305	303	296				
	70°C-1h, 90°C-1h, 150°C-2h	332	325	312	311				

Table 2.10. % Gel content of thermosets.

	Resin (A:B) Styrene (%)	DMESS-0.8 (1:9) 0	10	20	30
Curing conditions	150°C-1h, 175°C-1h, 200°C-5h	99.36	99.48	99.50	99.87
	150°C-1h, 175°C-1h, 200°C-2h	99.35	99.48	99.66	99.86
	150°C-1h, 175°C-1h	96.48	97.27	97.78	99.83
	120°C-2h	97.20	98.03	97.94	98.61
	120°C-1h	95.44	97.01	97.58	98.36
	120°C-0.5h	95.37	96.03	95.90	97.00
	90°C-1.5h	88.94	93.52	96.95	97.63
	90°C-1h	98.99	99.41	99.91	99.67
	120°C-1h, 150°C-3h	98.79	99.74	99.69	99.59
	90°C-1h, 120°C-1h, 150°C-3h	97.69	97.34	97.94	99.15
	70°C-1h, 90°C-1h, 120°C-1h	98.80	98.68	98.55	98.70
	70°C-1h, 90°C-1h, 150°C-2h	99.36	99.48	99.50	99.87

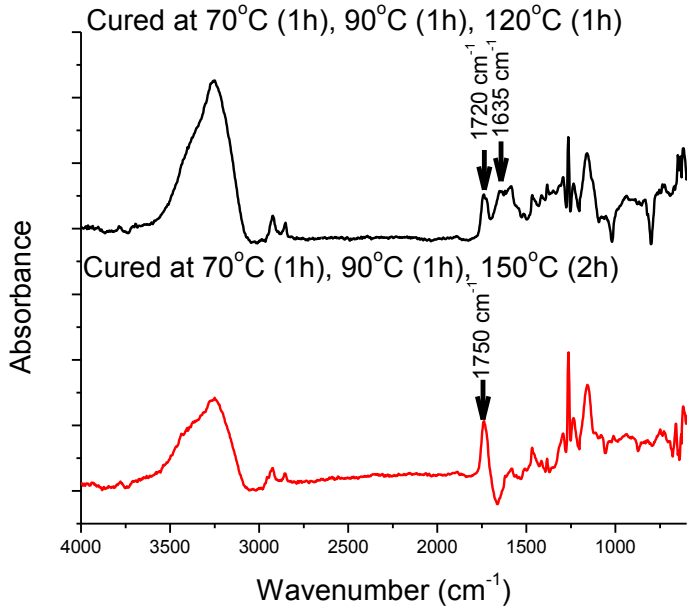

Figure 2.7. ATR-FTIR spectra of DMESS-0.8 (1:9) thermosets with 30% styrene cured at two different conditions.

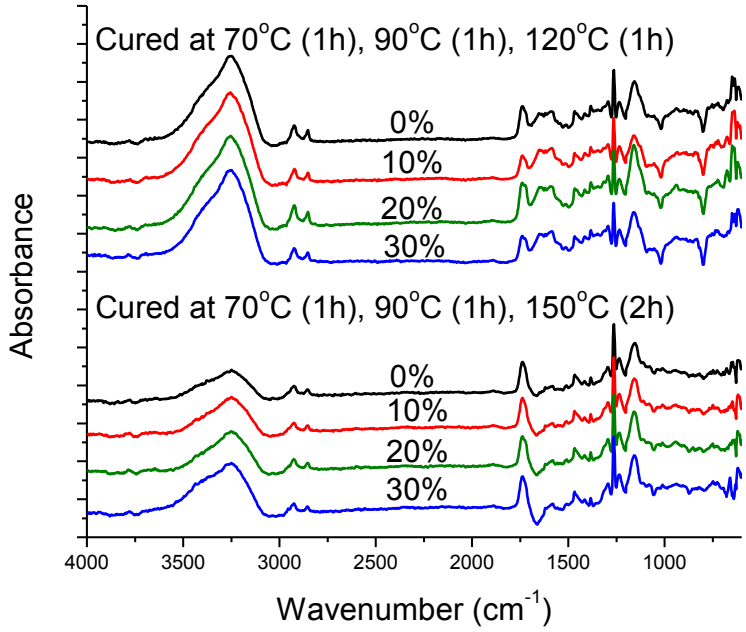

Figure 2.8. ATR-FTIR spectra of DMESS-0.8 (1:9) thermosets with various amounts of styrene cured at two different conditions.

2.4.3. Properties of the cured materials

2.4.3.1. Viscoelastic properties

DMTA was used to determine the glass transition temperatures (T_g) and crosslink densities (ν_e) of the thermosets. Table 2.11 shows a summary of the DMTA results. Figure 2.9 shows the temperature dependence of the storage modulus and tan delta of the thermosets. Broad tan delta curves are observed are due to the broad distribution of functionality in the soybean-oil derived polymers. The presence of a second phase is also indicated in the tan delta curve and may be attributed to the crosslinking of the epoxy groups with hydroxyl groups, which could also suggest heterogeneity in the polymer network structure. The T_g trend (Figure 2.10) shows direct proportionality with the degree of methacrylation, as well as the styrene content. Higher degree of methacrylation and styrene content resulted in higher T_g of the thermosets. In the same manner, the crosslink densities of the thermosets generally followed the same trend. As

the degree of methacrylation is increased, the polymer architecture has higher crosslink density, which leads to higher T_g.

Table 2.11. Glass transition temperatures (T_g), storage moduli (E') at T_g + 60°C, and crosslink densities (v_e) of thermosets of DMESS with different methacrylating agent ratios and different degrees of methacrylation cured at 70°C for 1 h, 90°C for 1 h, and 150°C for 2 h.

			Styrene (%)			
	A:B	% Methacrylation	0	10	20	30
T_g (°C)	1:9	90	88	94	101	113
		80	78	87	92	108
		70	74	85	96	103
	2:8	90	80	94	111	108
		80	81	90	99	114
E' (MPa) at T_g + 60°C	1:9	90	475.4	474.5	206.5	310.6
		80	741.8	619.1	632.1	707.0
		70	188.6	277.8	259.7	221.7
	2:8	90	219.3	400.7	308.9	311.9
		80	284.7	263.8	242.2	198.7
$v_e(10^4$ mol/m$^3)$	1:9	90	4.53	4.46	1.91	2.79
		80	7.24	5.91	5.96	6.72
		70	1.86	2.67	2.43	2.04
	2:8	90	2.16	3.84	2.89	2.87
		80	2.76	2.50	2.25	1.78

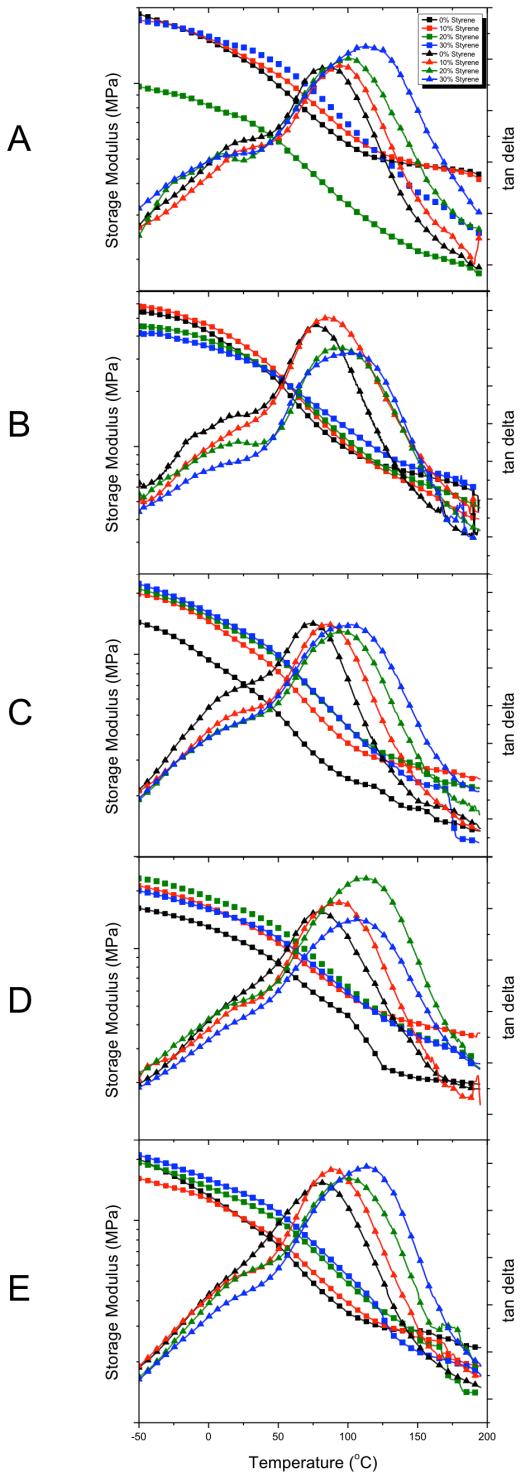

Figure 2.9. DMTA curves of thermosets with 0, 10, 20, and 30 percent by weight styrene content: A) DMESS-0.9 (1:9), B) DMESS-0.8 (1:9), C) DMESS-0.7 (1:9), D) DMESS-0.9 (2:8), and E) DMESS-0.8 (2:8).

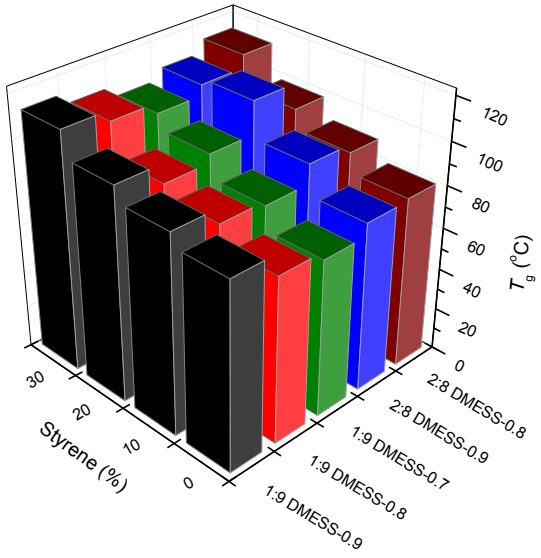

Figure 2.10. Glass transition temperatures as a function of degree of methacrylation and styrene content.

The dependence of crosslink density and T_g as a function of styrene content showed a similar trend to that reported by Yan and Webster.[36] They have discussed a more detailed reasoning behind this phenomenon. The highest T_g observed from this study was 114°C, which was from the resin that had 2:8 methacrylic acid to methacrylic anhydride ratio, 80% methacrylation, and contained 30% styrene. This result could be compared to that of Yan and Webster,[36] MESS-0.8 with 30% styrene, which gave a T_g of 130°C. The difference is attributed to the difference in curing conditions and the higher functionality of the resin. The high degree of methacrylation may cause the methacrylate groups to exhibit steric repulsion. The steric repulsion prevents intramolecular propagation of the DMESS resin and encourages intermolecular propagation of the styryl radicals leading to a lower crosslink density and T_g.

2.4.3.2. Tensile properties

Table 2.12 shows a summary of the tensile properties of the thermosets. Generally, the mechanical properties are related to the functionality and structure of the oligomers, as well as

the amount of styrene. Increasing amounts of styrene increase both the tensile strength and modulus but lower the elongation at break and toughness of the thermosets. The higher degree of functionality of the oligomers demonstrated the same effect as that of increasing styrene content. The modulus values of these thermosets are in the range of 0.6-1.0 GPa. As expected, the higher modulus values were mostly for thermosets with high degree of functionality (1:9 A:B 90% methacrylation, 1:9 A:B 80% methacrylation, and 2:8 A:B 90% methacrylation). The thermosets exhibited better elongation (3.1-6.0%) than those produced with MESS-0.8 (2.5-3.0%).[36] The increase in flexibility is attributed to the replacement of the hydroxyl groups with the methacrylate groups.

Table 2.12. Tensile properties of thermosets of DMESS with different methacrylating agent ratios and different degrees of methacrylation cured at 70°C for 1 h, 90°C for 1 h, and 150°C for 2 h.

			Styrene (%)			
	A:B	% Methacrylation	0	10	20	30
Tensile strength (MPa)	1:9	90	30.3 ± 2.2	26.8 ± 2.9	34.1 ± 2.4	25.5 ± 1.8
		80	23.6 ± 2.0	26.2 ± 4.1	25.5 ± 4.1	25.2 ± 5.0
		70	24.4 ± 4.0	20.9 ± 1.4	23.4 ± 1.2	24.4 ± 2.1
	2:8	90	23.0 ± 3.4	29.6 ± 4.0	32.3 ± 3.7	34.5 ± 3.6
		80	28.2 ± 3.5	25.1 ± 3.3	23.3 ± 3.6	26.5 ± 2.3
Young's modulus (MPa)	1:9	90	1085 ± 79	890 ± 78	1044 ± 70	816 ± 81
		80	868 ± 75	955 ± 32	1031 ± 75	1042 ± 66
		70	772 ± 47	678 ± 55	698 ± 31	658 ± 70
	2:8	90	865 ± 53	932 ± 94	986 ± 81	1040 ± 36
		80	745 ± 57	685 ± 22	786 ± 42	674 ± 33
% Elongation	1:9	90	4.4 ± 0.5	4.0 ± 0.4	4.6 ± 0.7	4.6 ± 1.9
		80	3.5 ± 0.9	3.5 ± 0.9	3.3 ± 0.6	3.1 ± 0.9
		70	5.6 ± 1.4	4.3 ± 0.7	4.6 ± 0.4	6.0 ± 1.4
	2:8	90	4.1 ± 0.8	4.4 ± 0.7	4.4 ± 0.3	4.5 ± 1.0
		80	6.0 ± 0.8	5.7 ± 1.2	3.7 ± 0.9	5.3 ± 0.5
Toughness (10^{-2} J)	1:9	90	6.0 ± 0.97	6.0 ± 0.68	6.9 ± 1.08	4.9 ± 1.34
		80	4.1 ± 1.96	4.6 ± 1.82	2.6 ± 0.71	3.5 ± 0.86
		70	5.5 ± 2.61	5.2 ± 1.42	6.0 ± 1.03	9.3 ± 2.59
	2:8	90	4.3 ± 1.45	4.7 ± 1.10	6.2 ± 0.90	6.0 ± 2.12
		80	8.4 ± 1.77	7.8 ± 2.55	4.6 ± 1.94	8.5 ± 0.89

2.4.3.3. Thermal stability and gel content

Table 2.13 shows a summary of the thermal stability and extent of cure as measured by thermogravimetric analysis and Soxhlet extraction, respectively. The thermal stability was measured by determining the temperatures of 5% weight loss ($T_{5\%}$). The $T_{5\%}$ of the thermosets are in the range of 311-334°C. The homopolymers of the resins displayed thermal stability dependence on degree of functionality. Thermosets with 1:9 A:B ratios had higher $T_{5\%}$ (331°C, 332°C, and 332°C) than 2:8 A:B ratios (326°C and 319°C). In contrast, thermosets containing styrene did not show any strong correlation with the thermal stability. The gel contents of the thermosets were generally very high (98.12-99.24%).

Table 2.13. Thermal degradation properties and gel content of thermosets of DMESS with different methacrylating agent ratios and different degrees of methacrylation cured at 70°C for 1 h, 90°C for 1 h, and 150°C for 2 h.

			Styrene (%)			
	A:B	% Methacrylation	0	10	20	30
$T_{5\%}$ (°C)	1:9	90	331	330	321	328
		80	332	325	312	311
		70	332	330	328	324
	2:8	90	326	334	325	324
		80	319	329	319	326
% Gel content	1:9	90	98.56	98.48	98.61	99.08
		80	98.80	98.68	98.55	98.70
		70	98.12	98.21	98.35	98.47
	2:8	90	98.67	98.85	98.92	99.17
		80	98.31	98.47	98.80	99.24

Figure 2.11 shows a simplified conceptual representation of the crosslink network of the thermosets. Figure 2.11A is a representation of a network, such as MESS, where hydroxyl groups are present. In this type of network, the presence of ether linkages are possible as well as unreacted epoxies. The hydroxyls provide hydrogen bonding that renders the thermosets to have good tensile strength and modulus. Figure 2.11B is representation of a highly methacrylated

network when the hydroxyls are replaced with methacrylate groups. In this case, the network is more tightly crosslinked. The thermosets generated have good tensile strength and modulus and better flexibility than the network formed in Figure 2.11A. If the methacrylation is decreased, the network appears to be highly crosslinked and also containing more hydroxyl groups as depicted in Figure 2.11C.

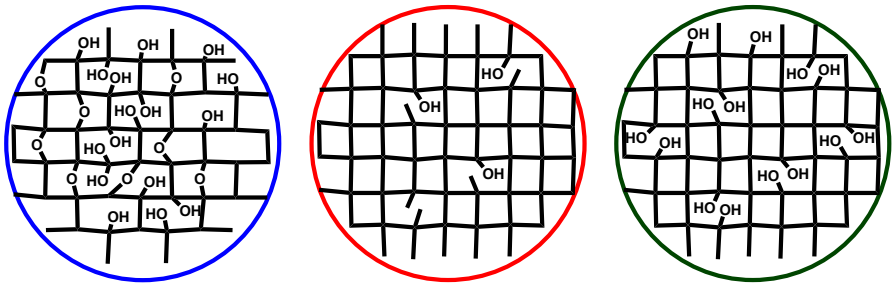

Figure 2.11. Simplified illustration of thermoset network: A) MESS-0.8, B) DMESS (highly methacrylated), and C) DMESS (lower methacrylation).

2.5. Conclusions

A one-pot, solvent-free synthesis of a highly functional methacrylated bio-based resin was developed. The degree of methacrylation was controlled by the amount and ratios of the methacrylating agents (methacrylic acid and methacrylic anhydride) used. Compared with MESS, DMESS has lower resin viscosity, which makes it more processible. DMESS resins required a much lower amount of styrene to achieve a similar formulation viscosity than that of MESS, enabling the reduction of styrene content. The curing schedule was studied and suitable curing time and temperatures were established. The crosslink densities of the resulting thermosets were much higher than the thermosets based from MESS due to the increased amount of methacrylate groups in the resin. As expected, highly methacrylated resins also provided higher T_gs. The trend observed was when styrene content was increased T_gs also increased.

Table 2.14 summarizes the general trends of the thermoset properties as a function of degree of methacrylation, acid-anhydride ratio and styrene content.

Table 2.14. General trends of thermoset properties.

Properties	Degree of methacrylation	Acid:Anhydride	% Styrene
T_g	↑	↑↓	↑
v_e	↑↓	↓	↓
Tensile strength	↑	↑↓	↑↓
Young's modulus	↑	↑↓	↑
% Elongation	↑↓	↑	↓
Toughness	↑↓	↑	↓

2.6. Acknowledgements

This work was supported by the National Science Foundation EPSCoR Award under Grant No. IIA-1355466.

2.7. References

1. Wool, R.; Sun, X. S., *Bio-based polymers and composites*. Academic Press: 2011.

2. Belgacem, M. N.; Gandini, A., *Monomers, polymers and composites from renewable resources*. Elsevier: 2011.

3. Raquez, J. M.; Deléglise, M.; Lacrampe, M. F.; Krawczak, P., Thermosetting (bio) materials derived from renewable resources: a critical review. *Progress in Polymer Science* **2010,** *35* (4), 487-509.

4. Deka, H.; Karak, N., Bio-based hyperbranched polyurethanes for surface coating applications. *Progress in Organic Coatings* **2009,** *66* (3), 192-198.

5. Lu, Y.; Larock, R. C., Novel polymeric materials from vegetable oils and vinyl monomers: preparation, properties, and applications. *ChemSusChem* **2009,** *2* (2), 136-147.

6. Kundu, P. P.; Larock, R. C., Novel conjugated linseed oil-styrene-divinylbenzene copolymers prepared by thermal polymerization. 1. Effect of monomer concentration on the structure and properties. *Biomacromolecules* **2005,** *6* (2), 797-806.

7. Henna, P. H.; Andjelkovic, D. D.; Kundu, P. P.; Larock, R. C., Biobased thermosets from the free-radical copolymerization of conjugated linseed oil. *Journal of Applied Polymer Science* **2007,** *104* (2), 979-985.

8. Valverde, M.; Andjelkovic, D.; Kundu, P. P.; Larock, R. C., Conjugated low-saturation soybean oil thermosets: Free-radical copolymerization with dicyclopentadiene and divinylbenzene. *Journal of Applied Polymer Science* **2008,** *107* (1), 423-430.

9. Andjelkovic, D. D.; Valverde, M.; Henna, P.; Li, F.; Larock, R. C., Novel thermosets prepared by cationic copolymerization of various vegetable oils—synthesis and their structure–property relationships. *Polymer* **2005,** *46* (23), 9674-9685.

10. Andjelkovic, D. D.; Larock, R. C., Novel rubbers from cationic copolymerization of soybean oils and dicyclopentadiene. 1. Synthesis and characterization. *Biomacromolecules* **2006,** *7* (3), 927-936.

11. Lu, Y.; Larock, R. C., Novel biobased nanocomposites from soybean oil and functionalized organoclay. *Biomacromolecules* **2006,** *7* (9), 2692-2700.

12. Li, F.; Larock, R. C., Synthesis, structure and properties of new tung oil-styrene-divinylbenzene copolymers prepared by thermal polymerization. *Biomacromolecules* **2003,** *4* (4), 1018-1025.

13. Khot, S. N.; Lascala, J. J.; Can, E.; Morye, S. S.; Williams, G. I.; Palmese, G. R.; Kusefoglu, S. H.; Wool, R. P., Development and application of triglyceride-based polymers and composites. *Journal of Applied Polymer Science* **2001,** *82* (3), 703-723.

14. Howie, J. K.; Schaefer, J. J.; Trout, J. E., Synthesis of polyol medium fatty acid polyesters. U.S. Patent No. 6,995,232: 7 Feb. 2006.

15. Corrigan, P. J., Synthesis of polyol fatty acid polyesters. U.S. Patent No. 6,620,952: 16 Sep. 2003.

16. Schaefer, J. J.; Trout, J. E., Synthesis of purified, partially esterified polyol polyester fatty acid compositions. U.S. Patent No. 6,887,947: 3 May 2005.

17. Pan, X.; Sengupta, P.; Webster, D. C., Novel biobased epoxy compounds: epoxidized sucrose esters of fatty acids. *Green Chemistry* **2011,** *13* (4), 965-975.

18. Pan, X.; Sengupta, P.; Webster, D. C., High biobased content epoxy–anhydride thermosets from epoxidized sucrose esters of fatty acids. *Biomacromolecules* **2011,** *12* (6), 2416-2428.

19. Pan, X.; Webster, D. C., Impact of structure and functionality of core polyol in highly functional biobased epoxy resins. *Macromolecular Rapid Communications* **2011,** *32* (17), 1324-1330.

20. Paramarta, A.; Webster, D. C., Bio-based high performance epoxy-anhydride thermosets for structural composites: The effect of composition variables. *Reactive and Functional Polymers* **2016,** *105*, 140-149.

21. Auvergne, R.; Caillol, S.; David, G.; Boutevin, B.; Pascault, J.-P., Biobased thermosetting epoxy: present and future. *Chemical Reviews* **2013,** *114* (2), 1082-1115.

22. Pan, X.; Webster, D. C., New biobased high functionality polyols and their use in polyurethane coatings. *ChemSusChem* **2012,** *5* (2), 419-429.

23. Yan, J.; Ariyasivam, S.; Weerasinghe, D.; He, J.; Chisholm, B.; Chen, Z.; Webster, D., Thiourethane thermoset coatings from bio-based thiols. *Polymer International* **2012,** *61* (4), 602-608.

24. Nelson, T. J.; Webster, D. C., Monomer-grafted sucrose ester resins. *Journal of Coatings Technology and Research* **2013,** *10* (4), 515-525.

25. Nelson, T. J.; Bultema, L.; Eidenschink, N.; Webster, D. C., Bio-based high functionality polyols and their use in 1K polyurethane coatings. *Journal of Renewable Materials* **2013,** *1* (2), 141-153.

26. Mosiewicki, M. A.; Aranguren, M. I., A short review on novel biocomposites based on plant oil precursors. *European Polymer Journal* **2013,** *49* (6), 1243-1256.

27. Wu, J. F.; Fernando, S.; Jagodzinski, K.; Weerasinghe, D.; Chen, Z., Effect of hyperbranched acrylates on UV-curable soy-based biorenewable coatings. *Polymer International* **2011,** *60* (4), 571-577.

28. Lu, J.; Khot, S.; Wool, R. P., New sheet molding compound resins from soybean oil. I. Synthesis and characterization. *Polymer* **2005,** *46* (1), 71-80.

29. La Scala, J.; Wool, R. P., Property analysis of triglyceride-based thermosets. *Polymer* **2005,** *46* (1), 61-69.

30. Can, E.; Küsefoğlu, S.; Wool, R. P., Rigid, thermosetting liquid molding resins from renewable resources. I. Synthesis and polymerization of soy oil monoglyceride maleates. *Journal of Applied Polymer Science* **2001,** *81* (1), 69-77.

31. Pfister, D. P.; Xia, Y.; Larock, R. C., Recent advances in vegetable oil-based polyurethanes. *ChemSusChem* **2011,** *4* (6), 703-717.

32. Desroches, M.; Escouvois, M.; Auvergne, R.; Caillol, S.; Boutevin, B., From vegetable oils to polyurethanes: synthetic routes to polyols and main industrial products. *Polymer Reviews* **2012,** *52* (1), 38-79.

33. Lu, Y.; Larock, R. C., New hybrid latexes from a soybean oil-based waterborne polyurethane and acrylics via emulsion polymerization. *Biomacromolecules* **2007,** *8* (10), 3108-3114.

34. Lu, Y.; Larock, R. C., Aqueous cationic polyurethane dispersions from vegetable oils. *ChemSusChem* **2010,** *3* (3), 329-333.

35. Petrović, Z. S., Polyurethanes from vegetable oils. *Polymer Reviews* **2008,** *48* (1), 109-155.

36. Yan, J.; Webster, D. C., Thermosets from highly functional methacrylated epoxidized sucrose soyate. *Green Materials* **2014,** *2* (3), 132-143.

37. Williams, G. I.; Wool, R. P., Composites from natural fibers and soy oil resins. *Applied Composite Materials* **2000,** *7* (5-6), 421-432.

38. Hosseini, N.; Ulven, C. A.; Azarmi, F.; Webster, D. C.; Nelson, T. J. In *Utilization of Flax Fibers and Glass Fibers in a Bio-Based Resin*, ASME 2014 International Mechanical Engineering Congress and Exposition, 2014; American Society of Mechanical Engineers: 2014; pp V014T11A041-V014T11A041.

39. Foulk, J. A.; Fuqua, M. A.; Ulven, C. A.; Alcock, M. M., Flax fibre quality and influence on interfacial properties of composites. *International Journal of Sustainable Engineering* **2010,** *3* (1), 17-24.

40. O'Donnell, A.; Dweib, M. A.; Wool, R. P., Natural fiber composites with plant oil-based resin. *Composites Science and Technology* **2004,** *64* (9), 1135-1145.

41. Lu, Y.; Larock, R. C., Fabrication, Morphology and Properties of Soybean Oil-Based Composites Reinforced with Continuous Glass Fibers. *Macromolecular Materials and Engineering* **2007,** *292* (10-11), 1085-1094.

42. Quirino, R. L.; Woodford, J.; Larock, R. C., Soybean and linseed oil-based composites reinforced with wood flour and wood fibers. *Journal of Applied Polymer Science* **2012,** *124* (2), 1520-1528.

43. Amiri, A.; Yu, A.; Webster, D.; Ulven, C., Bio-Based Resin Reinforced with Flax Fiber as Thermorheologically Complex Materials. *Polymers* **2016,** *8* (4), 153.

44. Taylor, C.; Amiri, A.; Paramarta, A.; Ulven, C.; Webster, D., Development and weatherability of bio-based composites of structural quality using flax fiber and epoxidized sucrose soyate. *Materials & Design* **2017,** *113*, 17-26.

45. Amiri, A.; Hosseini, N.; Ulven, C.; Webster, D. In *Advanced bio-composites made from methacrylated epoxidized sucrose soyate resin reinforced with flax fibers*, Proceedings of the 20th International Conference on Composite Materials, Copenhagen, Denmark, 2015; pp 19-24.

46. Hosseini, N.; Webster, D. C.; Ulven, C., Advanced biocomposite from highly functional methacrylated epoxidized sucrose soyate (MAESS) resin derived from vegetable oil and fiberglass fabric for composite applications. *European Polymer Journal* **2016,** *79*, 63-71.

47. La Scala, J.; Wool, R. P., Rheology of chemically modified triglycerides. *Journal of Applied Polymer Science* **2005,** *95* (3), 774-783.

48. Monono, E. M.; Bahr, J. A.; Pryor, S. W.; Webster, D. C.; Wiesenborn, D. P., Optimizing process parameters of epoxidized sucrose soyate synthesis for industrial scale production. *Organic Process Research & Development* **2015,** *19* (11), 1683-1692.

49. Monono, E. M.; Webster, D. C.; Wiesenborn, D. P., Pilot scale (10kg) production and characterization of epoxidized sucrose soyate. *Industrial Crops and Products* **2015,** *74*, 987-997.

50. Adekunle, K.; Åkesson, D.; Skrifvars, M., Synthesis of reactive soybean oils for use as a biobased thermoset resins in structural natural fiber composites. *Journal of Applied Polymer Science* **2010,** *115* (6), 3137-3145.

51. Adekunle, K.; Åkesson, D.; Skrifvars, M., Synthetic modification of reactive soybean oils for use as biobased thermoset resins in structural natural fiber composites. *Polymer Preprints* **2008,** *49* (1), 279.

52. Adekunle, K.; Åkesson, D.; Skrifvars, M., Biobased composites prepared by compression molding with a novel thermoset resin from soybean oil and a natural-fiber reinforcement. *Journal of Applied Polymer Science* **2010,** *116* (3), 1759-1765.

53. Environmental Protection Agency. Federal Register. 2003; Vol. 68, pp 19375-19443.

54. Humans, I. W. G. o. t. E. o. C. R. t.; World Health, O.; International Agency for Research on, C., *Some traditional herbal medicines, some mycotoxins, naphthalene and styrene*. World Health Organization: 2002.

CHAPTER 3. TUNABILITY OF DIMETHACRYLATED EPOXIDIZED SUCROSE SOYATE (DMESS): STRUCTURE-PROPERTY RELATIONSHIPS OF MODIFIED HIGHLY FUNCTIONAL BIO-BASED THERMOSETS

3.1. Abstract

The high functionality of epoxidized sucrose soyate (ESS) was exploited and its highly methacrylated derivatives were studied. ESS has been previously functionalized by methacrylation to synthesize a bio-based resin, methacrylated epoxidized sucrose soyate (MESS), for composite applications. These thermosets have shown high glass transition temperature (T_g) and good mechanical properties, but the resin viscosity was high due to hydrogen bonding. This was circumvented by further functionalization of the MESS to dimethacrylated epoxidized sucrose soyate (DMESS). The structure-property relationships of the thermosets produced were studied. Nevertheless, the thermosets produced from DMESS remained brittle. To maintain low resin viscosity and improve thermoset ductility, replacement of some methacrylate groups with various ester groups was hypothesized. The synthesis of these modified DMESS remained as a one-pot process involving the sequential slow addition of anhydrides mixed prior to addition. Formulations were made using varying amounts of styrene and free-radically cured using commercially available peroxyesters as initiators. The bio-based resins with 30% styrene gave much lower viscosities compared with commercial resins containing higher amount of styrene (33% and 45%). The thermosets produced had improved flexibility and toughness with only a slight drop in the glass transition temperature. The inclusion of the non-functional esters in the resin structure acted as internal plasticizers for the polymer system. The new sets of thermomechanical properties demonstrated tunability of the developed resin and opens up different avenues for end-use applications.

3.2. Introduction

Fluctuating costs and environmental concerns of petrochemicals have remained as the main motivator of sustainability in polymer science. Vegetable oils have been sought as chemical commodity to replace petrochemical sources due to their competitive cost, ready availability, built-in functionality, and numerous applications.[1-6] These oils are esters formed by glycerol and various fatty acids containing 8-24 carbon atoms and ranging from saturated to unsaturated types, depending on the plant type and source.[7, 8] Polymerization of unmodified vegetable oils is typically done via autoxidation through the fatty acid double bonds.[9] However, these crosslinking processes require prolonged periods of time to fully cure. Due to this, modification of vegetable oils has been extensively explored. One of the more common modifications utilized has been the epoxidation of these oils. This epoxidation has become one of the routes used in creating materials possessing tunable properties.

SEFOSE 1618U (sucrose soyate) is a sucrose ester of fatty acid from soybean oil, which was commercialized by Procter and Gamble (P&G) Chemicals as a reactive diluent for alkyds.[10-12] It has a rigid sucrose core and flexible fatty acid side chains. Webster *et al.* epoxidized the sucrose soyate and optimized the process suitable for large-scale production.[13-15] Epoxidized sucrose soyate (ESS) contains on average 11-12 epoxy groups per molecule and has shown promise in a wide range of crosslinking technologies.[16] This molecule has shown versatility in bio-based coatings applications such as polyurethanes[17], UV-curable[18], melamine-formaldehyde[19], acid-blocked[20], degradable[21, 22], and high performance coatings.[23, 24] Recently, ESS displayed exceptionally well in terms of its adhesive property in fiberboards when used with a suitable crosslinker and catalyst.[25] Fiber reinforced polymer (FRP) composites have been developed using bio-based thermosets as the polymer matrix.[26-33] ESS has also shown promise in

this application. High performance epoxy-anhydride thermosets for structural composites using ESS have shown high glass transition temperatures and Young's modulus.[23] Yan and Webster also studied novel bio-based methacrylated oligomers from ESS.[34] The thermosets produced from this resin gave improved thermomechanical properties that afforded them as FRP composite resin matrix.

Plasticizers are typically used as additives in polymer industries. These are relatively low molecular weight non-volatile compounds that soften materials.[35] Plasticizers alter the physical properties of a polymer by increasing the free volume of the overall polymer network. Consequently, the glass transition temperature is lowered while the flexibility, elongation, and toughness is increased. They also lower resin viscosity by increasing the mobility of the polymer chains making the material more processible.[36] Generally, plasticizers are classified as either external or internal. External plasticizers are not physically bound and may exude from the polymer while internal plasticizers are chemically bound within the polymer chain. The effects of external bio-based plasticizers such as epoxidized soybean oil (ESO) on thermomechanical properties of polymers have been studied.[37-39] Similarly, the effects of bound dangling chains on the thermomechanical properties of polymer have also been proven to function as immobile internal plasticizers.[40, 41] A recent review by Vieira *et al.*[42] discussed the current developments on natural-based plasticizers in the last decade.

In conjunction with flax and glass fibers, MESS has been investigated and shown interesting set of properties that displayed complex behavior.[43-45] When used with glass fibers, MESS had better adhesion to the fibers than the conventional vinyl ester resins.[46] Despite the improved thermomechanical properties of the MESS, its resin viscosity was high due to the hydrogen bonding of the secondary hydroxyl group generated from the epoxide ring-opening

reaction. The resin viscosity was successfully reduced when these hydroxyl groups were further substituted with methacrylates (Scheme 3.1). However, the thermosets from these resins resulted in highly crosslinked networks which made them very brittle. In principle, replacing some of the methacrylate groups with aliphatic esters would decrease the crosslink density and improve the ductility of these thermosets.

Therefore, the objective of this study was to investigate the effect of introducing immobile internal plasticizers on the thermal and mechanical properties of these highly functionalized bio-based resins. Moreover, the effect of the degree of functionality and length of the ester chains on the structure-property relationships were investigated. Bio-based resins containing some non-functional esters were synthesized and formulated into thermosets, and compared with dimethacrylated epoxidized sucrose soyate (DMESS). The DMESS control used in this study was functionalized 80% and had 1:9 methacrylic acid:methacrylic anhydride. The thermosets were thermally initiated and free-radically polymerized with styrene as a reactive diluent. The sets of thermomechanical properties were investigated and the structure-property relationships were elucidated.

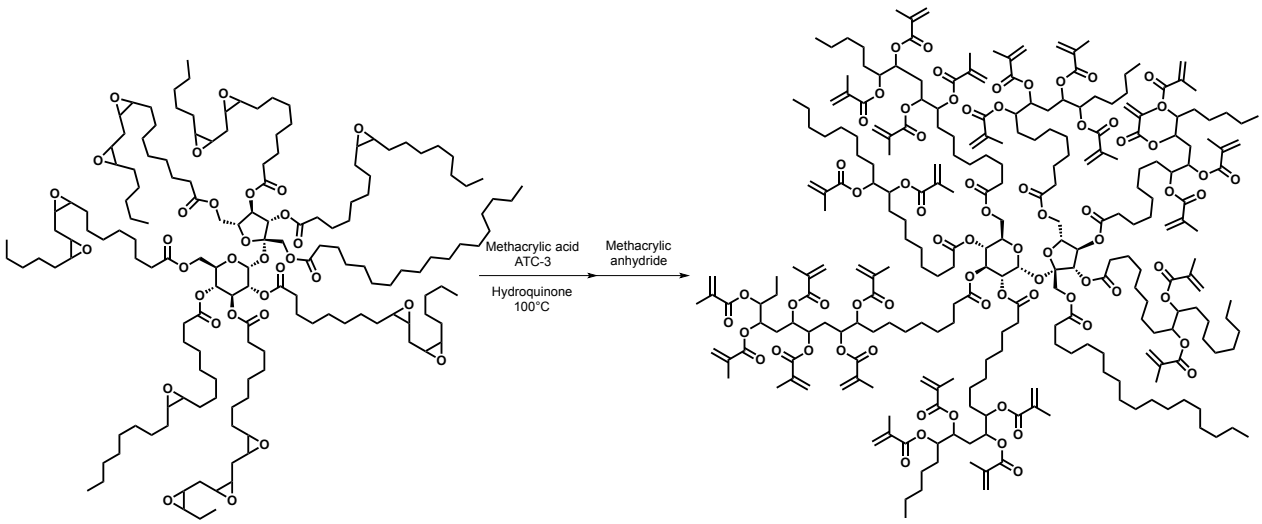

Scheme 3.1. Synthetic route to dimethacrylated epoxidized sucrose soyate (DMESS).[47]

3.3. Experimental

3.3.1. Raw materials

Sucrose soyate (SEFOSE 1618U) was provided by Procter & Gamble Chemicals (Cincinnati, OH, USA), which was the precursor of the starting material. The synthesis of epoxidized sucrose soyate (ESS) from sucrose soyate followed the procedure found in literature.[13-15] The epoxy equivalent weight (EEW) of ESS was determined by titration according to ASTM D 1652 and was calculated to be 244 g/eq. Methacrylic acid and methacrylic anhydride were purchased from Alfa Aesar (Ward Hill, Massachusetts, USA). ATC-3 was used as a catalyst and purchased from AMPAC Fine Chemicals (Rancho Cordova, CA, USA). ATC-3 is a solution of trivalent organic chromium complexes in phthalate esters. Acetic anhydride, propionic anhydride, butyric anhydride, hydroquinone, and styrene were purchased from Sigma Aldrich (St. Louis, MO, USA). All the reagents were used as received.

3.3.2. Synthesis of the DMESS resins containing non-functional esters

The synthesis of the resins involved a modification of a previously established protocol.[47] This was accomplished through successive ring-opening and substitution reactions using methacrylic acid and anhydrides, respectively. The reaction was heated to 100°C, using 1.0% (of total weight) catalyst, ATC-3 and 0.1% (of total weight) inhibitor, hydroquinone. The degree of functionalization was maintained at 80% for all the resins. The molar ratio of methacrylic acid to the anhydrides was also kept constant at 1:9. The amount of the second anhydride relative to the methacrylic anhydride was varied from 10% to 30% in each case. A typical procedure is as follows: ESS (100.00 g), methacrylic acid (2.82 g), hydroquinone (0.14 g) and ATC-3 (1.44 g) were placed into a four-necked reaction kettle equipped with a mechanical stirrer and a thermocouple. The mixture was heated to 100°C until the most of the acid has reacted.

Methacrylic anhydride (40.94 g) and acetic anhydride (3.01 g) were mixed together and added dropwise (~0.25 mL/minute). The reaction mixture was heated at 100°C until the acid number was less than 15. The resulting resin appeared as a dark green, viscous liquid. A summary of the amounts used for the synthesis or each resin is shown in Table 3.1.

Table 3.1. Amounts of the reagents used for the synthesis of the MASS, MPSS, and MBSS.

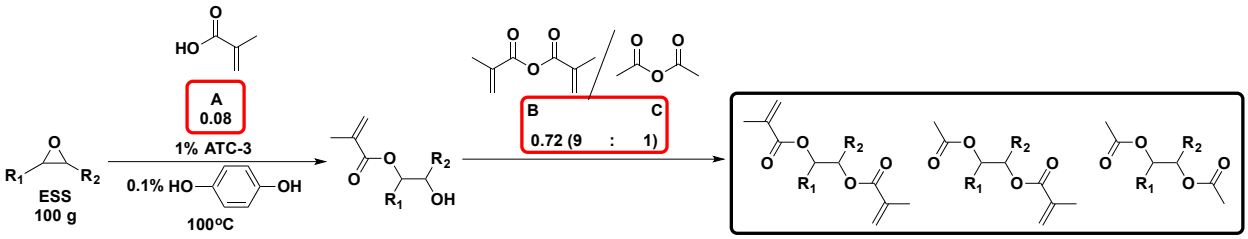

Resin	Second anhydride	B:C	Methacrylic anhydride (g) [B]	Second anhydride (g) [C]
MASS-0.1	Acetic anhydride	9:1	40.94	3.01
MASS-0.3	Acetic anhydride	7:3	31.84	9.04
MPSS-0.1	Propionic anhydride	9:1	40.94	3.84
MPSS-0.3	Propionic anhydride	7:3	31.84	11.52
MBSS-0.1	Butyric anhydride	9:1	40.94	4.67
MBSS-0.3	Butyric anhydride	7:3	31.84	14.00

3.3.3. Characterization of oligomers

Proton nuclear magnetic resonance spectroscopy (^{1}H-NMR) was used to aid in structure elucidation and conducted with a Bruker system, Ascend 400 MHz magnet with an Avance III HD console (Bruker BioSpin Corporation, Billerica, Massachusetts, USA), using deuterated chloroform ($CDCl_3$ as the solvent. Fourier transform infrared spectroscopy (FTIR) was used to confirm functional groups and was performed with a Thermo Scientific Nicolet 8700 with a detector type of DTGS KBr under nitrogen purge. Diluted thin films of the samples were applied on a KBr plate and the absorption spectra were taken with 32 scans at a resolution of 4 cm^{-1} in the range of 4000-400 cm^{-1}. Molecular weight of the resin was obtained using a GPC

system (EcoSEC HLC-8320GPC, Tosoh Bioscience, Japan) with a differential refractometer (DRI) detector. Separations were performed using two TSKgel SuperH3000 6.00 mm ID×15 cm columns. The temperature of the columns and detectors were set at 40°C. Tetrahydrofuran (THF) was used as the eluent with a flow rate of 0.35 mL min^{-1}. Samples were prepared at nominally 1 mg mL^{-1} in an aliquot of the eluent and allowed to dissolve at ambient temperature for several hours and the injection volume was 20 μL for each sample. Calibration was conducted using polystyrene standards (Agilent EasiVial PS-H 4 mL). Acid number titration was carried out according to ASTM D664. The viscosity of the resins was measured at 25°C using an ARES Rheometer (TA Instruments) operating from 0.1 rad/s to 500 rad/s with 0.1% strain. Weight percent solids of the resins were determined according to ASTM D 2369.

3.3.4. Curing of the resins

Formulations of the resins alone and with 10, 20, and 30 percent by weight styrene as the reactive diluent were prepared. Commercially available peroxyesters Luperox P, *tert*-butyl peroxybenzoate, (2% of total resin weight) and Luperox 10M75, *tert*-butyl peroxyneodecanoate, (2% of total resin weight) were utilized as free-radical initiators. All the ingredients were mixed thoroughly using a Flacktek Speedmixer before curing. The formulations were placed in a silicone mold and then cured. A typical procedure is as follows: Resin (4.50 g), styrene (0.50 g), Luperox P (0.10 g), and Luperox 10M75 (0.10 g) were placed in a 15-mL plastic vial. The contents were mixed for 5 minutes at 3500 rpm using the high-speed mixer. The mixture was then poured into the silicone mold, and cured in an oven at 70°C for 1 hour, 90°C for 1 hour, and 150°C for 2 hours. The mold was allowed to cool to room temperature before the cured thermosets were removed.

3.3.5. Characterization of thermosets

The extent of cure was evaluated using a Vertex 70 Fourier transform infrared spectrometer (Bruker Optics) with an attenuated total reflectance (ATR) accessory. The beam was irradiated an angle of 45° and the crystal was made of Germanium. A Q500 thermogravimetric analysis (TGA) system (TA Instruments) with a heating rate of 20°C/min from room temperature to 600°C under a continuous nitrogen flow, was used to determine the thermal stability of the thermosets. Instron 5542 system (Instron Corp., Norwood, MA, USA) with a strain rate of 0.2%/s was used to measure the tensile properties and ASTM D638 was followed to prepare dumbbell type V specimens. Specimen thicknesses were around 1.0 mm. At least 5 samples were measured for each thermoset and the averages and standard deviation were reported. A Q800DMA (TA Instruments) operating at 1 Hz and a heating rate of 5°C/min from -50°C to 200°C (dual cantilever mode) was used to determine the glass transition temperature (T_g). The tan δ peak was identified as the T_g. The storage modulus (E') in the rubbery plateau region was determined at 60°C above the T_g and used to calculate the crosslink density (v_e). Equation 3.1 from the rubber elasticity theory was used to calculate the crosslinking density using the storage modulus:

$$E' = 3v_eRT \qquad \text{(Equation 3.1)}$$

where E' is the thermoset storage modulus in the rubbery plateau region, R is the gas constant, and T is the absolute temperature. The gel content of the thermosets was determined in order to determine the extent of polymerization. This was done via solvent extraction using dichloromethane. A 500-mL flask containing 300 mL dichloromethane and boiling stones was equipped with a Soxhlet extractor, connected to a condenser. 1 g of the samples were weighed and placed inside the thimble, and extracted for 24 h by dichloromethane. The samples were

then dried in vacuum at 40°C for 3 hours and weighed. The gel content of the thermoset is calculated using Equation 3.2:

$$\%\ Gel\ Content = \frac{W_f}{W_i} X\ 100 \qquad \text{(Equation 3.2)}$$

where W_i is the weight of the thermoset sample prior to Soxhlet extraction, and W_f is the weight of the thermoset sample after the extraction.

3.4. Results and discussion

3.4.1. Synthesis and characterization of resins

A series of resins with varying ratios of anhydrides were synthesized following the route shown in Scheme 3.2: methacrylate-acetate epoxidized sucrose soyate (MASS), methacrylate-propionate epoxidized sucrose soyate (MPSS), and methacrylate-butyrate epoxidized sucrose soyate (MBSS).

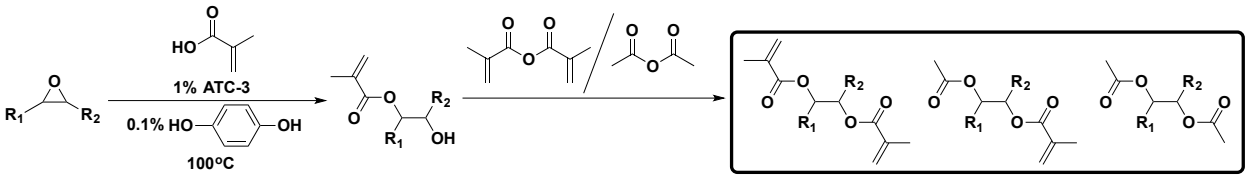

Scheme 3.2. Synthesis of MASS.

The presence of a mixture of anhydrides reacting with the hydroxyls complicates the reaction mechanism (Scheme 3.3). The reaction initially undergoes epoxide activation by the methacrylic acid. Once the methacrylated intermediate (Intermediate A, Scheme 3.3) is formed, either anhydride may react with the hydroxyl group. The reaction products will be a mixture of dimethacrylate and methacrylate-acetate compounds. In the case of acetic anhydride as the non-functional ester source, after the anhydrides react with the hydroxyl groups, acetic acid and methacrylic acid will be generated in the reaction. These acids will generate both intermediates A and B. These intermediates will then generate mixtures of dimethacrylate, methacrylate-

acetate, and diacetate products. When propionic anhydride and butyric anhydride were used, their corresponding intermediates and products were produced.

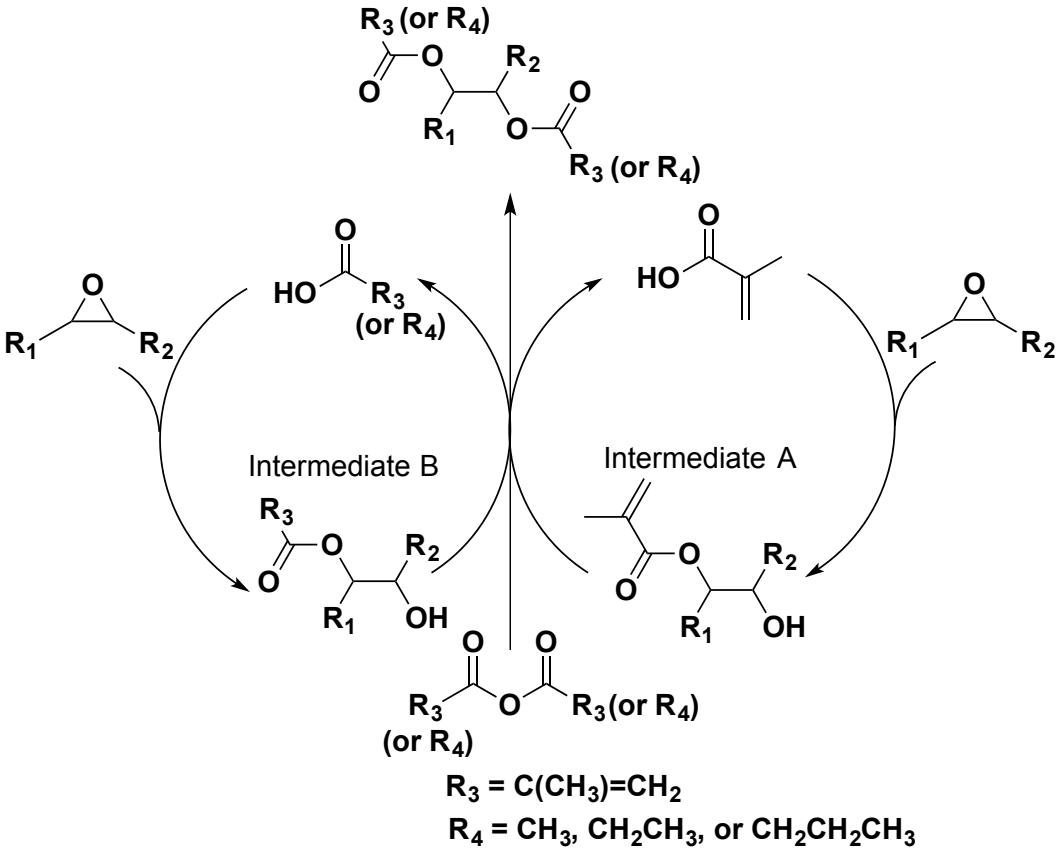

Scheme 3.3. Proposed mechanism of the MASS (or MPSS, MBSS) synthesis.

The proton NMR spectra (Figure 3.1) of the resins were very similar to each other. The main difference can be observed at the chemical shift around 5.2 ppm. This peak corresponds to the proton of the –CH- of the second methacrylate group of DMESS. The spectra show a decrease of this peak as the amount of the non-functional esters was increased, replacing some of the second methacrylate.

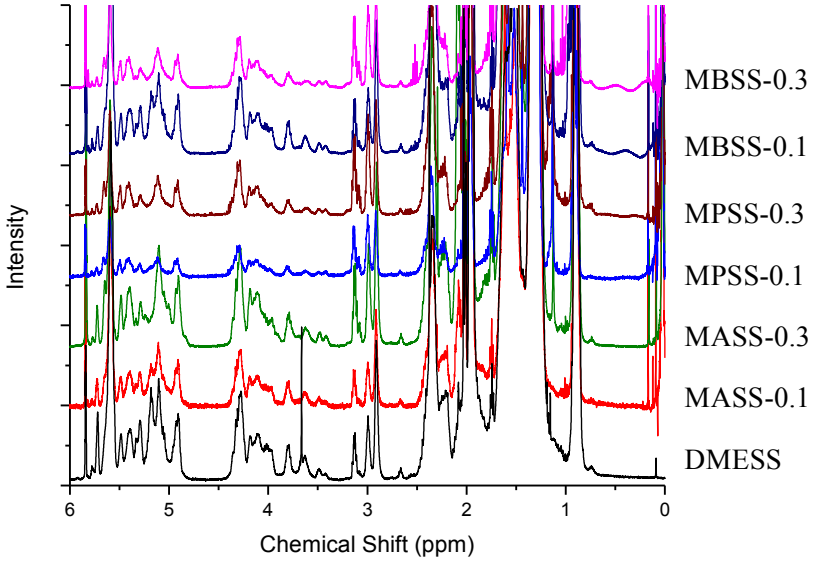

Figure 3.1. ^{1}H-NMR spectra of all the resins.

The FTIR spectra (Figure 3.2) of the resins showed all the functional groups present. The carbonyl region (Figure 3.2, right) showed that the non-conjugated carbonyl peak (~1750 cm^{-1}) increased and the methacrylate carbonyl peak (~1720 cm^{-1}) decreased as more non-functional esters replaced the methacrylate groups.

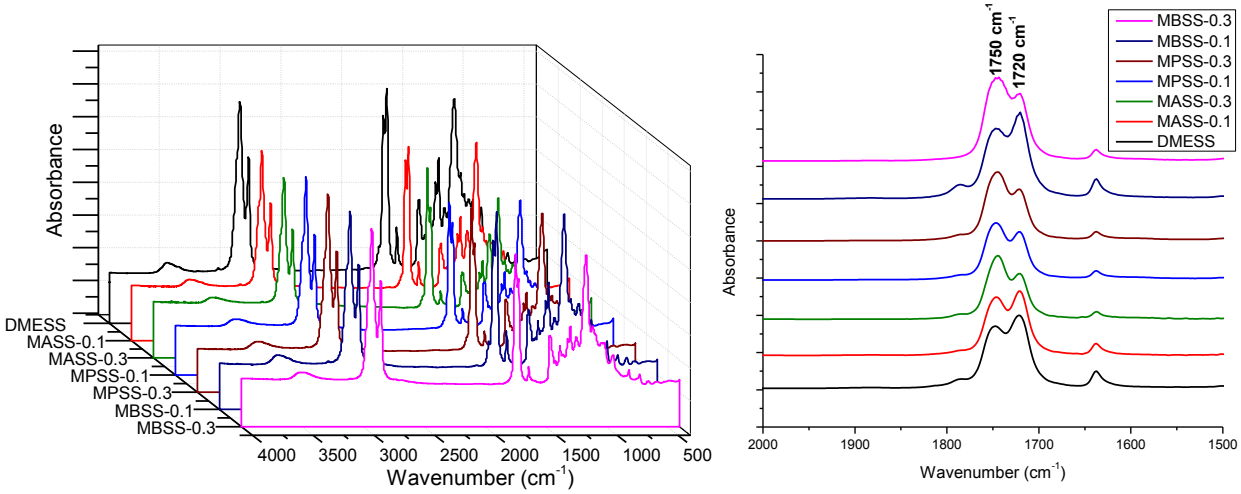

Figure 3.2. FTIR spectra of all the resins (left: full spectrum, right: carbonyl peaks).

Table 3.2 shows the summary of the properties of all the resins. The syntheses of the resins showed that the aliphatic anhydrides required shorter reaction times than methacrylic

anhydride. This could suggest that the reactions involving the aliphatic anhydrides are more reactive or kinetically favored than methacrylic anhydride. In all cases, the acid numbers were less than 15 and the solids were all in the range 94-99%. Figure 3.3 (left) shows the decreasing resin viscosity trend as the amount of styrene was increased. The trend also showed that viscosities decreased when the amount of non-functional esters was increased and when their chain length was increased. The presence of the non-functional esters reduces the resin viscosity by functioning as internal plasticizers. This effect became more apparent as their length increases. Generally, the viscosity decreases as more of the non-functional esters are added. In the case of MPSS-0.1, this was not observed. This is due to the lower conversion as reflected on the final acid number of 13 and lower solid content of 94.48% than the other resins. The number-average molecular weights (M_n) of the resins were generally lower than that of DMESS. Figure 3.3 (right) shows the GPC traces of the resins. The higher molecular weight shoulder could be due to the side reaction of the epoxy and hydroxyl group.

Table 3.2. Properties of the resins.

Resin	Time (Hours)	Acid Number	% Solids	Viscosity with styrene (mPa•s)				M_n	$Đ$
				0%	10%	20%	30%		
DMESS	47.5	7	99.90	67330	8530	2070	660	3900	1.012
MASS-0.1	25	4	99.09	46530	8270	1050	260	3750	1.011
MASS-0.3	24	8	98.08	24080	5290	950	220	3630	1.012
MPSS-0.1	24	13	94.48	12820	1520	360	120	3460	1.018
MPSS-0.3	18	8	97.81	14810	2420	470	150	3500	1.013
MBSS-0.1	39	13	96.22	25920	2850	560	160	3460	1.044
MBSS-0.3	17	11	97.28	7750	2120	440	130	3520	1.018

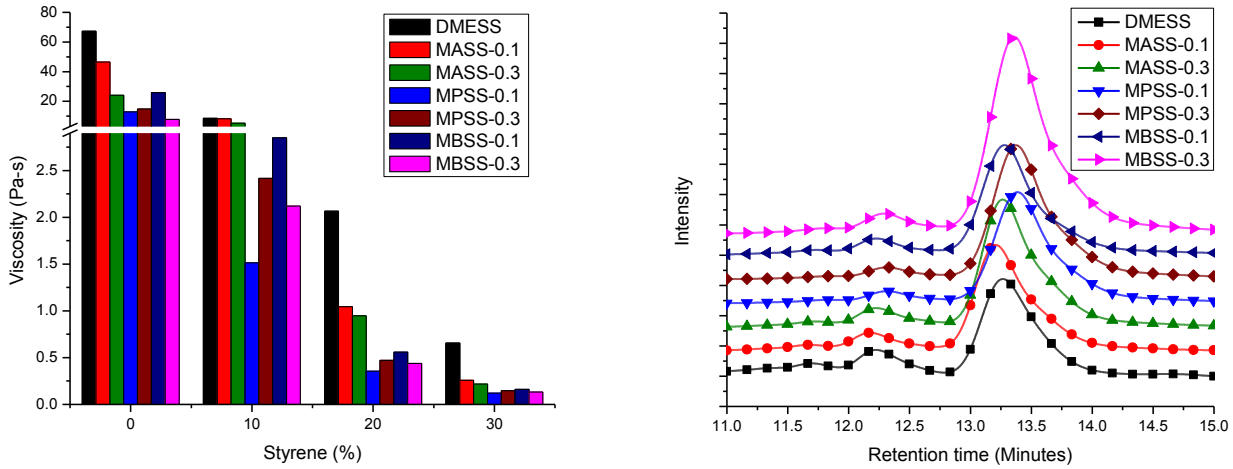

Figure 3.3. Viscosity of resins as a function of styrene content, degree of esterification, and ester chain length (left) and GPC traces (right).

3.4.2. Curing of the resins

The thermosets were polymerized via stepwise curing conditions of 70°C for 1 hour, 90°C for 1 hour, and 150°C for 2 hours. The extent of cure was determined by ATR-FTIR. The spectra (Figure 3.4) showed that thermosets from MPSS and MBSS cured much more efficiently than MASS. The presence of unreacted C=C peaks (~1635 cm^{-1}) were more pronounced for MASS in both cases (MASS-0.1 and MASS-0.3) than those of MPSS and MBSS. MASS contains shorter acetate groups and thus, lower free volume resulting in less mobility and crosslink efficiency.

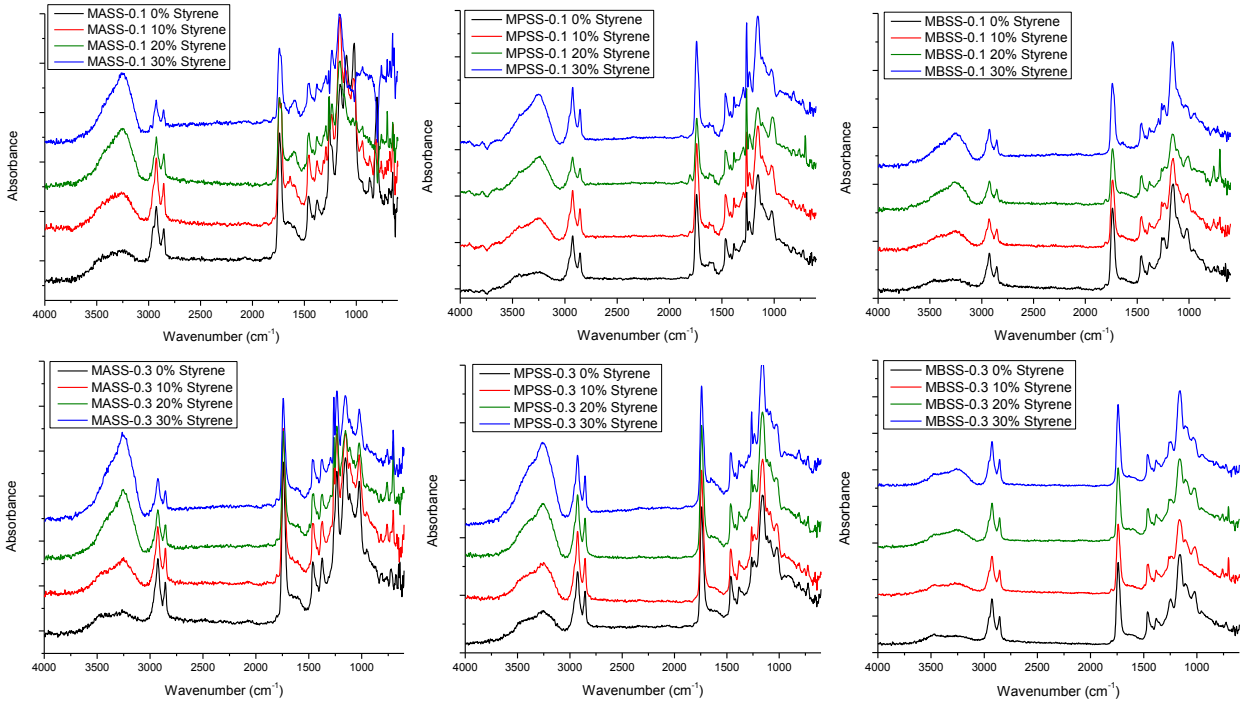

Figure 3.4. ATR-FTIR spectra of thermosets with 0, 10, 20, and 30 percent by weight styrene content : MASS-0.1 (top left), MASS-0.3 (bottom left), MPSS-0.1 (top center), MPSS-0.3 (bottom center), MBSS-0.1 (top right), and MBSS-0.3 (bottom right).

3.4.3. Properties of thermosets

3.4.3.1. Viscoelastic properties

The glass transition temperature (T_g) and crosslink density (ν_e) were characterized via dynamic mechanical thermal analysis (DMTA), and the results are summarized in Table 3.3. The T_g trend (Figure 3.5, top) shows direct proportionality to the styrene content and inverse proportionality to the degree of esterification and ester chain length. T_g increases as styrene content increases and decreases as more non-functional esters replaced the methacrylates. The ν_e showed inverse proportionality to the amount of styrene, as well as the degree of esterification and ester chain length (Figure 3.5, bottom). The non-functional esters do not participate in the crosslinking, therefore exists as dangling chains, which increase the distance between junctions and results in lower crosslink densities. The temperature dependence of storage modulus and tan

delta for the thermosets with varying styrene content is illustrated in Figure 3.6. The broad tan delta curves are due to the broad distribution of the functionality of the soybean oil-derived fatty acid chains. The presence of a second phase may be attributed to the ether linkages that resulted from the epoxy-hydroxyl side reactions, which suggests a heterogeneous polymer architecture.

Table 3.3. Glass transition temperatures (T_g), storage moduli (E') at T_g + 60°C, and crosslink densities (ν_e) of thermosets of DMESS, MASS, MPSS, and MBSS with different degrees of esterification.

		Styrene (%)			
	Resin	0	10	20	30
T_g (°C)	DMESS	78	87	92	108
	MASS-0.1	74	81	90	110
	MASS-0.3	65	71	78	83
	MPSS-0.1	65	66	77	81
	MPSS-0.3	52	63	66	63
	MBSS-0.1	75	80	84	95
	MBSS-0.3	59	45	67	73
E' (MPa) at T_g + 60°C	DMESS	741.8	619.1	632.1	707.0
	MASS-0.1	549.6	356.4	342.1	295.8
	MASS-0.3	155.9	126.1	132.0	136.6
	MPSS-0.1	48.1	46.1	49.2	51.4
	MPSS-0.3	115.6	29.4	31.2	89.7
	MBSS-0.1	184.5	142.3	269.9	142.8
	MBSS-0.3	36.6	26.8	28.6	21.9
$\nu_e(10^4$ mol/m$^3)$	DMESS	7.24	5.91	5.96	6.72
	MASS-0.1	5.42	3.45	3.25	2.67
	MASS-0.3	1.57	1.25	1.29	1.32
	MPSS-0.1	0.48	0.46	0.48	0.50
	MPSS-0.3	1.20	0.30	0.31	0.91
	MBSS-0.1	1.81	1.38	2.59	1.34
	MBSS-0.3	0.37	0.28	0.29	0.22

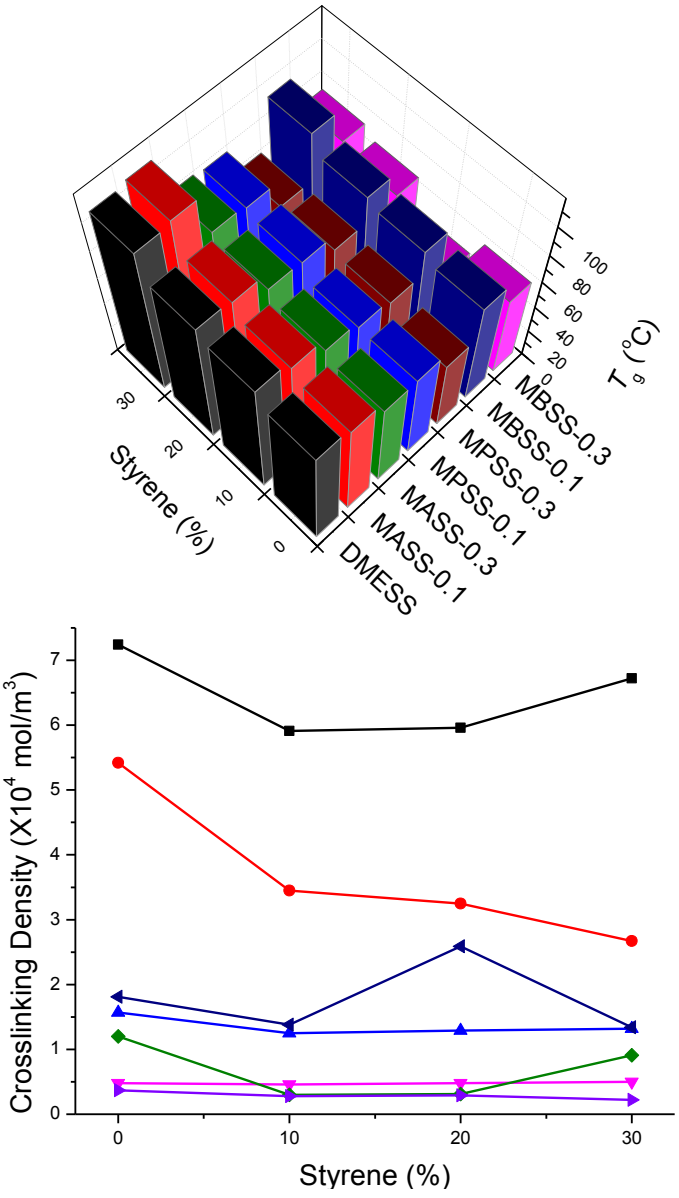

Figure 3.5. Glass transition temperature (top) and crosslink density (bottom) as a function of styrene content.

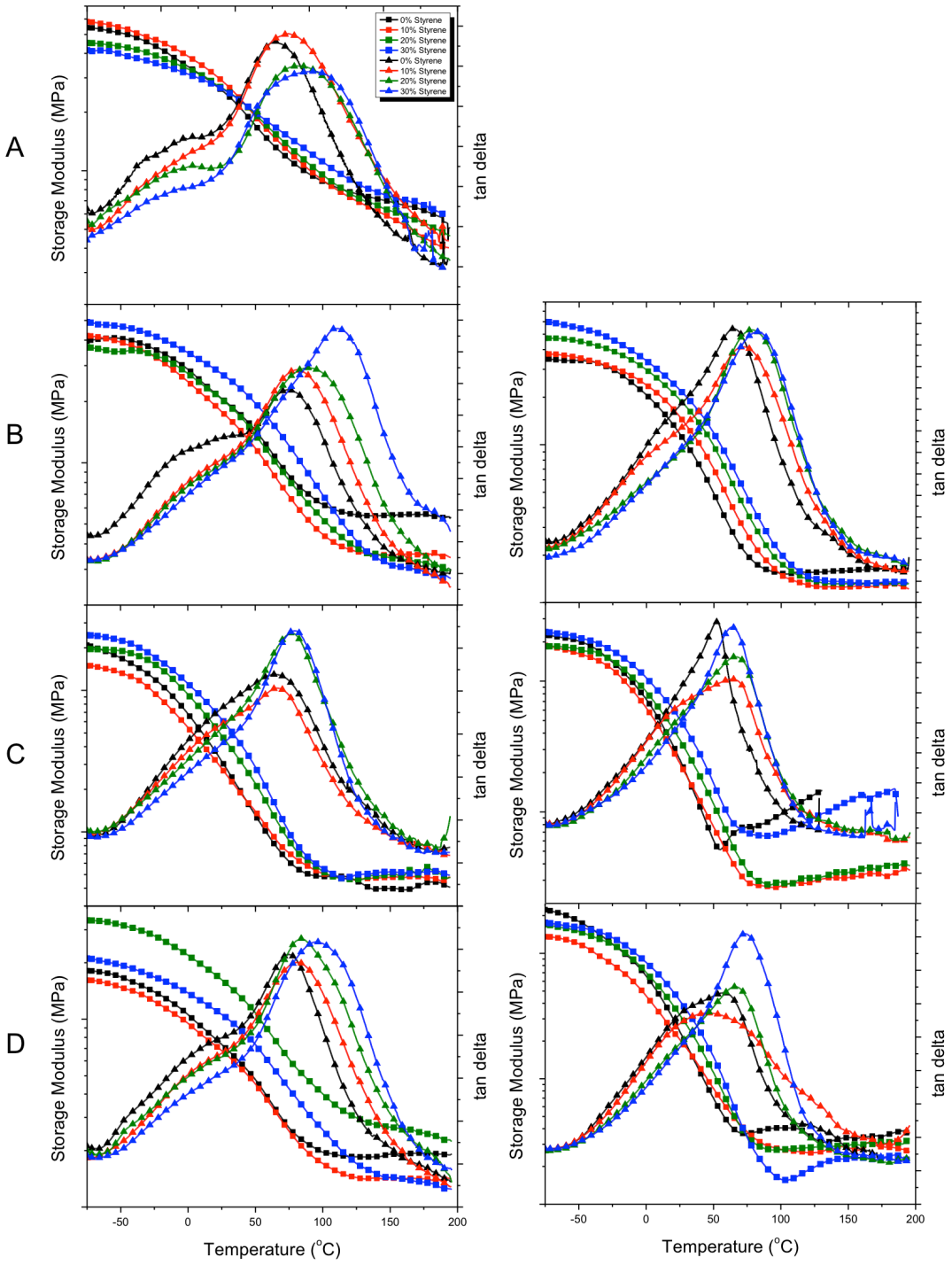

Figure 3.6. DMTA curves of thermosets with 0, 10, 20, and 30 percent by weight styrene content: A) DMESS B) MASS-0.1 (left), MASS-0.3 (right), C) MPSS-0.1 (left), MPSS-0.3 (right), D) MBSS-0.1 (left), MBSS-0.3 (right).

3.4.3.2. Tensile properties

The tensile properties of the thermosets are summarized in Table 3.4. The trend (Figure 3.7) shows that tensile strength, Young's modulus, % elongation, and toughness are directly proportional to styrene content. In terms of degree of esterification and ester chain length, tensile strength and Young's modulus (Figure 3.7, top left and top right, respectively) both decreased while % elongation and toughness (Figure 3.8, bottom left and bottom right, respectively) both increased.

Table 3.4. Tensile properties of thermosets of MASS, MPSS, and MBSS with different degrees of esterification.

Resin	Styrene (%)	Tensile Strength (MPa)	Young's Modulus (MPa)	Elongation (%)	Toughness ($X10^{-2}$ J)
DMESS	0	23.6 ± 2.0	868 ± 75	3.5 ± 0.9	4.1 ± 2.0
	10	26.2 ± 4.1	955 ± 32	3.5 ± 0.9	4.6 ± 1.8
	20	25.5 ± 4.1	1031 ± 75	3.3 ± 0.6	2.4 ± 0.7
	30	25.2 ± 5.0	1042 ± 66	3.1 ± 0.9	3.2 ± 2.1
MASS-0.1	0	22.8 ± 3.0	640 ± 72	5.6 ± 1.8	7.0 ± 3.8
	10	23.8 ± 2.6	642 ± 50	6.9 ± 1.6	10.2 ± 3.5
	20	25.2 ± 1.6	734 ± 27	6.6 ± 0.8	9.8 ± 2.1
	30	27.0 ± 2.7	722 ± 60	8.4 ± 1.3	12.4 ± 4.1
MASS-0.3	0	14.6 ± 1.3	269 ± 26	9.6 ± 1.8	8.0 ± 2.2
	10	14.7 ± 2.8	319 ± 17	8.9 ± 3.0	9.0 ± 5.5
	20	18.0 ± 1.5	422 ± 32	11.1 ± 1.5	11.8 ± 2.0
	30	18.8 ± 2.3	446 ± 60	9.7 ± 2.9	9.7 ± 3.6
MPSS-0.1	0	8.7 ± 0.7	232 ± 10	4.5 ± 0.6	1.6 ± 0.3
	10	11.5 ± 1.9	290 ± 35	5.6 ± 1.6	2.7 ± 1.1
	20	10.7 ± 1.5	283 ± 36	5.8 ± 1.4	4.0 ± 1.6
	30	7.6 ± 0.8	143 ± 10	11.4 ± 1.5	3.4 ± 0.7
MPSS-0.3	0	7.3 ± 1.3	95 ± 8	13.3 ± 2.9	4.7 ± 2.0
	10	8.7 ± 1.5	93 ± 17	15.4 ± 4.3	6.5 ± 3.1
	20	6.6 ± 0.8	99 ± 13	11.8 ± 3.2	5.8 ± 2.0
	30	7.4 ± 0.6	101 ± 12	14.6 ± 3.4	7.6 ± 2.1
MBSS-0.1	0	21.5 ± 3.5	629 ± 67	5.1 ± 1.2	5.5 ± 2.0
	10	15.6 ± 5.0	405 ± 143	6.9 ± 0.7	9.5 ± 1.8
	20	21.2 ± 6.8	576 ± 171	6.1 ± 1.8	8.2 ± 3.8
	30	23.1 ± 1.7	619 ± 46	7.6 ± 1.0	11.4 ± 2.1
MBSS-0.3	0	7.2 ± 1.1	106 ± 9	11.0 ± 2.2	3.7 ± 1.3
	10	8.1 ± 0.9	165 ± 17	9.5 ± 2.0	4.3 ± 1.4
	20	8.4 ± 1.3	119 ± 23	13.5 ± 3.5	7.1 ± 3.5
	30	8.9 ± 2.9	110 ± 47	18.4 ± 3.5	11.9 ± 3.8

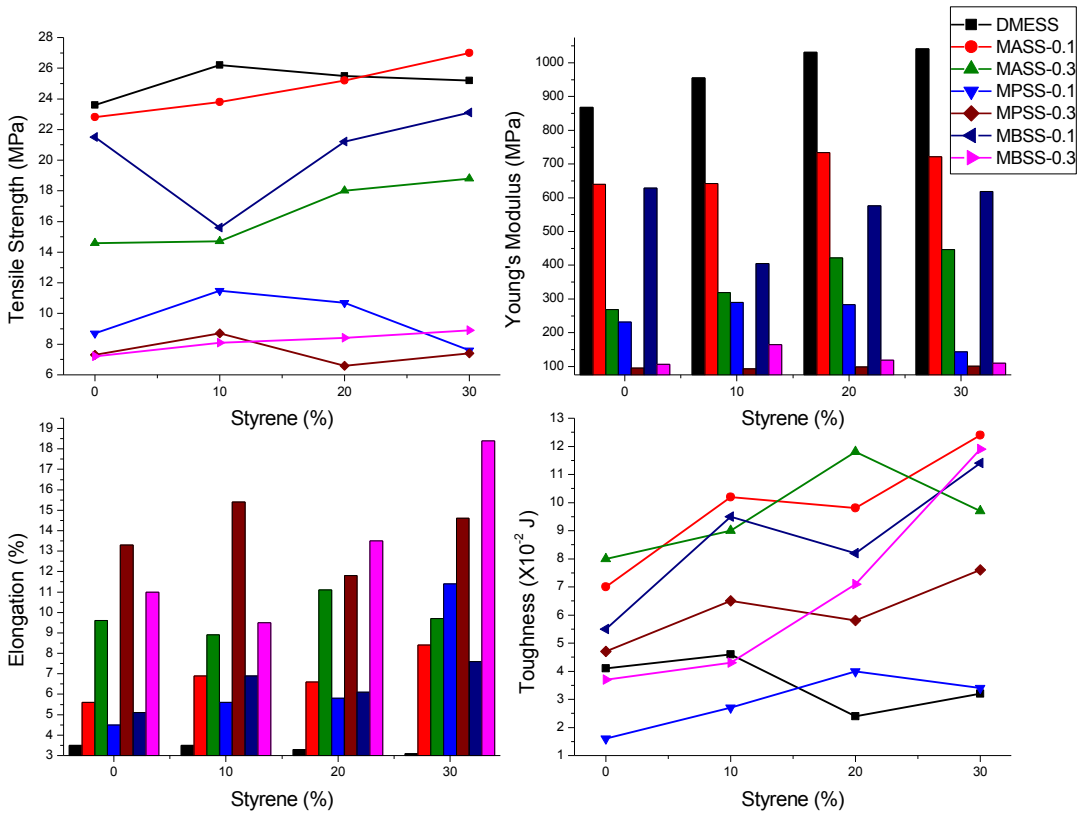

Figure 3.7. Tensile properties as a function of styrene content: tensile strength (top left), Young's modulus (top right), elongation (bottom left), and toughness (bottom right).

Figure 3.8 shows representative stress-strain curves of the thermosets. Introducing more non-functional ester groups to replace the methacrylate groups improves the flexibility of the thermosets and renders them ductile. The improvement in their toughness becomes more evident as the degree of esterification and chain length were increased (Figure 3.8B right and 3.8C right). As predicted, the tensile strength and Young's modulus displayed opposing effects against flexibility (% elongation) and toughness of the thermosets. The modulus values of these thermosets are in the range of 95-734 MPa. The lower modulus values were mostly for the thermosets with higher non-functional, longer chain ester groups (MPSS-0.3 and MBSS-0.3). The same thermosets exhibited 3-5 times elongation (9.5-18.4%) than DMESS (3.1-3.5%).

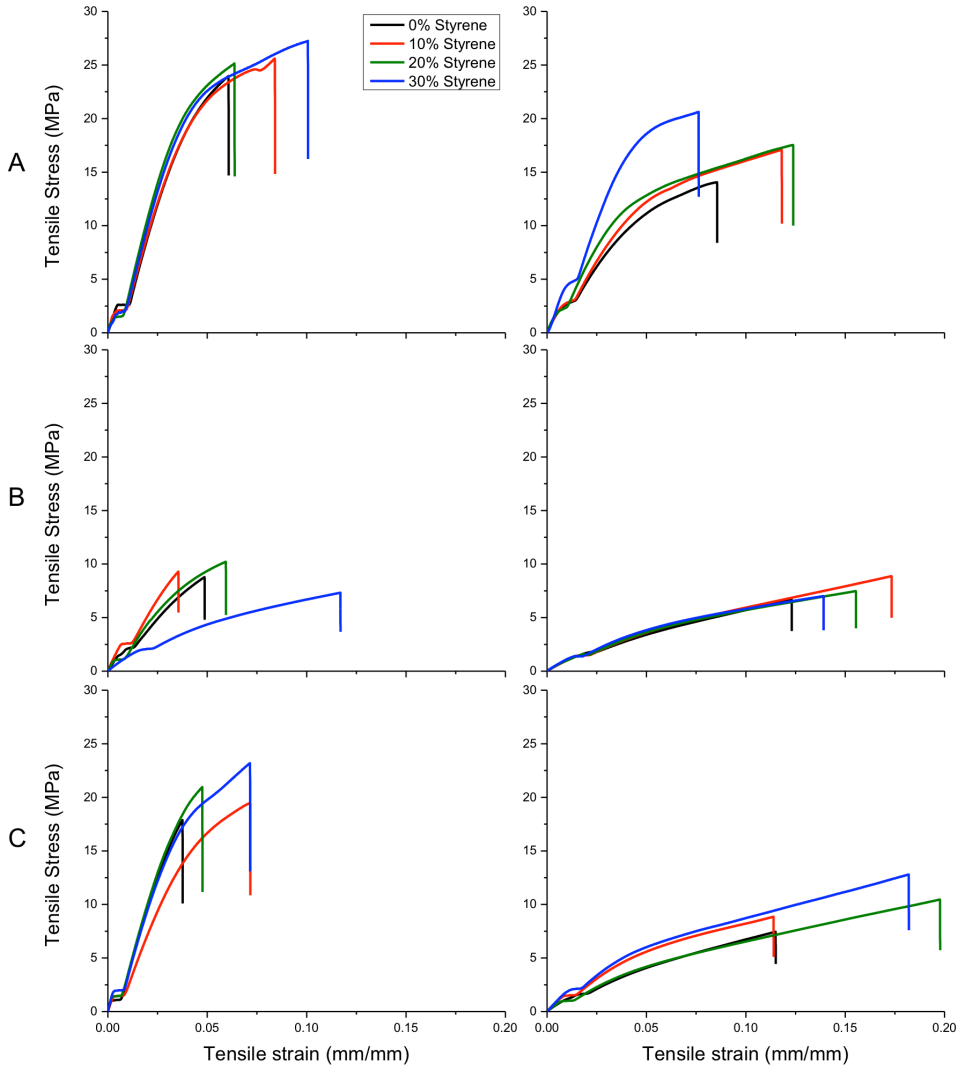

Figure 3.8. Stress-strain curve of thermosets with 0, 10, 20, and 30 percent by weight styrene content: A) MASS-0.1 (left), MASS-0.3 (right), B) MPSS-0.1 (left), MPSS-0.3 (right), C) MBSS-0.1 (left), MBSS-0.3 (right).

3.4.3.3. Thermal stability and gel content

The thermal stability of the thermosets was characterized via thermogravimetric analysis (TGA), the temperatures of 5% weight loss and % gel are listed on Table 3.5. 5% weight loss was observed at temperatures greater than 311°C for all the thermosets. Figure 3.9 (left) shows the 5% weight loss temperatures of all the thermosets containing 0, 10, 20 and 30% styrene. There was a slight improvement in the thermal stability of all the non-functional ester resin-

based thermosets (320-341°C) compared with the DMESS-based thermosets (311-332°C). The gel contents of all the thermosets were greater than 95% (Figure 3.9 right).

Table 3.5. Thermal degradation properties and gel content of thermosets of MASS, MPSS, and MBSS with different degrees of esterification.

		Styrene (%)			
	Resin	0	10	20	30
$T_{5\%}$ (°C)	DMESS	332	325	312	311
	MASS-0.1	341	338	325	340
	MASS-0.3	339	334	328	323
	MPSS-0.1	338	329	330	330
	MPSS-0.3	320	328	326	324
	MPSS-0.1	333	331	328	325
	MPSS-0.3	333	333	329	326
% Gel content	DMESS	98.80	98.68	98.55	98.70
	MASS-0.1	98.60	98.72	98.87	99.05
	MASS-0.3	98.11	98.22	98.81	99.40
	MPSS-0.1	97.29	97.84	97.96	98.20
	MPSS-0.3	96.64	96.11	97.41	95.36
	MPSS-0.1	97.74	98.71	98.81	99.18
	MPSS-0.3	96.35	97.60	97.12	98.81

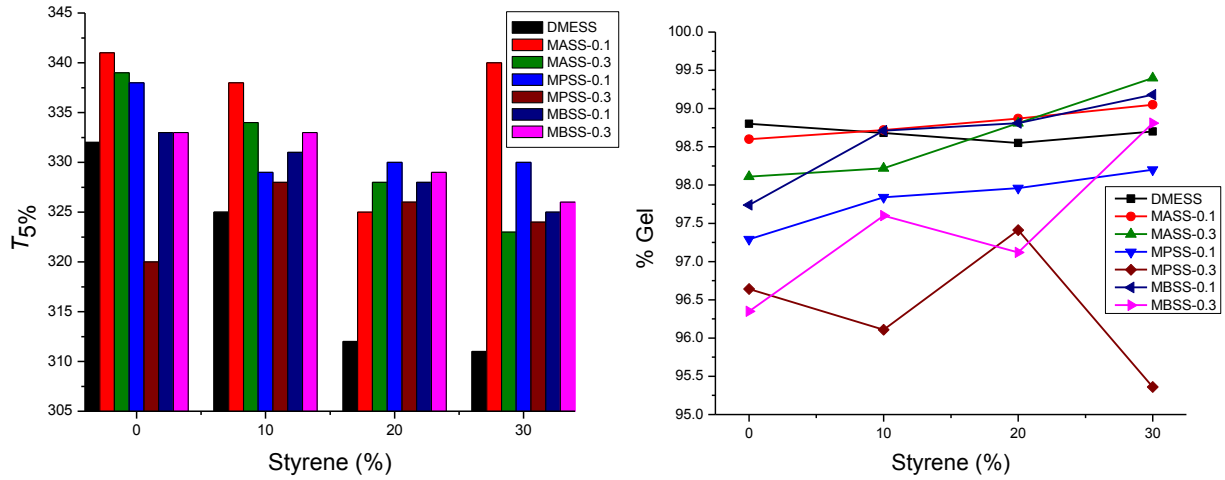

Figure 3.9. Thermal degradation properties (left) and gel content (right) as a function of styrene content.

Figure 3.10 is a depiction of the crosslink network of the thermosets. Figure 3.10A is a representation of a highly crosslinked network such as DMESS. Upon introduction of non-

functional ester groups, the junctions in the network become more distant from each other, lowering the crosslink density, allowing dangling chains to improve material toughness (Figure 3.10B). As the ester chain length is increased, the network loosens further (Figure 3.10C) and improvement of both toughness and flexibility is observed.

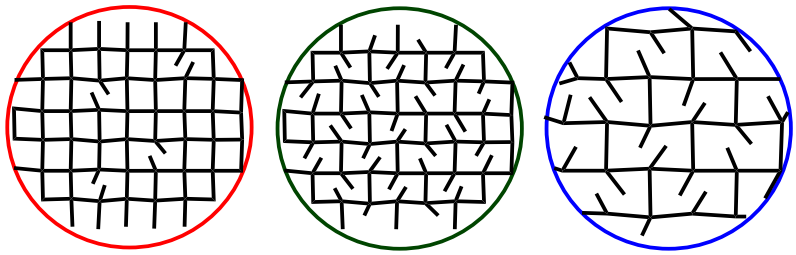

Figure 3.10. Simplified illustration of thermoset network: A) highly crosslinked B) short ester chains C) long ester chains.

3.5. Conclusions

A modified procedure based on a previously established synthetic protocol was developed for the syntheses of the highly functional bio-based resins. The process remained as a one-pot, solvent-free synthesis and required shorter reaction times. Tunability of the highly functional DMESS was demonstrated via incorporation of non-functional esters. Structure-property relationship studies established new sets of thermal and mechanical properties for the thermosets, which showed that DMESS may be tailored according to targeted applications due to its inherently high functionality. The resins with 30% styrene had lower viscosities (Figure 3.11 left) compared with DMESS (30% styrene) and commercially available vinyl esters, Derakane 411-350 (45% styrene) and Derakane 470-300 (33% styrene), which is a significant factor in processibility. Derakane 470-300 had a viscosity of 325 mPa•s with 33% styrene. This viscosity was achieved with the bio-based resins formulations using 31% styrene or less (Figure 3.11 right). Formulations with styrene generated expected trends: direct proportionality with T_g, tensile strength, Young's modulus, % elongation, and toughness. The inverse effect on v_e was

also expected from the inclusion of the non-functional esters into the network. Overall, non-functional esters successfully accomplished plasticizing the resins by further reducing viscosities and producing ductile thermosets. Thermomechanical properties mainly depended on ν_e and chemical compositions. Table 3.6 summarizes the general trends of the thermoset properties as a function of degree of esterification, ester chain length, and styrene content.

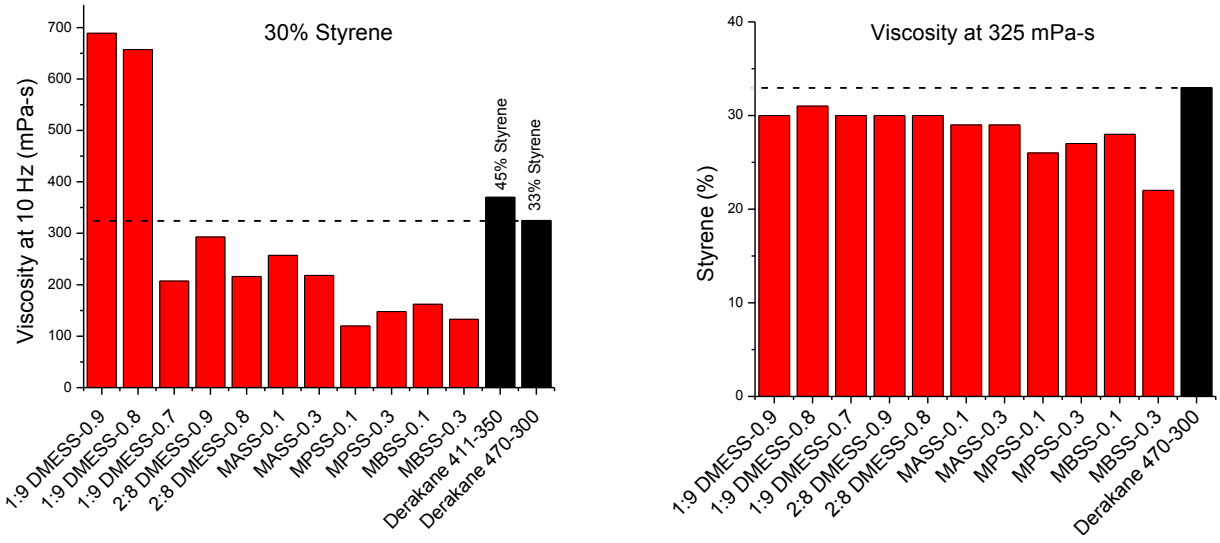

Figure 3.11. Viscosities of bio-based resins containing 30% styrene (left) and amounts of styrene used to achieve a formulation viscosity of 325 mPa•s (right).

Table 3.6. General trends of thermoset properties.

Properties	Degree of esterification	Ester chain length	% Styrene
T_g	↓	↓	↑
ν_e	↓	↓	↓
Tensile strength	↓	↑↓	↑
Young's modulus	↓	↓	↑
% Elongation	↑	↑	↑
Toughness	↑	↑	↑

3.6. Acknowledgements

This work was supported by the National Science Foundation EPSCoR Award under Grant No. IIA-1355466.

3.7. References

1. Liu, Z.; Kraus, G., *Green materials from plant oils*. Royal Society of Chemistry: 2014.

2. Xia, Y.; Larock, R. C., Vegetable oil-based polymeric materials: synthesis, properties, and applications. *Green Chemistry* **2010,** *12* (11), 1893-1909.

3. Miao, S.; Wang, P.; Su, Z.; Zhang, S., Vegetable-oil-based polymers as future polymeric biomaterials. *Acta biomaterialia* **2014,** *10* (4), 1692-1704.

4. Auvergne, R.; Caillol, S.; David, G.; Boutevin, B.; Pascault, J.-P., Biobased thermosetting epoxy: present and future. *Chemical Reviews* **2013,** *114* (2), 1082-1115.

5. Raquez, J. M.; Deléglise, M.; Lacrampe, M. F.; Krawczak, P., Thermosetting (bio) materials derived from renewable resources: a critical review. *Progress in Polymer Science* **2010,** *35* (4), 487-509.

6. de Espinosa, L. M.; Meier, M. A. R., Plant oils: the perfect renewable resource for polymer science?! *European Polymer Journal* **2011,** *47* (5), 837-852.

7. Belgacem, M. N.; Gandini, A., *Monomers, polymers and composites from renewable resources*. Elsevier: 2011.

8. Pfister, D. P.; Xia, Y.; Larock, R. C., Recent advances in vegetable oil-based polyurethanes. *ChemSusChem* **2011,** *4* (6), 703-717.

9. Soucek, M. D.; Khattab, T.; Wu, J., Review of autoxidation and driers. *Progress in Organic Coatings* **2012,** *73* (4), 435-454.

10. Howie, J. K.; Schaefer, J. J.; Trout, J. E., Synthesis of polyol medium fatty acid polyesters. U.S. Patent No. 6,995,232: 7 Feb. 2006.

11. Corrigan, P. J., Synthesis of polyol fatty acid polyesters. U.S. Patent No. 6,620,952: 16 Sep. 2003.

12. Schaefer, J. J.; Trout, J. E., Synthesis of purified, partially esterified polyol polyester fatty acid compositions. U.S. Patent No. 6,887,947: 3 May 2005.

13. Monono, E. M.; Bahr, J. A.; Pryor, S. W.; Webster, D. C.; Wiesenborn, D. P., Optimizing process parameters of epoxidized sucrose soyate synthesis for industrial scale production. *Organic Process Research & Development* **2015,** *19* (11), 1683-1692.

14. Monono, E. M.; Webster, D. C.; Wiesenborn, D. P., Pilot scale (10kg) production and characterization of epoxidized sucrose soyate. *Industrial Crops and Products* **2015,** *74*, 987-997.

15. Pan, X.; Sengupta, P.; Webster, D. C., Novel biobased epoxy compounds: epoxidized sucrose esters of fatty acids. *Green Chemistry* **2011,** *13* (4), 965-975.

16. Webster, D. C.; Sengupta, P. P.; Chen, Z.; Pan, X.; Paramarta, A., Highly functional epoxidized resins and coatings. U.S. Patent No. 9,096,773: 4 Aug 2015.

17. Pan, X.; Webster, D. C., New biobased high functionality polyols and their use in polyurethane coatings. *ChemSusChem* **2012,** *5* (2), 419-429.

18. Paramarta, A.; Pan, X.; Webster, D. C., Highly Functional Acrylated Biobased Resin System. *Radtech Report* **2013,** *1*, 26-32.

19. Nelson, T. J.; Bultema, L.; Eidenschink, N.; Webster, D. C., Bio-based high functionality polyols and their use in 1K polyurethane coatings. *Journal of Renewable Materials* **2013,** *1* (2), 141-153.

20. Kovash, C. S.; Pavlacky, E.; Selvakumar, S.; Sibi, M. P.; Webster, D. C., Thermoset Coatings from Epoxidized Sucrose Soyate and Blocked, Bio-Based Dicarboxylic Acids. *ChemSusChem* **2014,** *7* (8), 2289-2294.

21. Ma, S.; Webster, D. C.; Jabeen, F., Hard and flexible, degradable thermosets from renewable bioresources with the assistance of water and ethanol. *Macromolecules* **2016,** *49* (10), 3780-3788.

22. Ma, S.; Webster, D. C., Naturally occurring acids as cross-linkers to yield VOC-free, high-performance, fully bio-based, degradable thermosets. *Macromolecules* **2015,** *48* (19), 7127-7137.

23. Paramarta, A.; Webster, D. C., Bio-based high performance epoxy-anhydride thermosets for structural composites: The effect of composition variables. *Reactive and Functional Polymers* **2016,** *105*, 140-149.

24. Paramarta, A.; Webster, D. C., The exploration of Michael-addition reaction chemistry to create high performance, ambient cure thermoset coatings based on soybean oil. *Progress in Organic Coatings* **2017,** *108*, 59-67.

25. Sitz, E. D.; Bajwa, D. S.; Webster, D. C.; Monono, E. M.; Wiesenborn, D. P.; Bajwa, S. G., Epoxidized sucrose soyate—A novel green resin for crop straw based low density fiberboards. *Industrial Crops and Products* **2017**.

26. Zhang, C.; Garrison, T. F.; Madbouly, S. A.; Kessler, M. R., Recent Advances in Vegetable Oil-Based Polymers and Their Composites. *Progress in Polymer Science* **2017**.

27. Sengupta, S.; Ray, D., Vegetable Oil-Based Polymer Composites: Synthesis, Properties and Their Applications. *Handbook of Composites from Renewable Materials, Polymeric Composites* **2017,** *6*, 441.

28. Williams, G. I.; Wool, R. P., Composites from natural fibers and soy oil resins. *Applied Composite Materials* **2000,** *7* (5-6), 421-432.

29. Hosseini, N.; Ulven, C. A.; Azarmi, F.; Webster, D. C.; Nelson, T. J. In *Utilization of Flax Fibers and Glass Fibers in a Bio-Based Resin*, ASME 2014 International Mechanical Engineering Congress and Exposition, 2014; American Society of Mechanical Engineers: 2014; pp V014T11A041-V014T11A041.

30. Foulk, J. A.; Fuqua, M. A.; Ulven, C. A.; Alcock, M. M., Flax fibre quality and influence on interfacial properties of composites. *International Journal of Sustainable Engineering* **2010,** *3* (1), 17-24.

31. O'Donnell, A.; Dweib, M. A.; Wool, R. P., Natural fiber composites with plant oil-based resin. *Composites Science and Technology* **2004,** *64* (9), 1135-1145.

32. Lu, Y.; Larock, R. C., Fabrication, Morphology and Properties of Soybean Oil-Based Composites Reinforced with Continuous Glass Fibers. *Macromolecular Materials and Engineering* **2007,** *292* (10-11), 1085-1094.

33. Quirino, R. L.; Woodford, J.; Larock, R. C., Soybean and linseed oil-based composites reinforced with wood flour and wood fibers. *Journal of Applied Polymer Science* **2012,** *124* (2), 1520-1528.

34. Yan, J.; Webster, D. C., Thermosets from highly functional methacrylated epoxidized sucrose soyate. *Green Materials* **2014,** *2* (3), 132-143.

35. Sejidov, F. T.; Mansoori, Y.; Goodarzi, N., Esterification reaction using solid heterogeneous acid catalysts under solvent-less condition. *Journal of Molecular Catalysis A: Chemical* **2005,** *240* (1), 186-190.

36. Brazel, C. S.; Rosen, S. L., *Fundamental principles of polymeric materials*. John Wiley & Sons: 2012.

37. Park, S.-J.; Jin, F.-L.; Lee, J.-R., Thermal and mechanical properties of tetrafunctional epoxy resin toughened with epoxidized soybean oil. *Materials Science and Engineering: A* **2004,** *374* (1), 109-114.

38. Choi, J. S.; Park, W. H., Effect of biodegradable plasticizers on thermal and mechanical properties of poly (3-hydroxybutyrate). *Polymer Testing* **2004,** *23* (4), 455-460.

39. Choi, J. S.; Park, W. H. In *Thermal and mechanical properties of poly (3-hydroxybutyrate-co-3-hydroxyvalerate) plasticized by biodegradable soybean oils*, 2003; Wiley Online Library: pp 65-76.

40. Kono, M.; Hayashi, E.; Watanabe, M., Network polymer electrolytes with free chain ends as internal plasticizer. *Journal of the Electrochemical Society* **1998,** *145* (5), 1521-1527.

41. Zhang, Z.; Fang, S., Novel network polymer electrolytes based on polysiloxane with internal plasticizer. *Electrochimica Acta* **2000,** *45* (13), 2131-2138.

42. Vieira, M. G. A.; da Silva, M. A.; dos Santos, L. O.; Beppu, M. M., Natural-based plasticizers and biopolymer films: A review. *European Polymer Journal* **2011,** *47* (3), 254-263.

43. Amiri, A.; Yu, A.; Webster, D.; Ulven, C., Bio-Based Resin Reinforced with Flax Fiber as Thermorheologically Complex Materials. *Polymers* **2016,** *8* (4), 153.

44. Taylor, C.; Amiri, A.; Paramarta, A.; Ulven, C.; Webster, D., Development and weatherability of bio-based composites of structural quality using flax fiber and epoxidized sucrose soyate. *Materials & Design* **2017,** *113*, 17-26.

45. Amiri, A.; Hosseini, N.; Ulven, C.; Webster, D. In *Advanced bio-composites made from methacrylated epoxidized sucrose soyate resin reinforced with flax fibers*, Proceedings of the 20th International Conference on Composite Materials, Copenhagen, Denmark, 2015; pp 19-24.

46. Hosseini, N.; Webster, D. C.; Ulven, C., Advanced biocomposite from highly functional methacrylated epoxidized sucrose soyate (MAESS) resin derived from vegetable oil and fiberglass fabric for composite applications. *European Polymer Journal* **2016,** *79*, 63-71.

47. Webster, D. C.; Yu, A. Z., Biobased highly functional oligomers and thermosets therefrom. U.S. Patent No. 9,765,233: 19 Sep. 2017.

CHAPTER 4. HIGHLY FUNCTIONAL METHACRYLATED BIO-BASED RESINS FOR PHOTOCURABLE COATINGS

4.1. Abstract

Highly methacrylated bio-based resins methacrylated epoxidized sucrose soyate (MESS) and dimethacrylated epoxidized sucrose soyate (DMESS) were synthesized from epoxidized sucrose soyate (ESS). Formulations for these resins were developed and the thermomechanical properties of the thermosets produced were investigated and measured. The versatility of these resins was explored and applied to UV-curable coating applications. The resins were combined with various multifunctional reactive diluents and cured under UV light using a photoinitiator (Irgacure 1173) at a 4:1:0.25 ratio, respectively. Commercially available Bisphenol A glycerolate dimethacrylate (BisGMA) was used as the control. The extent of cure was determined using Attenuated Total Reflectance-Fourier transform infrared spectroscopy (ATR-FTIR). Thermomechanical properties were determined by thermogravimetric analysis (TGA), thermomechanical analysis (TMA), and atomic force microscopy (AFM). The curing kinetics was studied using real-time infrared spectroscopy equipped with a UV light. Shrinkage of the coatings was measured by the volume change before and after the curing process. Performance of the coatings was also evaluated by measuring the moisture uptake and abrasion resistance. Coatings made from these formulations displayed good solvent resistance and hardness due to the high crosslinking. The technology was extended to a visible light-cured system and initial results show promising applicability for dental applications.

4.2. Introduction

The popularity of plant oils as alternative sources to petroleum-based materials has been due to the rapidly rising costs of petrochemicals and its limited sources. In addition, plant oils

are readily available, highly abundant, low cost, and biodegradable.[1-6] They are generally made up of triglycerides containing various amounts of unsaturated functional groups, depending on the type of plant. The unsaturation sites on the fatty acids can be chemically modified to produce useful functional polymers. Procter and Gamble (P&G) Chemicals previously commercialized an alkyd diluent SEFOSE 1618U (sucrose soyate).[7-9] It is a structurally interesting molecule due to its rigid sucrose core and flexible fatty acid chains. Webster *et al.* further developed this molecule by transforming it into a more reactive molecule, epoxidized sucrose soyate (ESS) via the Prilezhaev epoxidation (Scheme 4.1).[10-12] ESS has proven itself to be versatile in terms of crosslinking technologies and bio-based coatings applications.[13-21] It has also shown promise in composites applications as a bio-based polymer matrix.[22-27] Thus, slowly gaining ground as a potential petrochemical alternative.

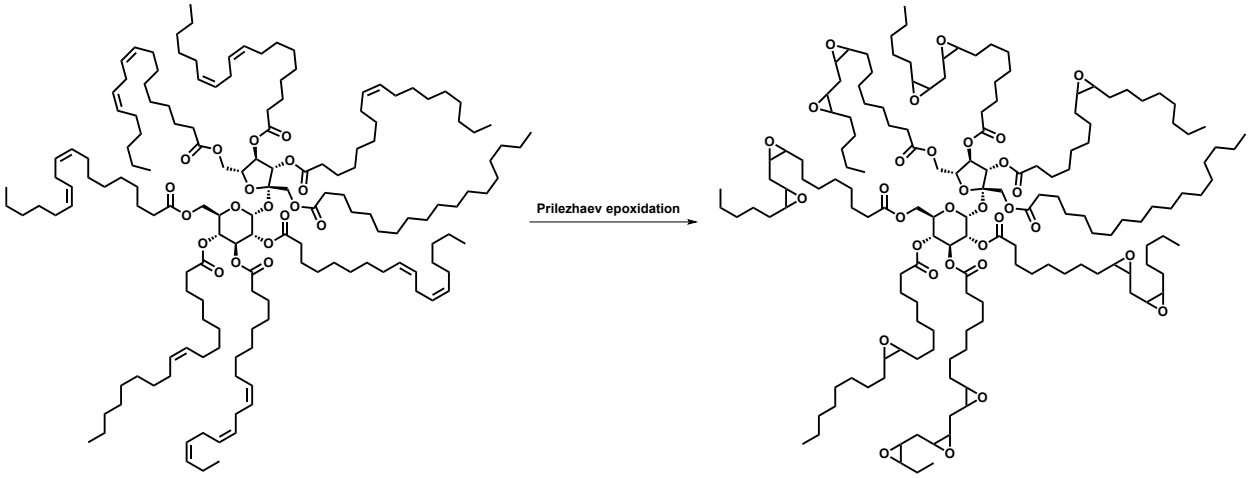

Scheme 4.1. Synthetic route of SEFOSE to ESS.

Bisphenol A (BPA) (Figure 4.1 left) is a widely used petrochemical that has earned its place in the world of plastics through the years due to its unique sets of properties and its easily modified structure. The phenolic hydroxyls are typically converted into other functional groups that provide unique sets of material properties. A more advanced derivative of BPA is bisphenol A glycerolate dimethacrylate (BisGMA) (Figure 4.1 right). BisGMA is an example of a

conventional epoxy methacrylate that is commonly used as a monomer due to its unique sets of properties. The phenyl ring provides chemical resistance, the ether linkage allows flexibility (toughness), the hydroxyl gives good adhesion, and the methacrylate is the reactive site for crosslinking. However, much research shows that BPA has adverse effects on humans.[28-30] Consequently, the replacement of BPA remains an actively sought research.

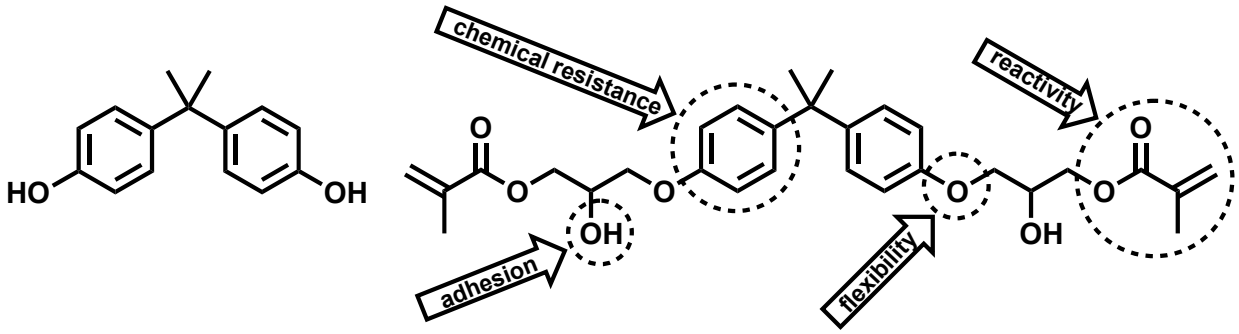

Figure 4.1. Structures of bisphenol A (BPA, left) and bisphenol A glycerolate dimethacrylate (BisGMA, right).

Webster *et al.*[31, 32] has developed bio-based methacrylated resins (methacrylated epoxidized sucrose soyate MESS and dimethacrylated epoxidized sucrose soyate DMESS, Figure 4.2) that have exhibited good thermomechanical properties and have been used as the polymer matrix in fiber reinforced polymer (FRP) composite applications. In these applications, the materials were crosslinked via thermally-initiated free-radical polymerization. These systems could likewise be crosslinked via photoinitiated free-radical polymerization. Acrylated counterparts of these molecules have been previously studied in UV-curable coatings.[15] The degree of acrylation was varied and different reactive diluents were used to lower resin viscosities. The coatings produced were hard and had good chemical and abrasion resistance.

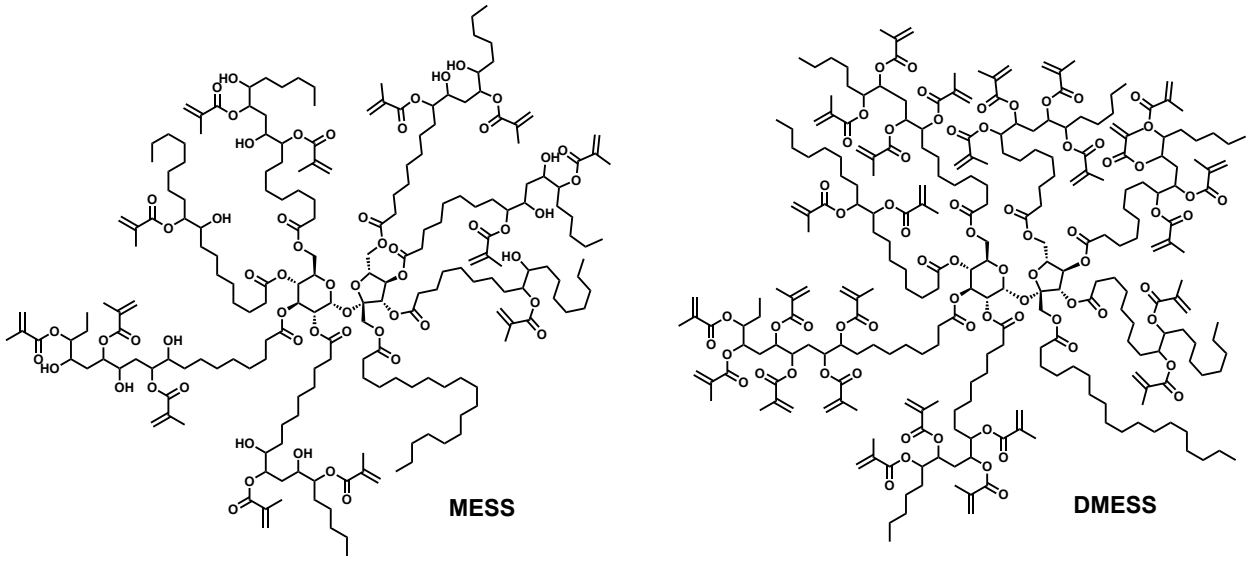

Figure 4.2. Structures of the bio-based methacrylated resins: MESS and DMESS.

In this study, the aim was to investigate the highly functional methacrylated bio-based resins as replacement for BPA-based resins in photopolymer applications. The reactivity of these methacrylated resins was exploited and its potential use in coating applications was explored. The resins were mixed with several methacrylated reactive diluents and applied onto substrates as coatings. The high functionality of the bio-based methacrylated resins would produce highly crosslinked coatings compared with the linear BisGMA. The degree of functionality of the bio-based resins can be controlled during its synthesis. This dictates the amount of hydroxyl groups present in the molecule, which controls the strength of the adhesion onto substrates. The formulations were cured by irradiation of ultraviolet (UV) light. The coatings properties were then evaluated and compared against the conventional BisGMA. The photopolymerization kinetics were also studied using infrared spectroscopy to monitor the reaction progress in real-time. Hardness was measured using König pendulum, pencil, and atomic force microscopy. Coating performance was investigated by evaluating the thermal stability, shrinkage, moisture uptake, and abrasion resistance.

4.3. Experimental

4.3.1. Materials

Bisphenol A glycerolate dimethacrylate (BisGMA) was purchased from Sigma Aldrich (St. Louis, MO, USA). The reactive diluents (Figure 4.3) ethylene glycol dimethacrylate (EGDMA), 1,4-butanediol dimethacrylate (1,4-BDDMA), polyethylene glycol dimethacrylate (PEG-200-DMA), and trimethylolpropane trimethacrylate (TMPTMA) were provided by Evonik. Irgacure 1173 (formerly Darocur 1173), 2-hydroxy-2-methyl-1-phenyl-propan-1-one, was provided by BASF. Camphorquinone (CQ) and ethyl 4-dimethylbenzoate (EDB) were purchased from VWR (Batavia, IL, USA). All reagents were used as received. Methacrylated epoxidized sucrose soyate (MESS) was synthesized following the procedure in the literature.[31] Dimethacrylated epoxidized sucrose soyate (DMESS) was synthesized using a developed protocol.[32]

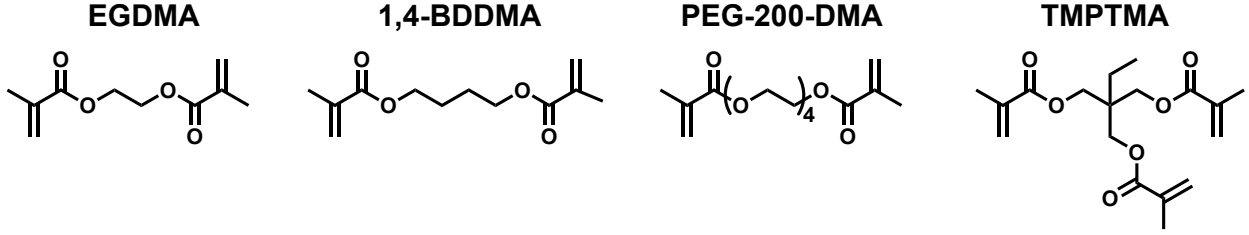

Figure 4.3. Structures of the reactive diluents (left to right): EGDMA, 1,4-BDDMA, PEG-200-DMA, and TMPTMA.

4.3.2. Coating formulations and curing

The methacrylated resins BisGMA, MESS, and DMESS were mixed with four different reactive diluents with weight ratios of 4:1 giving a total of 12 formulations. Irgacure 1173 was added at a concentration of 5% (based on total weight of resin and reactive diluent) to the formulation. The formulations were mixed for 5 minutes at 3500 rpm in a Flacktek high-speed mixer. Coatings were applied to a steel substrate (Q-Lab, QD-36) cleaned with acetone, as well

as Pine wood panels for adhesion testing, using a drawdown bar at a wet film thickness of 8 mil. The coatings were cured by exposure to UV irraditation (210-315 nm) for 40 seconds using a Fusion LC6B Benchtop Conveyer with an F300 Lamp of intensity ~1180 mW/cm^2 as determined by a UV Power Puck II (EIT Inc.).

The formulations were mixed for 5 minutes at 3500 rpm in a Flacktek high-speed mixer and the viscosities were measured at 25°C using an ARES Rheometer (TA Instruments) operating from 0.1 rad/s to 500 rad/s with 0.1% strain.

The conversion profiles for the photopolymerization with various reactive diluents were determined using real-time Infrared (RTIR) spectroscopy. The measurements were made using a Thermo Scientific Nicolet 8700 Infrared spectrometer with a Lesco Super Spot MK II fiber optic UV light (315-400 nm) with an irradiance of 50 mW/cm^2. The samples were irradiated with UV light for 180 seconds and scans were recorded every 2 seconds. The ratio of the peak area corresponding to the methacrylate unsaturation (C=C stretching at ~1630 cm^{-1}) was monitored and compared against the unchanging carbonyl peaks (~1725 cm^{-1}).

The extent of cure was evaluated using a Vertex 70 Fourier transform infrared (FTIR) spectrometer (Bruker Optics) with an attenuated total reflectance (ATR) accessory. The beam was irradiated an angle of 45° and the crystal was made of Germanium. Samples were placed directly on top of the crystal and absorption spectra were taken with 32 scans at a resolution of 4 cm^{-1} in the range of 4000-400 cm^{-1}.

The shrinkage of the cured coatings was reported as percent volume change before and after the curing process. The volume ($v = m/\rho$) of the uncured formulations (resin and reactive diluent) was calculated using the mass (m) of the uncured formulation and its density (ρ). The density was measured following ASTM D 1475. Similarly, the volume of the cured coatings on

a panel was calculated using its mass and density. The density was measured using the mass of a carefully cut out rectangular sample of the cured coating and its volume (length x width x thickness).

Formulations for the visible light-cured system were done similarly replacing Irgacure 1173 with camphorquinone (CQ) and ethyl 4-dimethylaminobenzoate (EDB) as Norrish II type photoinitiator. The ratio for the CQ/EDB was kept constant at 1:3 (by weight), respectively. The formulations were mixed by hand and pressed between two glass panels. The light source used to initiate the curing process (9 seconds) was a blue light-emitting diode (LED) 3M Ortholux^{TM} with a wavelength of 430 – 480 nm and intensity of 1600 mW/cm^2.

4.3.3. Coatings properties

The thickness of each of the cured panels was measured with a Byko-Test 8500 coating thickness gauge. Using the Gardner Micro-TRI-gloss measurement tool, the gloss of each formulation at 20°, 60°, and 85° was measured from the drawdown on the glass panel, along with the mean and standard deviation of each measurement. To determine hardness, the coatings were subjected to König pendulum hardness test following ASTM D 4366 and also with pencil hardness following ASTM D 3363. Adhesion to the substrate was characterized by crosshatch adhesion using ASTM D 3359. Flexibility was measured via conical mandrel bend (ASTM D 522), which measures slow deformation while reverse impact (ASTM D 2794) measures rapid deformation. Solvent resistance gives an indication of crosslink density and was measured using a modified version of ASTM D 5402. The head of a 26 ounce hammer was wrapped in 6 layers of cheesecloth and saturated with methyl ethyl ketone (MEK). This was then placed at the base of the coating and allowed to rub the coating back and forth, recording the number of double

rubs until coating failure was observed. Failure was reached when substrate was exposed. The hammer was rewet with MEK after 50 double rubs.

Nanoindentation measurements were carried out at room temperature with an AFM (Dimension 3100, Veeco, USA). The Berkovich indenter was a rectangular diamond tip (PDNISP, Bruker, USA) having a resonance frequency of about 70 kHz and an average spring constant of 284.14 N/m. The radius of curvature at the tip apex was nominally 40 nm and tip half angle is 42.28°. The deflection sensitivity of the indenter was determined by indenting on sapphire (Bruker, USA). The Z scan rate is set to 2.03Hz, which means that an indentation will take 0.49 second to execute. The load-displacement behavior of the coatings was measured in order to determine the mechanical properties. The mechanical properties, such as hardness and Young's modulus values, were calculated following the method by Oliver and Pharr.[33, 34]

Following the equations of Oliver and Pharr, hardness (H) is defined as[34]

$$H = \frac{F_{max}\,(h_{max})}{A(h_c)} \qquad \text{(Equation 4.1)}$$

where F_{max} is the maximum applied force, h_{max} is the displacement at maximum force, and $A(h_c)$ is the contact area as a function of the contact depth (h_c). The contact area and contact depth are defined as

$$A(h_c) = 24.56\, h_c^2 \qquad \text{(Equation 4.2)}$$

$$h_c = h_{max} - \frac{\varepsilon F_{max}}{S} \qquad \text{(Equation 4.3)}$$

where $\varepsilon = 0.75$ for the Berkovich indenter and S is the slope of the unloading curve.

The elastic modulus (E), commonly referred to as Young's modulus, in its reduced form, is defined as

$$E = E_r(1 - \nu^2) \qquad \text{(Equation 4.4)}$$

where E_r is the reduced elastic modulus and ν is the sample Poisson ratio. E_r is defined as

$$E_r = \frac{S}{2\beta}\sqrt{\frac{\pi}{A(h_c)}} \qquad \text{(Equation 4.5)}$$

where β = 1.034 for the Berkovich indenter.

A Q500 thermogravimetric analysis (TGA) system (TA Instruments) with a heating rate of 20°C/min from room temperature to 600°C under a continuous nitrogen flow, was used to determine the thermal stability of the thermosets. TMA of the samples was performed on a 2940 thermomechanical analyzer (TA Instruments). The probe used was a standard flat-tipped probe and the penetration load was kept constant at 0.050 N. As the samples softened at T_g, the probe position was accurately monitored by a movable-core linear variable differential transformer (LVDT). All the samples were run under helium atmosphere at a rate of 10°C/min from 0°C up to 200°C. The sample thicknesses ranged from 50-90 μm.

Abrasion tests were performed at room temperature on a TABER® Rotary Platform Abrasion Tester Model 5155 (TABER Industries) according to ASTM D 4060. The abrasion test involved 100 cycles of abrasion using a pair of CS10 resilient rubber wheels, each with a 250-g load, at 72 rpm. Coatings of 80-100 μm thicknesses were cured onto wooden discs with dimensions 4 inches diameter and 0.25 inch thickness. The initial and final weights of the samples were measured. Abrasion resistance of coatings was reported as average weight loss of triplicate samples.

Water absorption measurements were conducted via gravimetric process, which was based on ASTM D 570. Thermoset discs with dimensions 40 mm diameter and about 1 mm thickness were prepared and fully immersed in deionized water at room temperature (20°C). The sample weights were recorded after 1 week and 1 month immersions. Results were reported as percent moisture uptake.

4.4. Results and discussion

4.4.1. Coating formulations

The methacrylate resins were mixed with four different methacrylated reactive diluents. Three of the reactive diluents were linear difunctional methacrylates and one was a branched trifunctional methacrylate. A Norrish I type photoinitiator, 2-hydroxy-2-methyl-1-phenyl-propan-1-one, was used to promote the polymerization process. The coating formulations were applied onto steel substrates and photochemically cured. After ultraviolet irradiation, 2-hydroxy-2-methyl-1-phenyl-propan-1-one undergoes a homolytic cleavage and generates two free radical intermediates (Scheme 4.2). These intermediates then react with the double bonds from the methacrylates on both the resin and the reactive diluent to propagate.

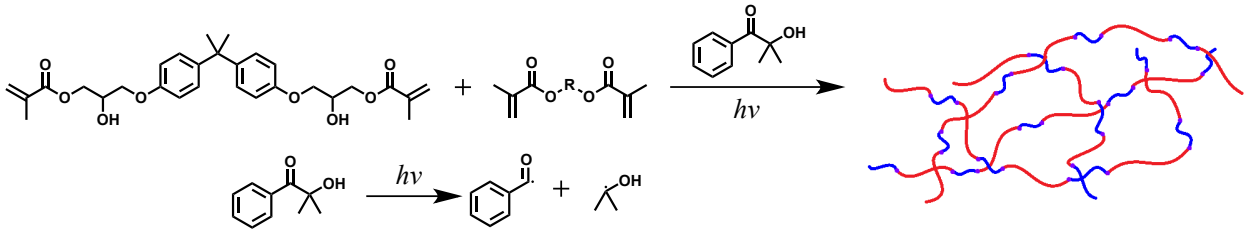

Scheme 4.2. Representative photoinitiated reaction of a methacrylated resin (BisGMA) with methacrylated reactive diluents and Irgacure 1173 as photoinitiator.

The viscosities of the methacrylated resins are high due to the hydroxyl groups that provide hydrogen bonding (BisGMA > MESS > DMESS). Addition of reactive diluents reduced the resin viscosity by breaking apart the intramolecular hydrogen bonding of the resins while inducing intermolecular hydrogen bonding between the resin and the reactive diluents. Table 4.1 shows the viscosities of the resins alone (123740-1055120 mPa•s) and with the reactive diluents (2380-24226 mPa•s). These were measured in order to study the compatibility of the reactive diluents and to reduce the viscosity to the lower range making them processible. The reactive diluents effectively reduced the viscosity of the control BisGMA more than the MESS

counterparts. This could be attributed to the linear structure of BisGMA which allows it to align with the reactive diluents and efficiently break the intramolecular hydrogen bonding. The trend in Figure 4.4 shows dramatic decrease in viscosity when the reactive diluents were added (2380-9481 mPa•s). EGDMA provided the formulation with the lowest viscosity within each group while TMPTMA gave the highest viscosity. Although increasing the chain length of the reactive diluent did not vary significantly, the trend seemed to suggest that the shorter chain reactive diluents were more effective than the longer ones. Furthermore, increasing the functionality of the reactive diluent proved that linear reactive diluents are more effective due to their higher mobility and sterically less hindered structure.

Table 4.1. Viscosities of the resins alone and with the reactive diluents.

Resin	Reactive Diluent	Abbr.	Viscosity at 10 Hz (mPa•s)
BisGMA	None		1055120
	EGDMA	BE	4134
	1,4-BDDMA	BB	7474
	PEG-200-DMA	BP	7814
	TMPTMA	BT	47367
MESS	None		591447
	EGDMA	ME	7101
	1,4-BDDMA	MB	7367
	PEG-200-DMA	MP	9481
	TMPTMA	MT	47062
DMESS	None		123740
	EGDMA	DE	2380
	1,4-BDDMA	DB	3921
	PEG-200-DMA	DP	5012
	TMPTMA	DT	24226

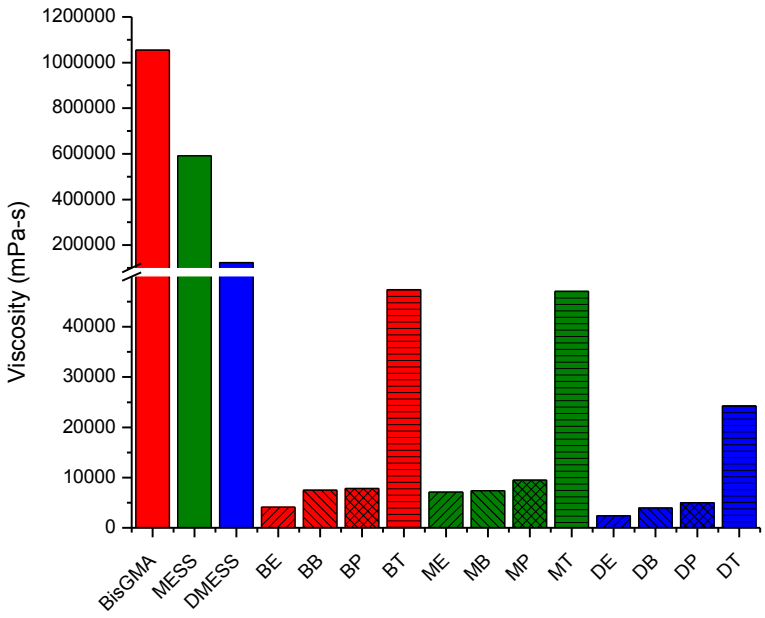

Figure 4.4. Viscosity of resins as a function of reactive diluents.

4.4.2. Photopolymerization kinetics

The conversion profiles (Figure 4.5) of the photopolymerizations with BisGMA reached 90% conversion at about 100 seconds while both MESS and DMESS reached the same conversion after about 90 seconds. Generally, the polymerization rates (R_p) were independent of the reactive diluents. In theory, varying the reactive diluents should have a direct proportionality effect on the reaction rate based on the photopolymerization rate equation (Equation 4.6):

$$R_p = k_p\,[\mathrm{M}]\left(\frac{\phi I_a}{k_t}\right)^{1/2} \qquad \text{(Equation 4.6)}$$

where [M] is the monomer (and reactive diluent) concentration, ϕ is the quantum efficiency, I_a is the absorbed light intensity, k_p is the propagation rate constant, and k_t is the termination rate constant.[35] However, the overall polymerization rate is controlled by the methacrylated resin concentration since it is 80% (by weight) of the total formulation and 20% reactive diluent. It has been previously shown that the polymerization kinetics of formulations containing BisGMA is largely dependent on BisGMA concentrations.[36] Thus, the effect of the reactive diluent

concentration is negligible. In all cases, final conversion was reached at about 180 seconds (Figure 4.5). Compared with acrylates, methacrylates are generally less reactive due to the methyl group in place of hydrogen. A similar study by Webster *et al.*[15] shows photopolymerization of acrylates reach final conversions after 20 seconds. The high functionality of the star-like architecture of the bio-based resins makes the structure sterically congested. Nevertheless, the conversion profiles showed 10% faster reaction rates compared with the conventional BisGMA. The results suggest that the propagation step of BisGMA is much slower than those of the bio-based resins or termination by combination is more favored than propagation ($k_t >> k_p$).

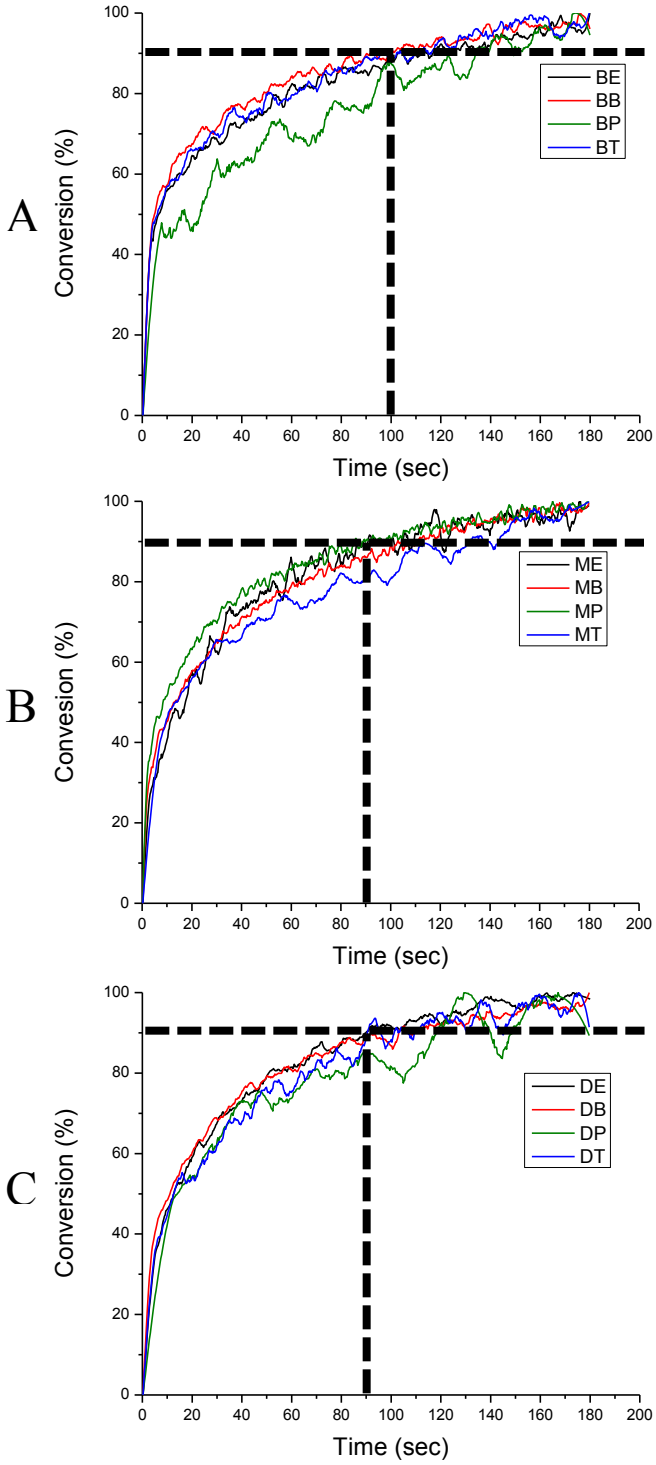

Figure 4.5. Conversion profiles of the different formulations: A) BisGMA series, B) MESS series, and C) DMESS series.

4.4.3. Curing study

The formulations were coated on steel and wood substrates, and cured via UV irradiation for 40 seconds (Figure 4.6). The extent of cure of the coatings on steel substrate was determined by ATR-FTIR. All the coatings were tack-free after UV exposure. However, the spectra (Figure 4.7) showed that BisGMA-based resins contained unreacted methacrylate groups due to the presence of C=C peaks (~1630 cm^{-1}) while both bio-based resins showed minimal C=C peaks. These results were consistent with the kinetics study, which showed that the photopolymerization of the control BisGMA had slower reaction rates. Likewise, this may be due to a faster termination rate than the propagation rate. BisGMA also shows absorption in the UV region (290-380 nm), which may slow down the polymerization rate due to the reduction of the initiator efficiency, Φ, as described by Equation 4.6.

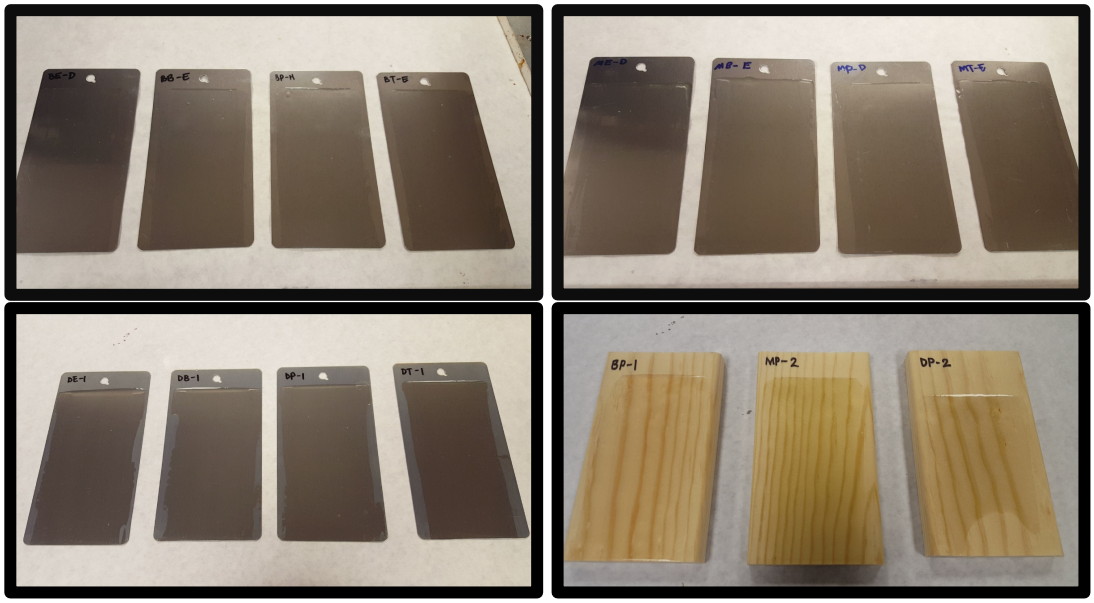

Figure 4.6. Pictures of coated steel substrates: BisGMA series (top left), MESS series (top right), DMESS series (bottom left), and Pine wood panels (bottom right).

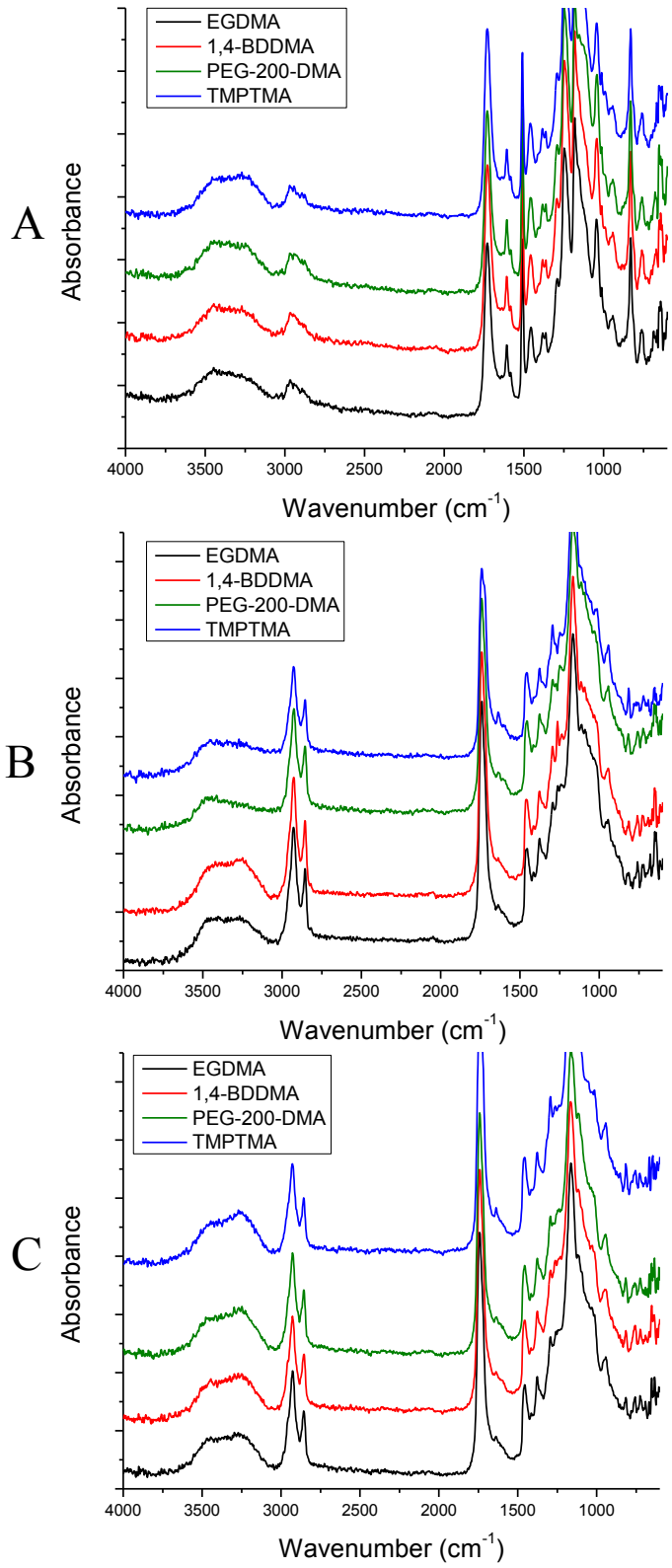

Figure 4.7. ATR-FTIR of coatings with different reactive diluents: A) BisGMA series, B) MESS series, and C) DMESS series.

4.4.4. Volumetric shrinkage

When monomer molecules undergo polymerization and form a polymer network, it is usually accompanied with a tighter or closer packing of the molecules. The volume reduction is typically referred as the polymerization shrinkage.[37-39] Table 4.2 shows a summary of the polymerization shrinkage reported as percent volume change. Generally, the shrinkage is around 3% and independent of the resin system. The measurements were based on densities before and after polymerization. A much more accurate method could be done using modern instrumentation developed by Lu *et al.*[40] The device is capable of measuring accurate and reproducible polymerization shrinkage stress data. They have also developed a novel experimental technique that could simultaneously measure stress and monitor the conversion by using the same instrument in tandem with a near-infrared (NIR) spectrometer with a fiber-optic system.[41] Stress relief could be done by modifying the viscoelastic properties or using fillers.[42]

Table 4.2. Volumetric shrinkage after polymerization.

Resing + Reactive Diluent	Average % Volume Change
BE	-3.28
BB	-3.60
BP	-1.02
BT	-2.20
ME	-4.72
MB	-4.69
MP	-1.70
MT	-3.18
DE	-2.78
DB	-3.11
DP	-3.47
DT	-3.27

(-) denotes decrease in change

4.4.5. Coating properties

Coating properties were determined and results were tabulated (Table 4.3). All the coatings performed well in terms of MEK double rub resistance (>400). Notable differences are

observed in the hardness of the coatings both in the König pendulum hardness and pencil hardness. Coatings based on the control BisGMA were harder compared with bio-based coatings. All the coatings were brittle as indicated by both reverse impact (< 4 in•lbs) and conical mandrel bend (0%) tests. The coatings gave poor adhesion on steel substrates. However, when Pine wood was used as substrate, coatings based on BisGMA and MESS gave good adhesion (5B) while DMESS-based coatings were inferior (2B-3B). BisGMA and MESS contain more hydroxyl groups that provide hydrogen bonding with the wood substrate. The gloss of the coatings was also measured (Table 4.4). At the high gloss angle (20°), all the coatings gave high gloss units (>70 GU).

Table 4.3. Coatings properties.

Resin + Reactive Diluent	Thickness (μm)	MEK Double Rub	König Pendulum Hardness (sec)	Reverse Impact (in•lbs)	Conical Mandrel (Elongation-at-break)	Pencil Hardness (gouge)	Crosshatch Adhesion[a]
BE	46.7	> 400	195	< 4	0%	6H	5B
BB	50.6	> 400	197	< 4	0%	6H	5B
BP	50.3	> 400	198	< 4	0%	6H	5B
BT	61.0	> 400	206	< 4	0%	8H	5B
ME	66.3	> 400	131	< 4	0%	2H	5B
MB	65.8	> 400	128	< 4	0%	2H	5B
MP	57.8	> 400	126	< 4	0%	H	5B
MT	60.2	> 400	135	< 4	0%	H	5B
DE	49.7	> 400	155	< 4	0%	H	3B
DB	44.5	> 400	152	< 4	0%	2H	3B
DP	46.8	> 400	143	< 4	0%	2H	3B
DT	56.0	> 400	140	< 4	0%	H	2B

[a] Pine wood substrate.

Table 4.4. Gloss measurements.

Resin + Reactive Diluent	Gloss		
	20°	60°	85°
BE	88 ± 8.2	100 ± 0.5	96 ± 0.4
BB	84 ± 4.4	99 ± 2.2	95 ± 3.0
BP	97 ± 1.5	100 ± 0.5	100 ± 0.6
BT	88 ± 6.4	100 ± 0.5	99 ± 0.4
ME	81 ± 2.0	90 ± 0.3	98 ± 0.3
MB	84 ± 0.4	91 ± 0.2	99 ± 0.3
MP	81 ± 0.8	91 ± 0.1	99 ± 0.3
MT	81 ± 1.5	90 ± 0.7	99 ± 0.6
DE	74 ± 2.8	90 ± 1.0	96 ± 1.7
DB	79 ± 2.6	90 ± 0.6	98 ± 0.9
DP	79 ± 3.2	91 ± 0.2	99 ± 1.5
DT	72 ± 6.2	87 ± 1.8	97 ± 1.2

4.4.6. Thermomechanical properties

The hardness and Young's modulus of the coatings were also quantified via AFM nanoindentation technique. Figure 4.8 is an example of an indented image of the surface of the coatings and Figure 4.9 is a representative load-displacement graph of the coatings. Figure 4.10 shows the hardness and Young's modulus as functions of resin and reactive diluents, which were calculated based on the work done by Oliver and Pharr.[33] The conventional BisGMA showed significantly higher hardness (>300 MPa) than the bio-based resins (<100 MPa), which remained consistent with the results from König pendulum hardness and pencil hardness tests. The Young's modulus values follow the same trend as the hardness. The linear structure of BisGMA has a greater probability of creating a closely packed arrangement than the star-like structure of the bio-based resins. Its linearity could also favor effective hydrogen bonding between the hydroxyl groups of the polymer chains. MESS and DMESS have more methacrylate functionality per molecule, however, BisGMA forms a closely packed arrangement, which seems contribute to the hardness.

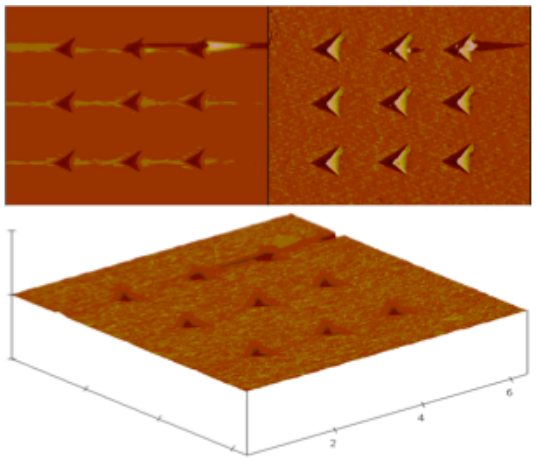

Figure 4.8. AFM images of samples after indentation.

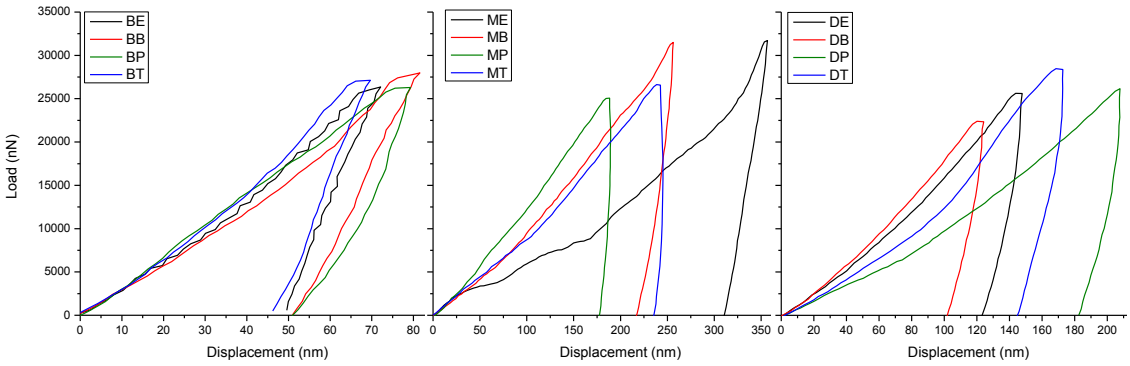

Figure 4.9. Representative load-displacement curves of the samples: BisGMA series (left), MESS series (center), and DMESS series (right).

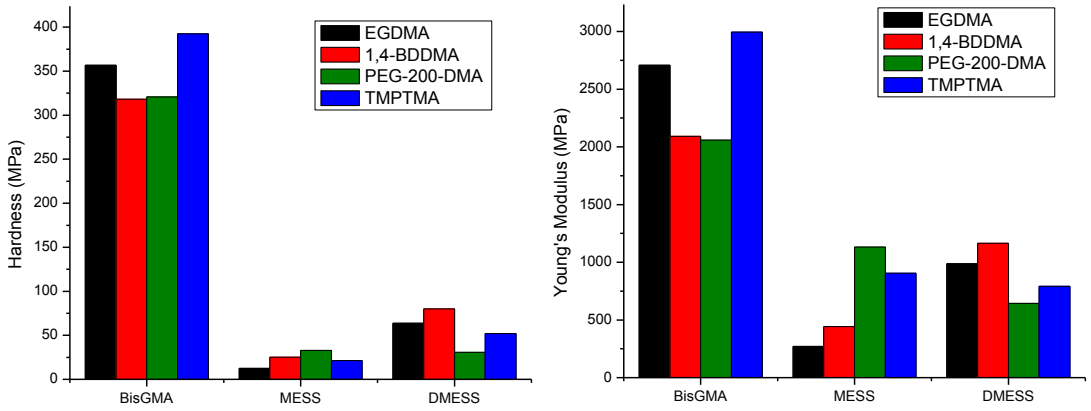

Figure 4.10. Hardness (left) and Young's modulus (right) of the coatings measured via AFM nanoindentation.

Thermal degradation studies (Table 4.5) were performed via thermal gravimetric analysis (TGA). Results showed that the bio-based thermosets had 5% weight loss at the temperature range of 240-259°C, which was relatively comparable with BisGMA-based thermosets (247-258°C). All the thermosets exhibited a one-step decomposition profile. The T_g was determined by measuring the dimensional changes against temperature using the thermomechanical analyzer (TMA). The T_g of the bio-based coatings were in the range of 52-67°C while that of BisGMA-based coatings proved to be difficult to measure via thermomechanical analysis. Due to presence of unreacted methacrylates, the thermograms suggest that the network is highly heterogeneous. Random arrangements of the hard and soft domains resulted in indistinguishable transitions on the thermograms.

Table 4.5. Thermal degradation and glass transition temperature.

Resin + Reactive Diluent	$T_{5\%}$ (°C)[a]	T_g (°C)[b]
BE	247	nd
BB	258	nd
BP	240	nd
BT	251	nd
ME	240	65
MB	247	66
MP	256	52
MT	252	66
DE	228	67
DB	247	57
DP	270	59
DT	259	62

[a] measured by TGA [b] measured by TMA

4.4.7. Abrasion resistance

The UV-cured coatings easily delaminated after polymerizing onto metal substrates. However, very good adhesion was observed when cured onto wooden substrates. Hence, potential applications could include coatings for wooden furniture and floor laminates. One of the more common properties of coatings used in these applications is its resistance to abrasion.

Figure 4.11 shows the appearance of the coatings before and after the testing. Loss of surface gloss was observed in all cases. Table 4.6 shows the mass loss of the coatings after subjecting them to 100 cycles of abrasions on a TABER abraser. Overall, the mass loss of the bio-based coatings was comparable with the BisGMA-based coatings.

Figure 4.11. Representative coated Pine wood discs before (top) and after (bottom) abrasions.

Table 4.6. Mass loss of coatings after 100 cycles of abrasions.

Resin + Reactive Diluent	Mass loss (mg ± std dev)
BE	4.9 ± 1.5
BB	5.7 ± 2.3
BP	4.0 ± 1.5
BT	5.0 ± 1.1
ME	6.9 ± 2.1
MB	5.3 ± 0.1
MP	6.0 ± 0.8
MT	5.5 ± 0.7
DE	5.7 ± 1.0
DB	4.4 ± 1.1
DP	5.8 ± 0.4
DT	6.5 ± 2.0

4.4.8. Moisture uptake

The moisture uptake of thermosets can be tested by measuring the amount of water absorbed after immersions. Table 4.7 shows the weight gain after 1 week and 1 month of water immersions, and Figure 4.12 shows the appearance of the thermosets after 1 month of immersion. Visually, the samples have very good clarity and did not show any differences compared with both 1 week immersions and pre-immersions.

Table 4.7. Percent moisture uptake after 1 week and 1 month immersions.

Resin + Reactive Diluent	After 1 week (% ± std dev)	After 1 month (% ± std dev)
BE	2.11 ± 0.14	4.28 ± 0.63
BB	1.78 ± 0.29	3.55 ± 0.26
BP	2.03 ± 0.05	3.99 ± 0.18
BT	1.58 ± 0.08	3.41 ± 0.47
ME	0.95 ± 0.01	2.15 ± 0.58
MB	0.84 ± 0.09	1.70 ± 0.66
MP	0.91 ± 0.11	2.15 ± 0.31
MT	0.82 ± 0.10	2.15 ± 0.23
DE	0.50 ± 0.01	1.70 ± 0.53
DB	0.43 ± 0.07	1.78 ± 0.07
DP	0.54 ± 0.05	1.46 ± 0.19
DT	0.44 ± 0.06	1.38 ± 0.71

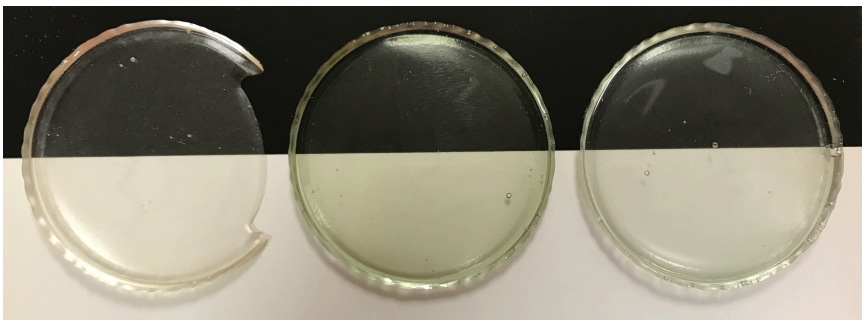

Figure 4.12. Representative moisture uptake samples after 1month immersion: BE (left), ME (center), and DE (right).

Figure 4.13 shows a decreasing trend on the amount of water absorbed by the thermosets. The trend indicates that the bio-based thermosets are more hydrophobic than the BisGMA series

(DMESS > MESS > BisGMA). The higher water absorption of the thermosets of MESS and BisGMA compared with DMESS is due to the presence of the hydroxyl groups on both MESS and BisGMA, which allows for more hydrogen bonding interactions with water. This became more evident after 1 month of immersion. The trend also shows that, although MESS and BisGMA contain hydroxyl groups, the amount of water absorbed by MESS is more similar to DMESS. This is due to the similarity of their sterically congested structure wherein the hydroxyl groups are less accessible for hydrogen bonding with water due to the hydrophobic fatty acid chains. DMESS has less moisture uptake than MESS since it contains less hydroxyl groups. On the other hand, the hydroxyl groups of BisGMA are more accessible for hydrogen bonding with water due to its linear structure.

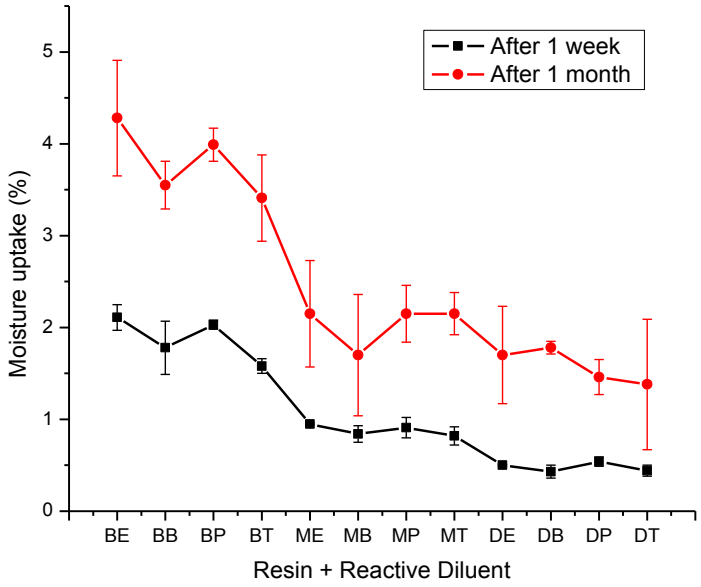

Figure 4.13. Moisture uptake (%) after 1 week and 1 month as a function of resin and reactive diluent.

4.4.9. Visible light-cured system

Applicability of the UV-curable system to a visible light-curable system was investigated by using the appropriate initiator, camphorquinone/ethyl 4-dimethylaminobenzoate (CQ/EDB), and light source combination, blue LED. Scheme 4.3 represents the reaction and the initiation

mechanism that occurs during the photopolymerization process. Four different methods of application were investigated (Figure 4.14). First, a conventional drawdown on a steel substrate was performed but due to the limited coverage of the light source, inconsistent exposure resulted in a tacky coating. Second, a drawdown with reduced surface area ensuring complete exposure to the light source still gave tacky coatings. Third, droplets were deposited onto steel substrates, however, polymerization occurred on the surface but not in the bulk of the droplets. The results from these methods suggested interference of oxygen in the polymerization. Therefore, the fourth method was designed to minimize coating exposure to air while allowing visible light to pass through the substrates (Figure 4.14 IV).

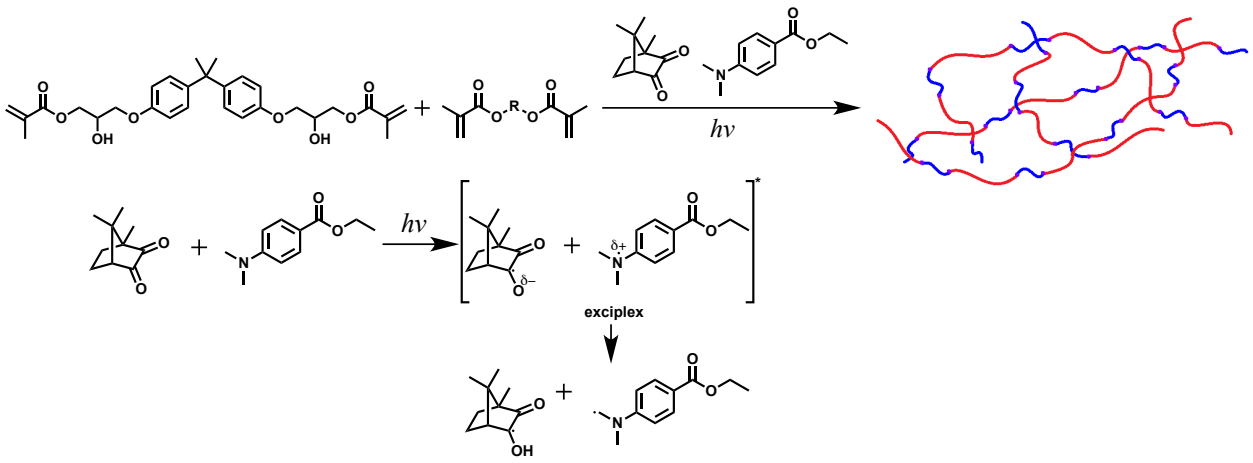

Scheme 4.3. Representative photoinitiated reaction of a methacrylated resin (BisGMA) with methacrylated reactive diluents and CQ/EDB as the photoinitiator system.

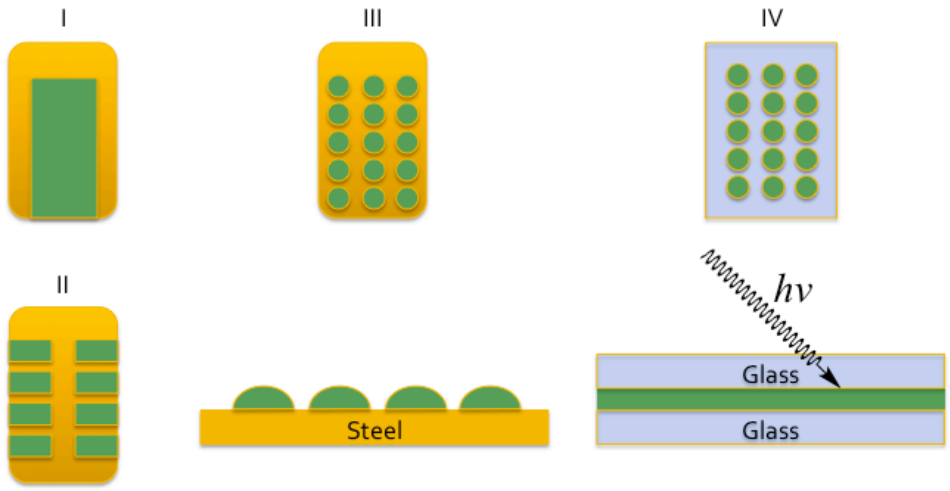

Figure 4.14. Methods of application on steel and glass substrates: I. conventional drawdown (steel), II. drawdown with reduced surface area (steel), III. droplets (steel), and IV. droplets pressed between glass panels.

Exposure times were monitored every 3 second intervals up to 18 seconds. The coatings were tack-free after 9 seconds and the mechanical properties were measured using AFM nanoindentation. Both the Young's modulus values and hardness of the coatings (Figure 4.15) from the bio-based resins afforded comparable values with that of the conventional BisGMA. Surface analysis using ATR-FTIR (Figure 4.16) confirmed the presence of unreacted carbon-carbon double bonds (~1635 cm^{-1}) in all cases from exposure time 3 to 18 seconds, even when the coatings were tack-free.

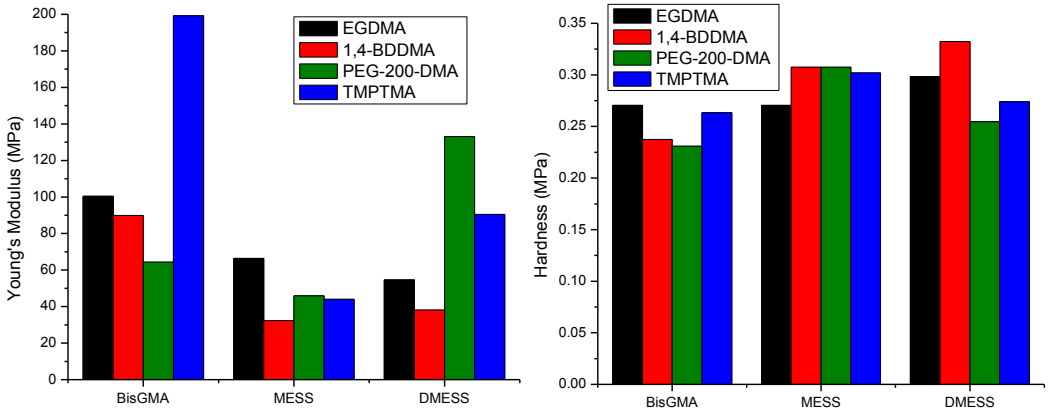

Figure 4.15. Young's modulus (left) and hardness (right) of the formulations cured for 9 seconds, measured using AFM nanoindentation.

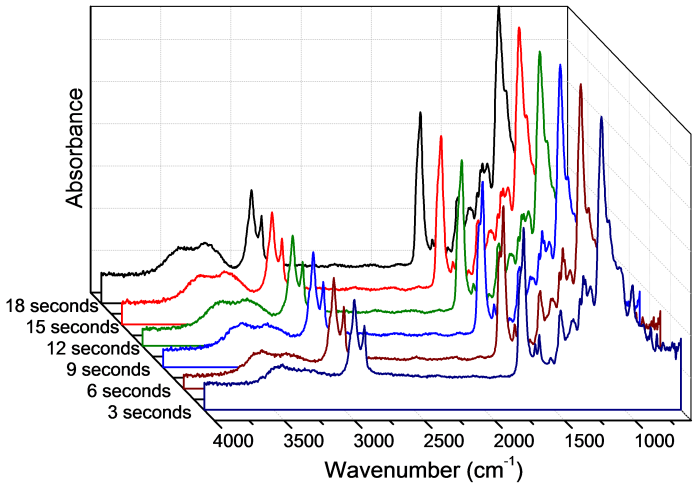

Figure 4.16. Representative ATR-FTIR spectra of formulations exposed at different times.

Thermal stabilities were measured via thermogravimetric analysis. Table 4.8 summarizes the temperatures at 5% weight loss and are all in the range of 205-251°C. As a whole, the visible light-cured coatings degraded at temperatures much lower than the UV-cured coatings. This decrease in thermal stability is indicative of less crosslinked or cured coatings.

Table 4.8. Thermal stabilities of the formulations cured for 9 seconds.

Resin + Reactive Diluent	$T_{5\%}$ (°C)[a]
BE	227
BB	205
BP	226
BT	247
ME	237
MB	233
MP	237
MT	233
DE	241
DB	251
DP	235
DT	235

[a] measured by TGA

Initial curing attempts for the visible light-curable system revealed necessitation of oxygen inhibition. The most direct course of action taken was the addition of an oxygen

scavenger such as 2,6-Di-*tert*-butyl-4-methylphenol (BHT) (Figure 4.17). Another strategy attempted was performing the curing process under inert atmosphere (Figure 4.18). Both approaches resulted in tacky surfaces even after the irradiation exposure was extended up to 60 seconds.

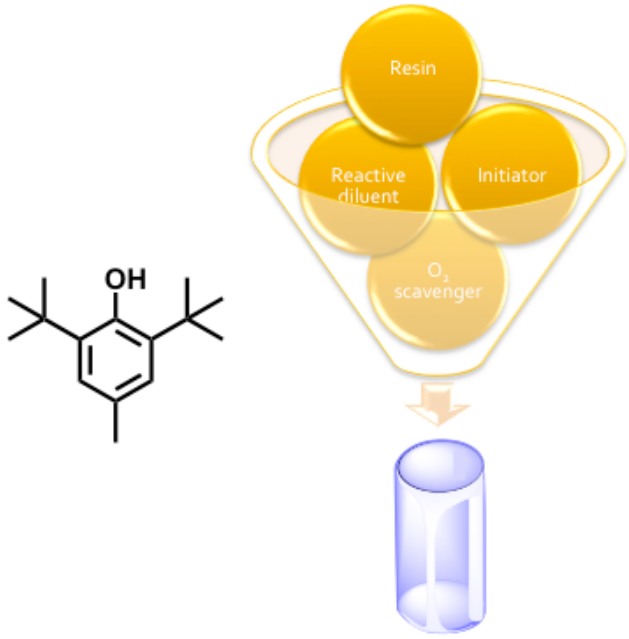

Figure 4.17. Structure of BHT and formulation components of the visible light-curable system.

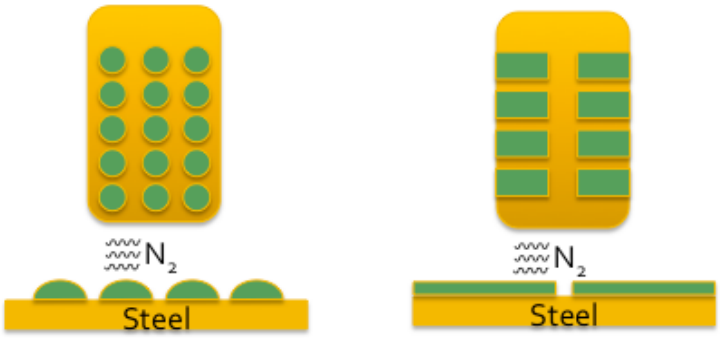

Figure 4.18. Inert condition setup: steady flow of nitrogen over the surface of the coating.

4.5. Conclusions

Exploration of the versatility of the highly methacrylated resins was done by performing photopolymerization using UV light and testing their performance against a conventional methacrylate, BisGMA. When the bio-based resins were formulated with methacrylated reactive diluents, the viscosities of the resultant mixture were dramatically reduced; thus, no solvent was used. The kinetics study showed that the bio-based systems cured at least 10% faster than the control. The extent of cure was determined via ATR-FTIR and showed that the bio-based systems were more efficient in conversion. The volumetric shrinkages of the systems were all comparable with each other. Thermal degradation also showed comparable stability ($T_{5\%}$ 228-270°C). In terms of hardness, the control was much better as proven by the König pendulum hardness, pencil hardness, and AFM nanoindentation. Young's modulus was also measured using AFM nanoindentation and also showed better results from the control. The glass transition temperatures of the bio-based systems were mostly around 60°C while that of the BisGMA were not determined. The TMA thermograms of the control showed multiple transitions which could be attributed to the unreacted methacrylate groups. All the coatings showed high gloss and high solvent resistance. Adhesion was proven to be weak on metal substrates but good on wood substrates, which is primarily attributed to the hydrogen bonding. The same reason justifies the greater water absorption of BisGMA and MESS systems than that of DMESS. In terms of abrasion resistance, the bio-based coatings performed relatively similar to the BisGMA-based coatings. Collectively, the properties show that these resins could be potentially used as coatings for wooden floor laminates or resins in restorative dental applications.

This technology was extended to a visible light-curable system for developing bio-based restorative dental materials. Initial results showed a fast curing system (9 seconds) using a blue

light-emitting diode (LED). The hardness and modulus revealed comparable performance against the control. However, the extent of cure proved incomplete conversion and thus, optimization of curing conditions need to be pursued.

4.6. Acknowledgements

This work was supported by the National Science Foundation EPSCoR Award under Grant No. IIA-1355466.

4.7. References

1. Xia, Y.; Larock, R. C., Vegetable oil-based polymeric materials: synthesis, properties, and applications. *Green Chemistry* **2010,** *12* (11), 1893-1909.

2. Raquez, J. M.; Deléglise, M.; Lacrampe, M. F.; Krawczak, P., Thermosetting (bio) materials derived from renewable resources: a critical review. *Progress in Polymer Science* **2010,** *35* (4), 487-509.

3. de Espinosa, L. M.; Meier, M. A. R., Plant oils: the perfect renewable resource for polymer science?! *European Polymer Journal* **2011,** *47* (5), 837-852.

4. Auvergne, R.; Caillol, S.; David, G.; Boutevin, B.; Pascault, J.-P., Biobased thermosetting epoxy: present and future. *Chemical Reviews* **2013,** *114* (2), 1082-1115.

5. Liu, Z.; Kraus, G., *Green materials from plant oils*. Royal Society of Chemistry: 2014.

6. Miao, S.; Wang, P.; Su, Z.; Zhang, S., Vegetable-oil-based polymers as future polymeric biomaterials. *Acta Biomaterialia* **2014,** *10* (4), 1692-1704.

7. Howie, J. K.; Schaefer, J. J.; Trout, J. E., Synthesis of polyol medium fatty acid polyesters. U.S. Patent No. 6,995,232: 7 Feb. 2006.

8. Corrigan, P. J., Synthesis of polyol fatty acid polyesters. U.S. Patent No. 6,620,952: 16 Sep. 2003.

9. Schaefer, J. J.; Trout, J. E., Synthesis of purified, partially esterified polyol polyester fatty acid compositions. U.S. Patent No. 6,887,947: 3 May 2005.

10. Pan, X.; Sengupta, P.; Webster, D. C., Novel biobased epoxy compounds: epoxidized sucrose esters of fatty acids. *Green Chemistry* **2011,** *13* (4), 965-975.

11. Monono, E. M.; Bahr, J. A.; Pryor, S. W.; Webster, D. C.; Wiesenborn, D. P., Optimizing process parameters of epoxidized sucrose soyate synthesis for industrial scale production. *Organic Process Research & Development* **2015,** *19* (11), 1683-1692.

12. Monono, E. M.; Webster, D. C.; Wiesenborn, D. P., Pilot scale (10kg) production and characterization of epoxidized sucrose soyate. *Industrial Crops and Products* **2015,** *74*, 987-997.

13. Webster, D. C.; Sengupta, P. P.; Chen, Z.; Pan, X.; Paramarta, A., Highly functional epoxidized resins and coatings. Google Patents: 2015.

14. Pan, X.; Webster, D. C., New biobased high functionality polyols and their use in polyurethane coatings. *ChemSusChem* **2012,** *5* (2), 419-429.

15. Paramarta, A.; Pan, X.; Webster, D. C., Highly Functional Acrylated Biobased Resin System. *Radtech Report* **2013,** *1*, 26-32.

16. Nelson, T. J.; Bultema, L.; Eidenschink, N.; Webster, D. C., Bio-based high functionality polyols and their use in 1K polyurethane coatings. *Journal of Renewable Materials* **2013,** *1* (2), 141-153.

17. Kovash, C. S.; Pavlacky, E.; Selvakumar, S.; Sibi, M. P.; Webster, D. C., Thermoset Coatings from Epoxidized Sucrose Soyate and Blocked, Bio‐Based Dicarboxylic Acids. *ChemSusChem* **2014,** *7* (8), 2289-2294.

18. Ma, S.; Webster, D. C.; Jabeen, F., Hard and flexible, degradable thermosets from renewable bioresources with the assistance of water and ethanol. *Macromolecules* **2016,** *49* (10), 3780-3788.

19. Ma, S.; Webster, D. C., Naturally occurring acids as cross-linkers to yield VOC-free, high-performance, fully bio-based, degradable thermosets. *Macromolecules* **2015,** *48* (19), 7127-7137.

20. Paramarta, A.; Webster, D. C., Bio-based high performance epoxy-anhydride thermosets for structural composites: The effect of composition variables. *Reactive and Functional Polymers* **2016,** *105*, 140-149.

21. Paramarta, A.; Webster, D. C., The exploration of Michael-addition reaction chemistry to create high performance, ambient cure thermoset coatings based on soybean oil. *Progress in Organic Coatings* **2017,** *108*, 59-67.

22. Hosseini, N.; Ulven, C. A.; Azarmi, F.; Webster, D. C.; Nelson, T. J. In *Utilization of Flax Fibers and Glass Fibers in a Bio-Based Resin*, ASME 2014 International Mechanical Engineering Congress and Exposition, 2014; American Society of Mechanical Engineers: 2014; pp V014T11A041-V014T11A041.

23. Amiri, A.; Hosseini, N.; Ulven, C.; Webster, D. In *Advanced bio-composites made from methacrylated epoxidized sucrose soyate resin reinforced with flax fibers*, Proceedings of the 20th International Conference on Composite Materials, Copenhagen, Denmark, 2015; pp 19-24.

24. Hosseini, N.; Webster, D. C.; Ulven, C., Advanced biocomposite from highly functional methacrylated epoxidized sucrose soyate (MAESS) resin derived from vegetable oil and fiberglass fabric for composite applications. *European Polymer Journal* **2016,** *79*, 63-71.

25. Amiri, A.; Yu, A.; Webster, D.; Ulven, C., Bio-Based Resin Reinforced with Flax Fiber as Thermorheologically Complex Materials. *Polymers* **2016,** *8* (4), 153.

26. Taylor, C.; Amiri, A.; Paramarta, A.; Ulven, C.; Webster, D., Development and weatherability of bio-based composites of structural quality using flax fiber and epoxidized sucrose soyate. *Materials & Design* **2017,** *113*, 17-26.

27. Sitz, E. D.; Bajwa, D. S.; Webster, D. C.; Monono, E. M.; Wiesenborn, D. P.; Bajwa, S. G., Epoxidized sucrose soyate—A novel green resin for crop straw based low density fiberboards. *Industrial Crops and Products* **2017**.

28. Rochester, J. R., Bisphenol A and human health: a review of the literature. *Reproductive toxicology* **2013,** *42*, 132-155.

29. Ejaredar, M.; Lee, Y.; Roberts, D. J.; Sauve, R.; Dewey, D., Bisphenol A exposure and children's behavior: A systematic review. *Journal of Exposure Science and Environmental Epidemiology* **2017,** *27* (2), 175-183.

30. Pergialiotis, V.; Kotrogianni, P.; Christopoulos-Timogiannakis, E.; Koutaki, D.; Daskalakis, G.; Papantoniou, N., Bisphenol A and adverse pregnancy outcomes: a systematic review of the literature. *The Journal of Maternal-Fetal & Neonatal Medicine* **2017**, 1-8.

31. Yan, J.; Webster, D. C., Thermosets from highly functional methacrylated epoxidized sucrose soyate. *Green Materials* **2014,** *2* (3), 132-143.

32. Webster, D. C.; Yu, A. Z., Biobased highly functional oligomers and thermosets therefrom. U.S. Patent No. 9,765,233: 19 Sep. 2017.

33. Oliver, W. C.; Pharr, G. M., Measurement of hardness and elastic modulus by instrumented indentation: Advances in understanding and refinements to methodology. *Journal of Materials Research* **2004,** *19* (1), 3-20.

34. Jee, A.-Y.; Lee, M., Comparative analysis on the nanoindentation of polymers using atomic force microscopy. *Polymer Testing* **2010,** *29* (1), 95-99.

35. Odian, G., *Principles of Polymerization*. John Wiley & Sons: 2004.

36. Lovelh, L. G.; Newman, S. M.; Bowman, C. N., The effects of light intensity, temperature, and comonomer composition on the polymerization behavior of dimethacrylate dental resins. *Journal of Dental Research* **1999,** *78* (8), 1469-1476.

37. Loshaek, S.; Fox, T. G., Cross-linked polymers. I. Factors influencing the efficiency of cross-linking in copolymers of methyl methacrylate and glycol dimethacrylates1. *Journal of the American Chemical Society* **1953,** *75* (14), 3544-3550.

38. Patel, M. P.; Braden, M.; Davy, K. W. M., Polymerization shrinkage of methacrylate esters. *Biomaterials* **1987,** *8* (1), 53-56.

39. Venhoven, B. A. M.; De Gee, A. J.; Davidson, C. L., Polymerization contraction and conversion of light-curing BisGMA-based methacrylate resins. *Biomaterials* **1993,** *14* (11), 871-875.

40. Lu, H.; Stansbury, J. W.; Dickens, S. H.; Eichmiller, F. C.; Bowman, C. N., Probing the origins and control of shrinkage stress in dental resin-composites: I. Shrinkage stress characterization technique. *Journal of Materials Science: Materials in Medicine* **2004,** *15* (10), 1097-1103.

41. Lu, H.; Stansbury, J. W.; Dickens, S. H.; Eichmiller, F. C.; Bowman, C. N., Probing the origins and control of shrinkage stress in dental resin composites. II. Novel method of simultaneous measurement of polymerization shrinkage stress and conversion. *Journal of Biomedical Materials Research Part B: Applied Biomaterials* **2004,** *71* (1), 206-213.

42. Boaro, L. C. C.; Gonçalves, F.; Guimarães, T. C.; Ferracane, J. L.; Versluis, A.; Braga, R. R., Polymerization stress, shrinkage and elastic modulus of current low-shrinkage restorative composites. *Dental Materials* **2010,** *26* (12), 1144-1150.

CHAPTER 5. CATALYZED NON-ISOCYANATE POLYURETHANE (NIPU) COATINGS FROM BIO-BASED CYCLIC CARBONATES

5.1. Abstract

Concerns on the use of isocyanates as starting materials for polyurethanes (PUs) have risen due to their effects on human health after exposure and also because the synthesis involves the use of phosgene. Polyurethanes are highly versatile materials used in widespread industries such as automotive, building, construction, and packaging. They have also been used in the medical field as flexible and rigid foams, adhesives, coatings, thermoplastic, or thermoset materials. Traditionally, PUs are synthesized from polyols and isocyanates. In order to circumvent the concerns, much research has been devoted to exploring alternative approaches to the synthesis of PUs. Non-isocyanate polyurethane (NIPU) synthesis using cyclic carbonates has gained popularity as one of the new approaches.

In this study, novel bio-based resins are synthesized by converting epoxidized sucrose soyate (ESS) into carbonated sucrose soyate (CSS) under super critical conditions. Initial studies have shown promise in systems where CSS is crosslinked with multifunctional amines generating coatings with good solvent resistance. This study will focus on studying the effect of catalysts and developing formulations of bio-based non-isocyanate polyurethane coatings.

5.2. Introduction

Polyurethanes (PUs) are a general class of polymers that have been widely used in a wide variety of applications such as apparel, appliances, building, construction, flooring, and athletic equipment.[1, 2] PUs have continued to attract the attention due to their high elasticity, hydrolytic stability, and good resistance to abrasion, chemicals, and solvents. PUs have also found their utility in biomedical applications as foams, adhesives, etc.[3, 4] However, one of the greater

challenges of polyurethanes is in their preparation. The classical approach in synthesizing polyurethanes involves the reaction of polyols with polyisocyanates (Scheme 5.1). Increased concerns on the effects of isocyanate exposure on human health spurred the interest in exploration of non-traditional approaches in manufacturing polyurethanes.[5, 6] Additionally, the precursor of isocyanates involves the use of phosgene, which is another chemical that requires special precautions.

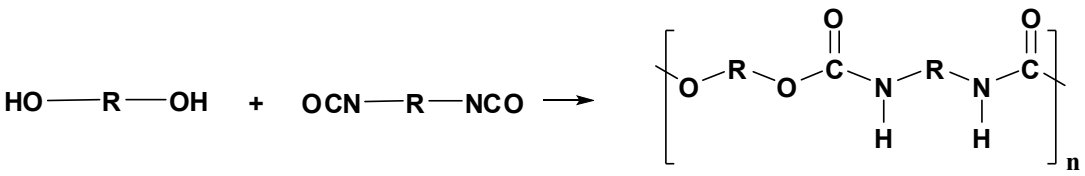

Scheme 5.1. Synthetic route of polyurethanes from polyols and polyisocyanates.

Rokicki *et al.*[7] published a comprehensive review on the syntheses, properties, and applications of non-isocyanate polyurethanes (NIPUs). Included in the synthesis section are the alternative routes in synthesizing polyurethanes. The non-traditional approaches were generally classified into: polycondensation reactions, rearrangement reactions, ring-opening polymerizations (ROPs), and step-growth polyaddition. Polycondensation reactions included reactions between chloroformates and amines or carbamates and alcohols. Rearrangement reactions mostly consisted of carboxylic acid derivatives undergoing rearrangement in the presence of alcohols. These rearrangement reactions were Curtius rearrangement of acyl azides, Hoffman rearrangement of carboxamides, and Lossen rearrangement of hydroxamic acids. For the ring-opening polymerizations, the starting compounds are cyclic urethanes, which unravels into polyurethanes. Step-growth polyaddition of cyclic carbonates and amines were found to be the most promising approach among the different alternative routes (Scheme 5.2).

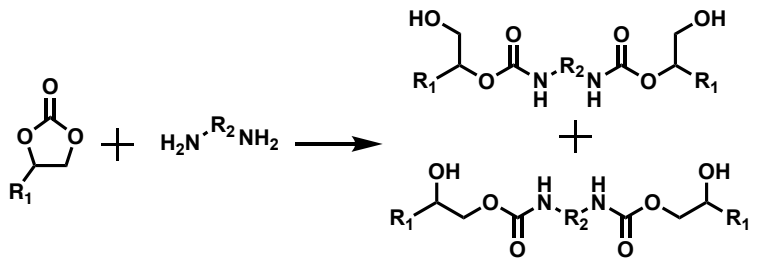

Scheme 5.2. Synthetic route of polyurethanes from cyclic carbonates and amines.

The polyurethane product formed by a cyclic carbonate with an amine contains hydroxyl groups (also called polyhydroxyurethanes PHUs), which is a difference from the polyurethane formed by the traditional polyol and polyisocyanate reaction. Terminal cyclic carbonates may form either primary or secondary hydroxyl groups depending on the cleavage due to reaction conditions and/or the substituent adjacent to it (Scheme 5.2). Several reviews in the field of NIPUs have been published in the last few years.[8-12] Much research has been devoted in this field and investigative work has been done on synthesis, reaction parameters, mechanistic studies, kinetic studies, properties, applications in coatings, composites, construction, and biomedical fields.

One of the more direct preparations of cyclic carbonates is via the epoxide precursors.[13-15] Epoxidized soybean oil (ESBO) is obtained from renewable resources and used in the production of thermoset resins. The high reactivity of the epoxide group makes its transformation easily accessible to form other functional groups. Converting ESBO to carbonated soybean oil (CSBO) has been studied, as well as their application in producing NIPUs.[16-18]

Sucrose soyate (SEFOSE 1618U, Figure 5.1), made by Procter & Gamble (P&G) Chemicals[19-21], was converted via the Prilezhaev reaction to epoxidized sucrose soyate (ESS, Figure 5.2).[22] Two of the interesting features of ESS are the rigid sucrose core and the higher functionality per molecule (11-12 functional groups). Hypothetically, molecules containing

higher functionalities, such as ESS, could generate high crosslink densities at any given degree of conversion. Webster has explored several crosslinking technologies offered by ESS (Figure 5.2) in coatings applications and found that crosslink densities are much higher than the soybean oil counterparts.[23-30]

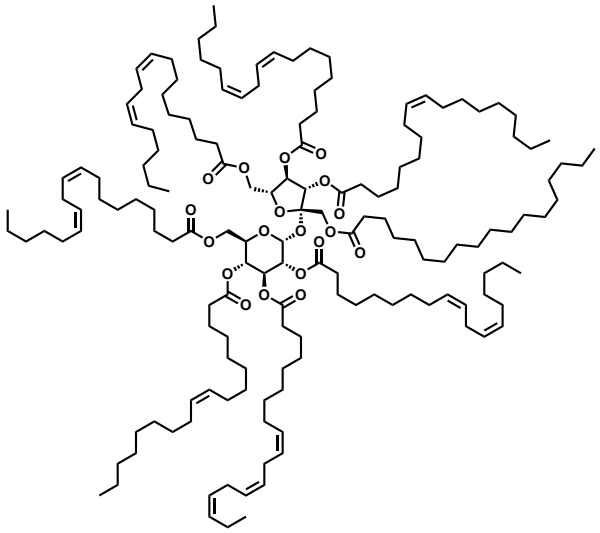

Figure 5.1. Structure of sucrose soyate (SEFOSE 1618U).

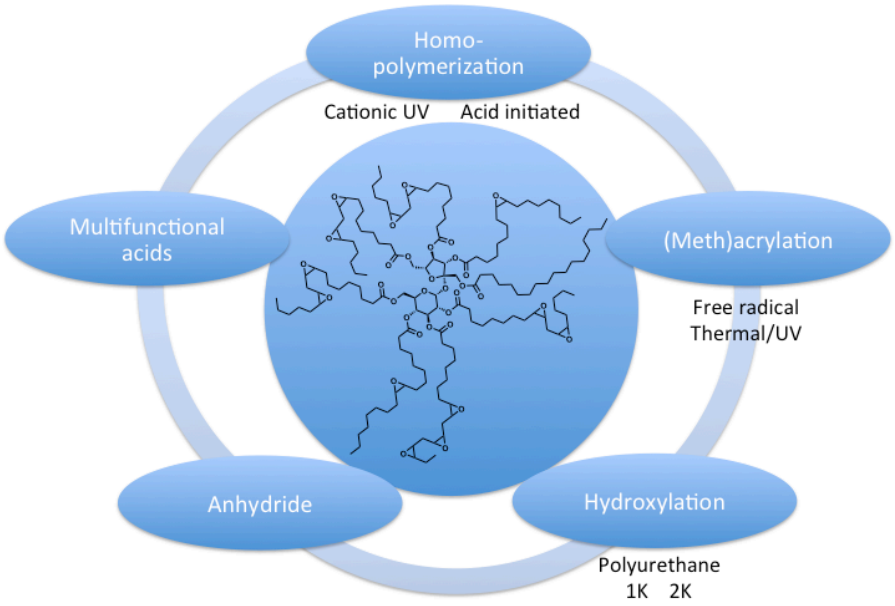

Figure 5.2. Crosslinking technologies of ESS.

The main objective of the study was to develop non-isocyanate polyurethane coatings from bio-based resins through the crosslinking reaction of internal cyclic carbonates and amines. The main drawback for this crosslinking reaction is the high temperature requirement. In order to overcome this hurdle, catalysis was applied in this study. Ultimately, a cooperative catalysis was deemed necessary to achieve successful crosslinking. Optimization of curing conditions was performed and the coating properties were evaluated and compared against CSBO.

5.3. Experimental

5.3.1. Raw materials

Epoxidized soybean oil (ESBO, Vikoflex 7170) was provided by Arkema (Philadelphia, PA, USA). Epoxidized sucrose soyate (ESS) was previously synthesized from sucrose soyate (SEFOSE 1618U), which was provided by Procter and Gamble Chemicals (Cincinnati, OH, USA), following the protocol from the literature.[31-33] The epoxy equivalent weight (EEW) of ESS was determined by titration according to ASTM D 1652 and was calculated to be 249 g/eq. Toluene, *tert*-Butylammonium bromide (TBAB), xylene, 2-heptanone (MAK), 1,5,7-triazabicyclo[4.4.0]dec-5-ene (TBD), and 1,8-diazabicyclo[5.4.0]undec-7-ene (DBU) were purchased from Sigma Aldrich (St. Louis, MO, USA). Ethyl 3-ethoxypropionate (EEP) was provided by Eastman (Kingsport, TN, USA). Lithium trifluoromethanesulfonate (LiOTf) was purchased from TCI America (Portland, OR, USA). Ethyl acetate and tris(2-aminoethyl)amine (TAEA) were purchased from Alfa Aesar (Ward Hill, Massachusetts, USA).

5.3.2. Synthesis of cyclic carbonates

The general reaction for the synthesis of cyclic carbonates from epoxides is shown in Scheme 5.3. The parameters for the synthesis is to run the reaction under supercritical conditions. The syntheses of the control, carbonated soybean oil (CSBO), and carbonated

sucrose soyate (CSS) followed this protocol.[34] The epoxy equivalent weight (EEW) of the starting materials and the cyclic carbonate products were determined by titration according to ASTM D 1652 and used to determine the conversion.

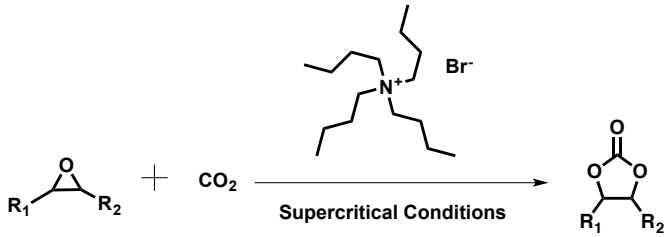

Scheme 5.3. Synthesis of cyclic carbonates from epoxides.

5.3.2.1. Synthesis of carbonated soybean oil (CSBO)

CSBO (Scheme 5.4, right) was synthesized by reacting CO_2 with epoxidized soybean oil (Scheme 5.4, left) (ESBO) (1000 g) under supercritical CO_2 conditions at 140°C and 152 bar and stirred at 222 rpm for 18 h in an 8-L high pressure reactor by Parr Instruments using 5.00 wt% (based on epoxidized soybean oil) of tetrabutylammonium bromide (TBAB) as catalyst (50 g). After reaction, the CO_2 pressure was released upon venting. The reactor was allowed to cool down to 40°C and the viscous amber product was collected. The mixture was dissolved in 1000 mL ethyl acetate and filtered. The mixture was then washed with brine solution to extract the catalyst. Both water and ethyl acetate were removed via rotary evaporator.

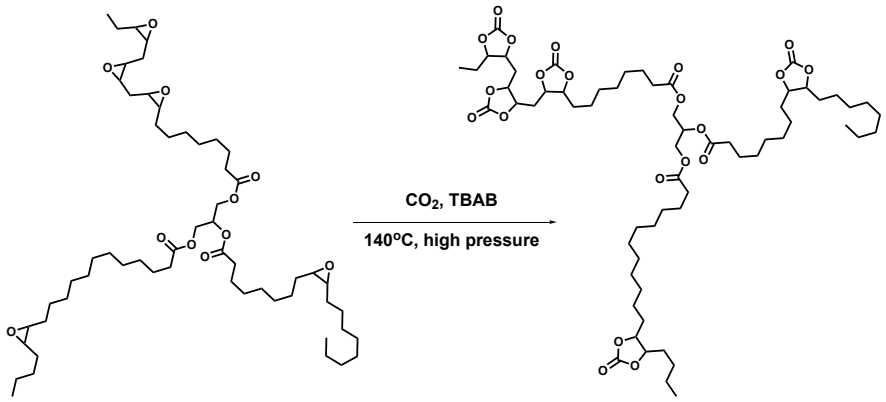

Scheme 5.4. Synthetic route of ESBO to CSBO under supercritical conditions.

5.3.2.2. Synthesis of carbonated sucrose soyate (CSS)

CSS (Scheme 5.5, right) was synthesized by reacting CO_2 with epoxidized sucrose soyate (ESS) (1000 g) in toluene (1:1 wt ratio) under supercritical CO_2 conditions at 140°C, 131 bar, and stirred at 222 rpm for 20 hours in an 8-L high pressure reactor using 5.00 wt% (based on ESS) of tetrabutylammonium bromide (TBAB) as catalyst (50 g). After reaction, the CO_2 pressure was released upon venting. The reactor was allowed to cool down to 40°C and the viscous amber mixture were collected. The mixture was dissolved in 1050 mL ethyl acetate and filtered. The mixture was then washed with brine solution to extract the catalyst. Toluene, water, and ethyl acetate were removed via rotary evaporator. Wiped film evaporator was used to further remove trace toluene from the mixture.

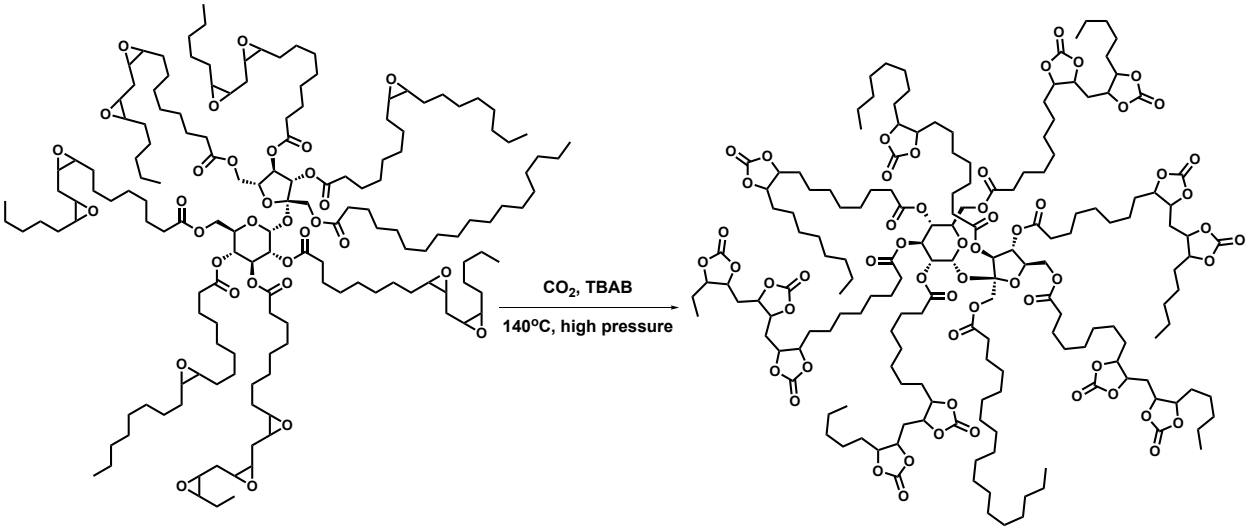

Scheme 5.5. Synthetic route of ESS to CSS under supercritical conditions.

5.3.3. Characterization of cyclic carbonates

Weight percent solids of the resins were determined according to ASTM D 2369. Measurements were performed in triplicate and the average was reported. The viscosity of the resins was measured at 25°C using an ARES Rheometer (TA Instruments) operating from 0.1 rad/s to 500 rad/s with 0.1% strain. Densities were measured following ASTM D 1475.

Functional groups were confirmed using Fourier transform infrared spectroscopy (FTIR) and was performed with a Thermo Scientific Nicolet 8700 with a DTGS KBr detector under nitrogen purge. Thin films of the samples were applied on a KBr plate and the absorption spectra were taken with 32 scans at a resolution of 4 cm^{-1} in the range of 4000-400 cm^{-1}. Proton nuclear magnetic resonance spectroscopy (^{1}H-NMR) was used in structure elucidation and conducted with a Bruker system, Ascend 400 MHz magnet with an Avance III HD console (Bruker BioSpin Corporation, Billerica, Massachusetts, USA), using deuterated chloroform ($CDCl_3$) as the solvent. The number-average molecular weight (M_n) of the resins were obtained using a GPC system (EcoSEC HLC-8320GPC, Tosoh Bioscience, Japan) with a differential refractometer (DRI) detector. Separations were performed using two TSKgel SuperH3000 6.00 mm ID×15 cm columns. The temperature of the columns and detectors were maintained at 40°C. Tetrahydrofuran (THF) was used as the eluent with a flow rate of 0.35 mL min^{-1}. Samples were prepared at nominally 1 mg mL^{-1} in an aliquot of the eluent and dissolved at ambient temperature for several hours and the injection volume was 20 µL for each sample. Polystyrene standards (Agilent EasiVial PS-H 4 mL) were used to perform calibration measurements.

5.3.4. Coating formulations

The catalysts (1.0 wt% of resin) and solvents (35.0 wt%) were added to the carbonated resins and stirred with a magnetic stir bar for 15 minutes. The mixture was sonicated for 20 minutes at room temperature to remove air bubbles. The amine crosslinker was then added to the mixture and then homogenized. Coatings were prepared on bare steel panels at 8 mils wet film thickness and subsequently cured at 80°C for 45 minutes.

5.3.5. Coating properties

The thickness of the coatings on the panels was measured with a Byko-Test 8500 coating thickness gauge. Using the Gardner Micro-TRI-gloss measurement tool, the gloss of each formulation at 20°, 60°, and 85° was measured from the drawdown on the glass panel, along with the mean and standard deviation of each measurement. To determine hardness, the coatings were first subjected to König pendulum hardness following ASTM D 4366 and also with pencil hardness following ASTM D 3363. Adhesion to the substrate was characterized by crosshatch adhesion using ASTM D 3359. Flexibility was measured via conical mandrel bend (ASTM D 522), which measures slow deformation while reverse impact (ASTM D 2794) measures rapid deformation. Solvent resistance gives an indication of crosslink density and was measured using a modified version of ASTM D 5402. The head of a 26-ounce hammer was wrapped in 6 layers of cheesecloth and saturated with methyl ethyl ketone (MEK). This was then placed at the base of the coating and allowed to rub the coating back and forth, recording the number of double rubs until coating failure was observed. Failure was reached when substrate was exposed. The hammer was rewet with MEK after 50 double rubs.

A Q500 thermogravimetric analysis (TGA) system (TA Instruments) with a heating rate of 20°C/min from room temperature to 600°C under a continuous nitrogen flow, was used to determine the thermal stability of the thermosets. A DSC Q1000 (TA Instruments) with heating and cooling rates of 10°C/min at a heat/cool/heat cycle scanned from 0°C to 100°C under nitrogen atmosphere, was used to measure the glass transition temperatures (T_g) of the coatings.

The extent of cure was evaluated using a Vertex 70 Fourier transform infrared (FTIR) spectrometer (Bruker Optics) with an attenuated total reflectance (ATR) accessory. The beam was irradiated an angle of 45° and the crystal was made of Germanium. Samples were placed

directly on top of the crystal and absorption spectra were taken with 32 scans at a resolution of 4 cm^{-1} in the range of 4000-400 cm^{-1}.

5.4. Results and discussion

5.4.1. Synthesis and characterization of cyclic carbonates

The catalytic mechanism of synthesizing cyclic carbonates from epoxides is shown in Scheme 5.6. Under supercritical conditions, the *t*-butylammonium ion activates the epoxide ring followed by the nucleophilic attack by the bromide ion. The activated intermediate then attacks the carbon dioxide and undergoes rearrangement to form the carbonate intermediate. The last step is the formation of the cyclic carbonate, which simultaneously allows the bromide to leave and the catalyst to be released.

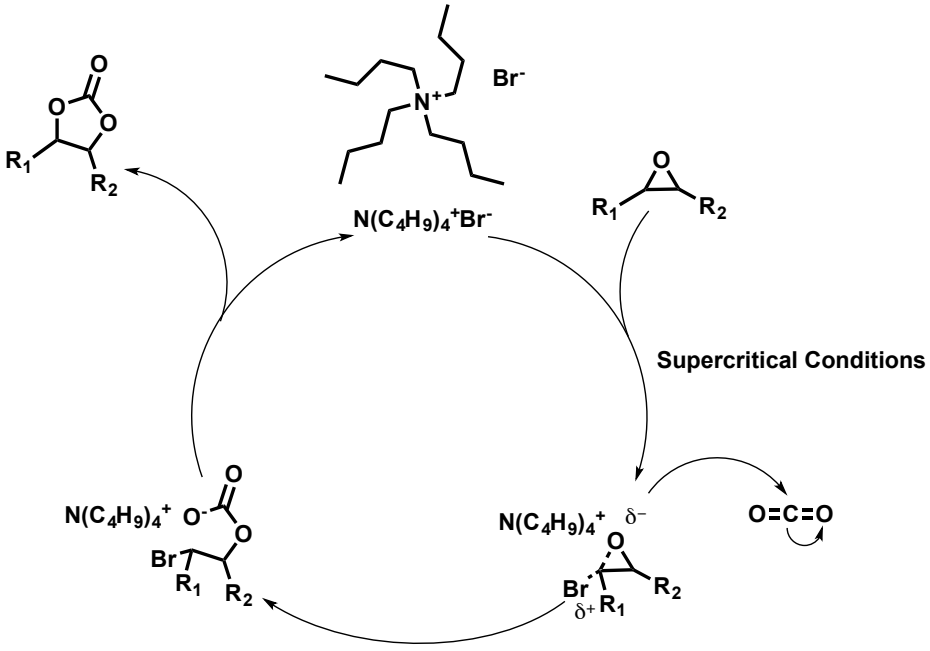

Scheme 5.6. Reaction mechanism of the catalytic synthesis of cyclic carbonates from epoxides.

Table 5.1 shows a summary of the properties of ESBO, ESS, CSBO, and CSS. The increase in density of ESBO to CSBO and ESS to CSS is characteristic of the carbonation. The noticeable increase of M_n from ESBO to CSBO and ESS to CSS is also an indication that the

epoxies have been converted to carbonates. The epoxy functionality was calculated using the number-average molecular weight from GPC and epoxy equivalent weight (EEW). The EEW's were determined by epoxy titration according to ASTM D 1652. CSBO gave an epoxy functionality of 0.25, which indicates a small amount of unreacted epoxies, while CSS gave an epoxy functionality of 3.98, which indicates a considerable amount of unreacted epoxies. From this, the carbonate functionalities were determined to be 4.14 and 7.41 for CSBO and CSS, respectively. The viscosities also dramatically increased from 4.20 Pa•s to 45.52 Pa•s for ESBO to CSBO and 0.97 Pa•s to 1382 Pa•s for ESS to CSS which also suggests conversion of epoxy groups to carbonate groups.

Table 5.1. Resin properties.

Resin	Density	% Solids	M_n	EEW	EW	Epoxy functionality	Carbonate functionality	Viscosity (Pa•s)
ESBO	0.994	99.78	1000	228	228	4.39	-	4.20
ESS	0.997	96.37	2836	249	249	11.39	-	0.97
CSBO	1.0907	95.82	1413	5743	341	0.25	4.14	45.52
CSS	1.1098	97.58	3254	818	439	3.98	7.41	1382

Figure 5.3 shows the FTIR spectra of CSBO and CSS, which confirm the presence of the carbonyl peak formed by the carbonate groups. The ratio of the carbonate carbonyl peak to the ester carbonyl peak is larger due to the higher molecular functionality of CSS than CSBO. Figure 5.4 shows the proton NMR spectra of CSBO and CSS. The peaks corresponding to the protons of the carbonates are identified (Figure 5.4). However, both spectra show peaks from the epoxy protons, which indicates incomplete conversion. This was likewise evident from their corresponding calculated epoxy and carbonate functionalities.

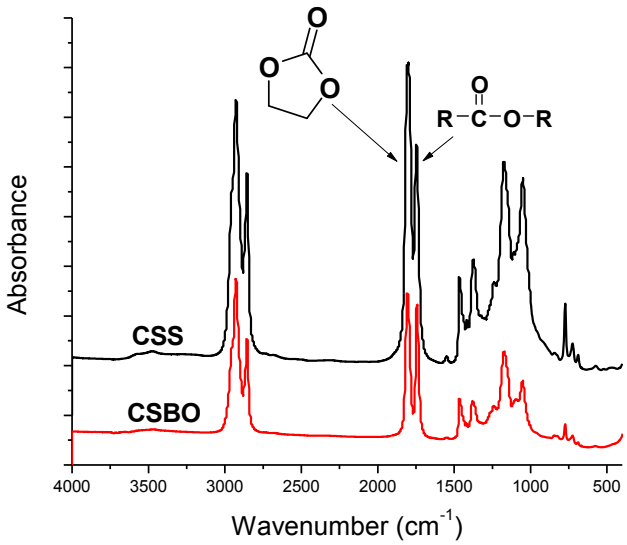

Figure 5.3. FTIR spectra of CSBO and CSS.

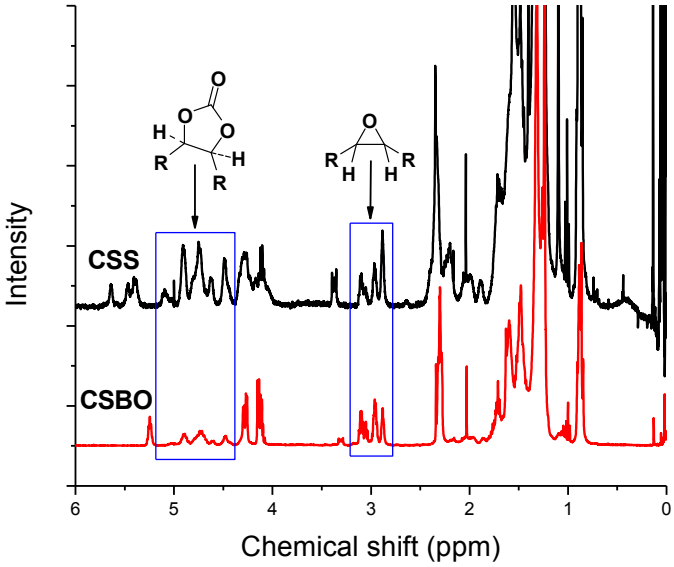

Figure 5.4. ^{1}H-NMR spectra of CSBO and CSS.

5.4.2. Coating formulations

Four different organic solvents were chosen to be evaluated for CSS solubility: EEP, toluene, xylene, and MAK. Solvent compatibility was determined by weighing equal amounts of the resin and solvent, and recording the time it takes to reach homogeneity. The viscosity was qualitatively labeled as low, mid, or high viscosity. Observations are tabulated in Table 5.2. The

solubility and compatibility of the catalyst, TBD (Figure 5.5), were also determined in a similar fashion using the same set of solvents. Results are summarized in Table 5.3. Toluene and MAK were identified as solvents that effectively solubilized both the resin and catalyst.

Table 5.2. Resin solubility in organic solvents.

Solvent	Mass of CSS (g)	Mass of Solvent (g)	Time (sec)	Observations
EEP	0.5413	0.5076	349	mid viscosity
Toluene	0.4978	0.5016	294	mid viscosity
Xylene	0.5138	0.5060	302	high viscosity
MAK	0.5334	0.5405	264	low viscosity

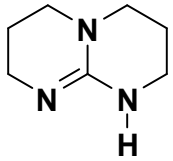

Figure 5.5. Structure of triazabicyclo[4.4.0]dec-5-ene (TBD).

Table 5.3. Catalyst solubility in organic solvents.

Solvent	Solution of TBD	Time (sec)	Solubility
EEP	5%	60	-
Toluene	5%	10	+
Xylene	5%	60	-
MAK	5%	18	+

Formulations of CSS, amine crosslinker, TBD, and solvents, cured at 120°C for 3 hours, were studied (Scheme 5.7). The amine crosslinker chosen was tris(2-aminoethyl)amine (TAEA) since it has previously showed promising coating properties for the uncatalyzed NIPU coatings. The curing condition of 120°C for 3 hours was obtained from Poussard *et al*.[16] The appropriate amount of solids for the formulations was varied beginning from 45% and gradually increased to 75% (Table 5.4). Formulations containing 45% solids spread out as they were coated onto steel substrates and resulted to tacky coatings. On the contrary, 70% and 75% solids formulations

prematurely gelled. Formulations with 60% and 65% solids afforded coatings with good wettability and no premature gelation was observed.

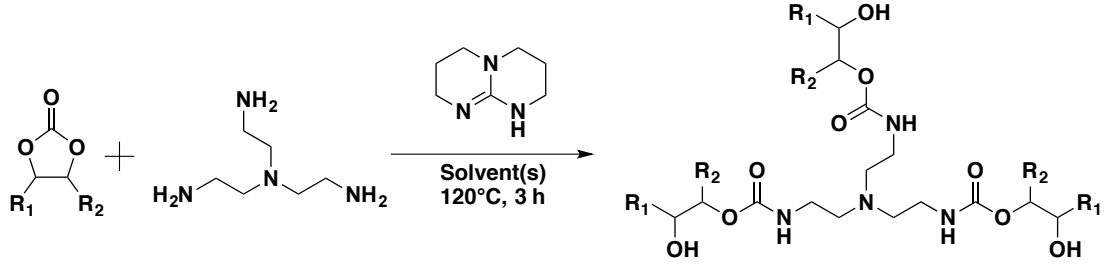

Scheme 5.7. Crosslinking reaction of CSS with TAEA catalyzed by TBD.

Table 5.4. Optimization of solids content of coating formulations.

Solids content (%)	Solvent(s)	Observations
45	MAK/Toluene	Viscosity too low
60	Toluene	Good coating
65	Toluene	Good coating
70	Toluene/EEP	Low MEK DRs/ Formulation gels
75	MAK/EEP	Fast gelling

Note: Formulations with TAEA and 5% TBD were cured at 120°C for 3 hours.

The effect of catalyst amount on solvent resistance was also studied. Table 5.5 summarizes the results and the trend suggests that increasing the amount of catalyst has the effect of reducing the solvent resistance. The formulation containing 5% TBD (entry 2) gave a more visually aesthetic coating than the one with 3% TBD (entry 1). However, the solvent resistance was compromised and decreased from 230 MEK double rubs (DRs) to 70 MEK DRs. At 8% TBD (entry 3), premature gelation was observed and solvent resistance provided 25 MEK DRs.

Table 5.5. Effect of catalyst amount on solvent resistance.

Entry	% TBD	Observations	MEK DRs
1	3	Slight turbidity	230
2	5	Good coating	70
3	8	Fast gelling	25

Note: Formulations with TAEA were 60% solids, in toluene, and cured at 120°C for 3 hours.

EEP has been used as a tailing solvent in coating formulations due to its high boiling point. Table 5.6 shows a summary of the effect of EEP in combination with toluene and MAK. In all cases where EEP was used as tailing solvent, the EEP to main solvent ratio was 1:3 by weight. The addition of EEP seemed to have opposing effects on solvent resistance (compare entries 1 and 3 against entries 2 and 4). In the absence of the catalyst (entries 5 and 6), the solvent resistance dramatically improved from 150 to 275 MEK DRs (compare entries 3 and 5) and 62 to >400 MEK DRs (compare entries 4 and 6). Without the use of EEP, hazy coatings were produced while its presence improves the overall coating appearance. From these results, it was determined that EEP/toluene (1:3 w/w) was the best solvent system.

Table 5.6. Effect of EEP on solvent resistance.

Entry	Solvent(s)	% TBD	MEK DRs
1	MAK	5	327
2	Toluene	5	50
3	EEP/MAK (1:3 w/w)	5	150
4	EEP/Toluene (1:3 w/w)	5	62
5	EEP/MAK (1:3 w/w)	0	275
6	EEP/Toluene (1:3 w/w)	0	>400

Note: Formulations with TAEA were 65% solids and cured at 120°C for 3 hours.

As can be seen, increasing the amount of TBD reduces crosslinking of the network as determined by MEK resistance. A study by Lambeth *et al.*[35] showed that TBD is a dual activating catalyst (Figure 5.6). The intermediate formed increases the nucleophilicity of the hydroxyl group, which could undergo intramolecular reaction with a proximal cyclic carbonate and result in lower crosslink density.

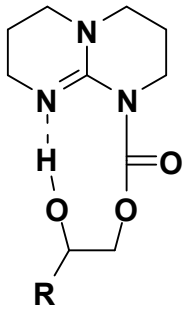

Figure 5.6. Structure of intermediate of TBD and carbonate during dual activation.[35]

5.4.3. Coatings properties

DBU (Figure 5.7) is another common catalyst used for PU synthesis and is structurally analogous to TBD. However, DBU only has a single active site. The activity of DBU was investigated and compared with TBD-catalyzed coatings. Table 5.7 summarizes the coating properties of the formulations with varying catalyst amount and cured at 120°C for 3 hours. Generally, all the coatings showed similar results in pencil hardness, crosshatch adhesion, reverse impact test, and conical mandrel bend. Reverse impact test showed that without any catalyst, the CSS-based coating (entry 14) failed at 96 in•lbs while addition of 1% DBU improved it to 128 in•lbs (entry 12) and 1% TBD improved it to 172 in•lbs (entry 10). It seemed that the solvent resistance and reverse impact results of the coatings were at best with CSS (entry 10) with 1% TBD. The trends (Figure 5.8) also indicate a higher dependence of the coating performance on the resin (CSS > CSBO).

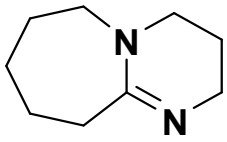

Figure 5.7. Structure of 1,8-diazabicyclo[5.4.0]undec-7-ene (DBU).

Table 5.7. Coating properties with varying catalyst type and amount.

Entry	Resin	Catalyst	% catalyst	Thickness (μm)	MEK DRs	König Pendulum Hardness (sec)	Pencil Hardness	Crosshatch Adhesion	Reverse Impact (in•lbs)	Conical Mandrel (Elongation-at-break)
1	CSBO	TBD	5	63.8	170	27	4H	5B	172	>28%
2	CSS			53.4	93	22	2H	5B	172	>28%
3	CSBO	DBU		54.3	90	28	3H	5B	172	>28%
4	CSS			52.6	265	67	2H	5B	172	>28%
5	CSBO	TBD	3	43.3	93	31	3H	5B	172	>28%
6	CSS			51.6	187	34	2H	5B	172	>28%
7	CSBO	DBU		54.9	68	27	3H	5B	172	>28%
8	CSS			51.3	226	59	2H	5B	172	>28%
9	CSBO	TBD	1	50.0	75	29	3H	5B	172	>28%
10	CSS			51.1	>400	65	2H	5B	172	>28%
11	CSBO	DBU		59.2	56	26	3H	5B	172	>28%
12	CSS			50.7	>400	68	2H	5B	128	>28%
13	CSBO	None		79.1	65	28	2H	5B	172	>28%
14	CSS			58.2	>400	60	3H	5B	96	>28%

Note: Formulations with TAEA were 65% solids, in EEP:toluene (1:3), and cured at 120°C for 3 hours.

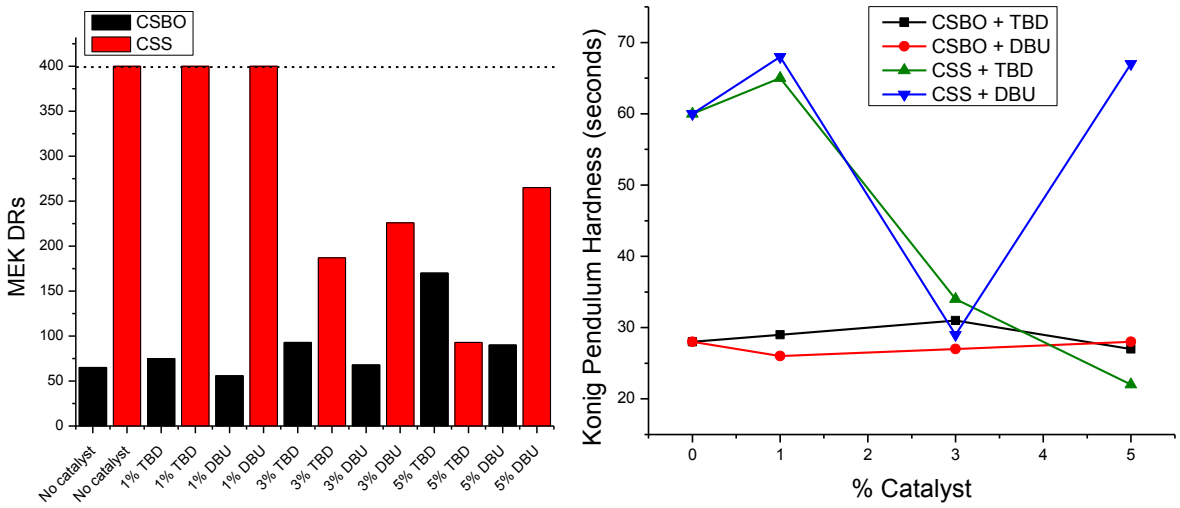

Figure 5.8. Solvent resistance (left) and König pendulum hardness (right) as functions of catalyst and catalyst amount.

5.4.4. Curing studies

5.4.4.1. Effect of catalysts

The MEK DR results in Table 5.7 showed that CSS gave >400 with 1% of TBD or DBU. On the other hand, CSBO gave its highest solvent resistance at 170 MEK DRs when 5% of TBD was used. For this reason, it was hypothesized that mixing TBD and DBU could potentially have a synergistic effect to achieve an optimized catalyzed formulation for both resins. Table 5.8 summarizes the coating properties of formulations with mixed catalysts. Overall, the coatings retained their performance in terms of pencil hardness, crosshatch adhesion, reverse impact, and conical mandrel bend. Unfortunately, mixing TBD and DBU resulted in antagonistic effect and compromised the solvent resistance (<400 MEK DRs, Figure 5.9 left) in every case (entries 3-8). Nonetheless, the König pendulum hardness remained higher for CSS-based coatings (Figure 5.9 right) than the CSBO controls.

Table 5.8. Coating properties with mixed catalysts.

Entry	Resin	% catalyst	Thickness (μm)	MEK DRs	König Pendulum Hardness (sec)	Pencil Hardness	Crosshatch Adhesion	Reverse Impact (in•lbs)	Conical Mandrel (Elongation-at-break)
1	CSBO	3% TBD	43.3	93	31	3H	5B	172	>28%
2	CSS		51.6	187	34	2H	5B	172	>28%
3	CSBO	2% TBD + 1% DBU	51.4	161	28	4H	5B	172	>28%
4	CSS		48.6	196	53	2H	5B	172	>28%
5	CSBO	1.5% TBD + 1.5% DBU	52.4	132	26	4H	5B	172	>28%
6	CSS		68.0	123	55	3H	5B	112	>28%
7	CSBO	1% TBD + 2% DBU	49.0	141	25	4H	5B	172	>28%
8	CSS		46.5	97	72	3H	5B	172	>28%
9	CSBO	3% DBU	54.9	68	27	3H	5B	172	>28%
10	CSS		51.3	226	59	2H	5B	172	>28%

Note: Formulations were 65% solids, in EEP:toluene (1:3), and cured at 120°C for 3 hours.

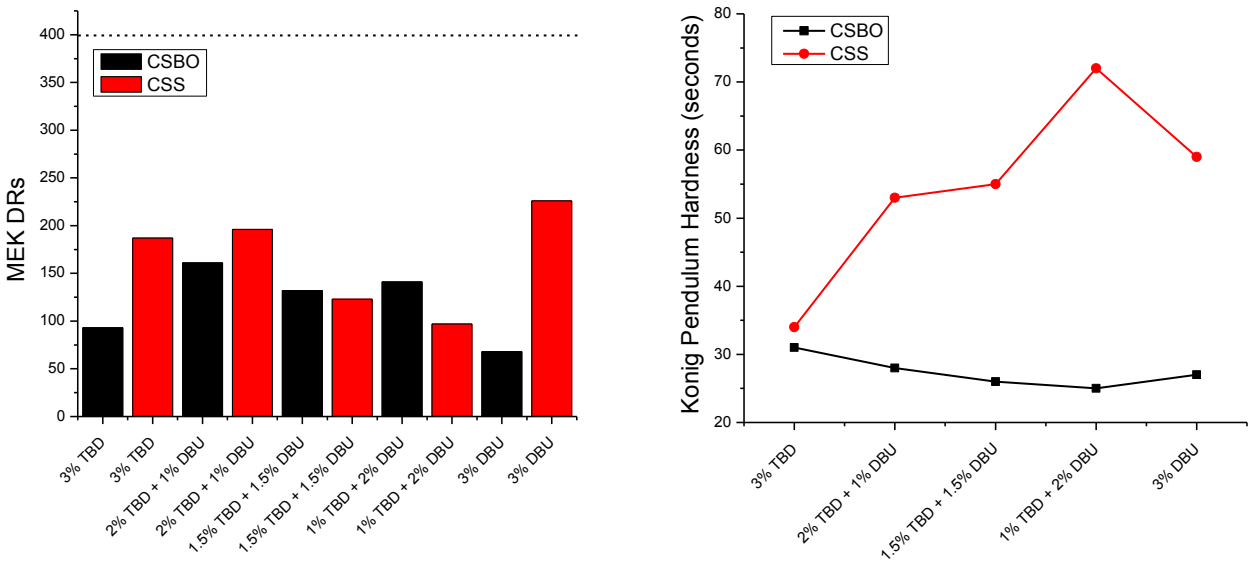

Figure 5.9. Solvent resistance (left) and König pendulum hardness (right) as a function of catalyst systems.

5.4.4.2. Effect of temperature

The crosslinking reaction of cyclic carbonates and amines require high temperatures in order to proceed to completion. The addition of catalysts aids the reaction by lowering the activation energy of the system. Since TBD has been shown to catalyze the crosslinking reaction, the effect of the cure temperature was investigated in order to determine the lowest possible temperature required to maintain the high solvent resistance of the coatings. Table 5.9 summarizes the temperature study. Once again, pencil hardness, crosshatch adhesion, impact, and conical mandrel bend retained their performance as seen previously. Lowering the temperature (100°C and 80°C) resulted in compromised solvent resistance (<400 MEK DRs, Figure 5.10 left). König pendulum hardness consistently gave better results with CSS-based coatings than CSBO-based coatings (Figure 5.10 center). In conjunction with solvent resistance, the reverse impact results decreased from 172 to 128 in•lbs at the cure temperature of 80°C (Figure 5.10, right).

Table 5.9. Coating properties at different curing temperatures.

Entry	Resin	1% catalyst	Curing schedule (°C, hours)	Thickness (μm)	MEK DRs	König Pendulum Hardness (sec)	Pencil Hardness	Crosshatch Adhesion	Reverse Impact (in•lbs)	Conical Mandrel (Elongation -at-break)
1	CSBO	TBD	120, 3	50.0	75	29	3H	5B	172	>28%
2	CSS			51.1	>400	65	2H	5B	172	>28%
3	CSBO	DBU		59.2	56	26	3H	5B	172	>28%
4	CSS			50.7	>400	68	2H	5B	128	>28%
5	CSBO	TBD	100, 3	74.8	44	33	2H	5B	172	>28%
6	CSS			56.9	166	62	2H	5B	172	>28%
7	CSBO	DBU		69.9	34	35	2H	5B	172	>28%
8	CSS			55.5	237	68	2H	5B	172	>28%
9	CSBO	TBD	80, 3	54.4	124	23	2H	5B	128	>28%
10	CSS			55.2	197	49	2H	5B	128	>28%
11	CSBO	DBU		41.2	45	21	2H	5B	128	>28%
12	CSS			56.0	171	48	2H	5B	128	>28%

Note: Formulations were 65% solids, in EEP:toluene (1:3), and cured at 120°C for 3 hours.

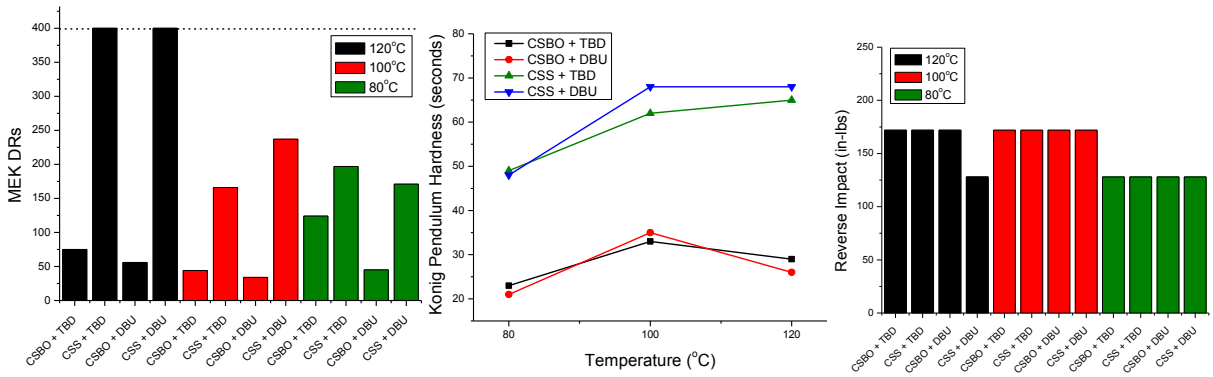

Figure 5.10. Solvent resistance (left), König pendulum hardness (center), and reverse impact (right) as a function of temperature.

5.4.4.3. Cooperative catalysis

Lombardo *et al.*[36] demonstrated cooperative catalysis of a Lewis acid and Lewis base pair in the crosslinking of terminal cyclic carbonates with amines. The best pair was found to be LiOTf as the Lewis acid and TBD as the Lewis base (equimolar). Scheme 5.8 shows the proposed mechanism of the cooperative catalysis. First, LiOTf activates the cyclic carbonate by increasing the electrophilicity of the carbonyl. Then, TBD attacks the activated carbonate to form a tetrahedral intermediate, which collapses to the activated carbamate. The activated carbamate undergoes nucleophilic attack by an amine and subsequent deprotonation of the amine by TBD generates the NIPU and releases the TBD.

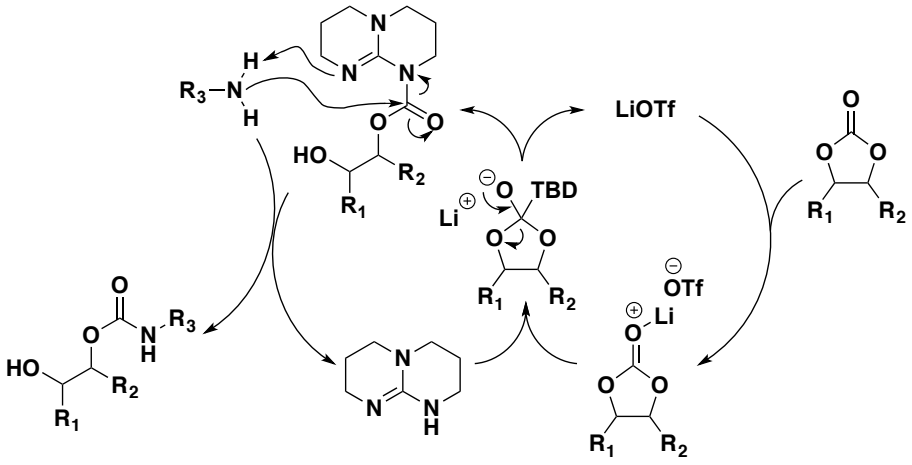

Scheme 5.8. Cooperative catalysis mechanism.

Table 5.10 summarizes the coating properties of the formulations with 1:1 catalyst:LiOTf at different curing conditions. When cured at 100°C without LiOTf (Table 9, entries 5-8), the coating solvent resistance are <400 MEK DRs. However, addition of LiOTf dramatically increased the solvent resistance to >400 (entries 1, 2, and 4) and 346 MEK DRs (entry 3). When the temperature was reduced to 80°C, the CSS formulations remained high (>400 and 371 MEK DRs, entries 6 and 8). Shortening the cure time from 3 hours to 45 minutes did not affect the solvent resistance of CSS-based coatings (>400 MEK DRs, entries 10 and 12) while the CSBO-based ones were reduced from 193 to 122 and 119 to 109 MEK DRs. Due to the promising results, ambient cure condition was also investigated (entries 13-16). CSS-based coatings gave 227 and 224 MEK DRs after one week. Cornille *et al.*[37] recently published their work detailing the effects of cyclic carbonate structure and solvents on forming NIPUs at room temperature. Figure 5.11 shows the differences in solvent resistance (left) and König pendulum hardness (right) of CSS-based coatings to that of CSBO-based coatings as a result of the higher functionality of CSS.

Table 5.10. Coating properties of formulations with 1:1 catalyst:LiOTf.

Entry	Resin	1% catalyst	Curing schedule (°C, time)	Thickness (μm)	MEK DRs	König Pendulum Hardness (sec)	Pencil Hardness	Crosshatch Adhesion	Reverse Impact (in•lbs)	Conical Mandrel (Elongation-at-break)
1	CSBO	TBD	100, 3 h	57.9	>400	47	HB	5B	172	>28%
2	CSS			61.8	>400	83	H	5B	144	>28%
3	CSBO	DBU		53.8	346	51	B	5B	172	>28%
4	CSS			59.1	>400	63	H	5B	144	>28%
5	CSBO	TBD	80, 3 h	52.5	193	46	3H	5B	172	>28%
6	CSS			51.7	>400	95	3H	5B	144	>28%
7	CSBO	DBU		55.0	119	33	2H	5B	172	>28%
8	CSS			49.1	371	81	2H	5B	144	>28%
9	CSBO	TBD	80, 45 min	44.2	122	18	HB	5B	172	>28%
10	CSS			45.5	>400	37	H	5B	172	>28%
11	CSBO	DBU		47.2	109	16	HB	5B	172	>28%
12	CSS			34.2	>400	38	H	5B	172	>28%
13	CSBO	TBD	RT, 1 week	51.5	87	29	3B	5B	172	>28%
14	CSS			56.3	227	56	2B	5B	172	>28%
15	CSBO	DBU		55.7	118	17	4B	5B	172	>28%
16	CSS			53.9	224	54	2B	5B	172	>28%

Note: Formulations were 65% solids and in EEP:toluene (1:3).

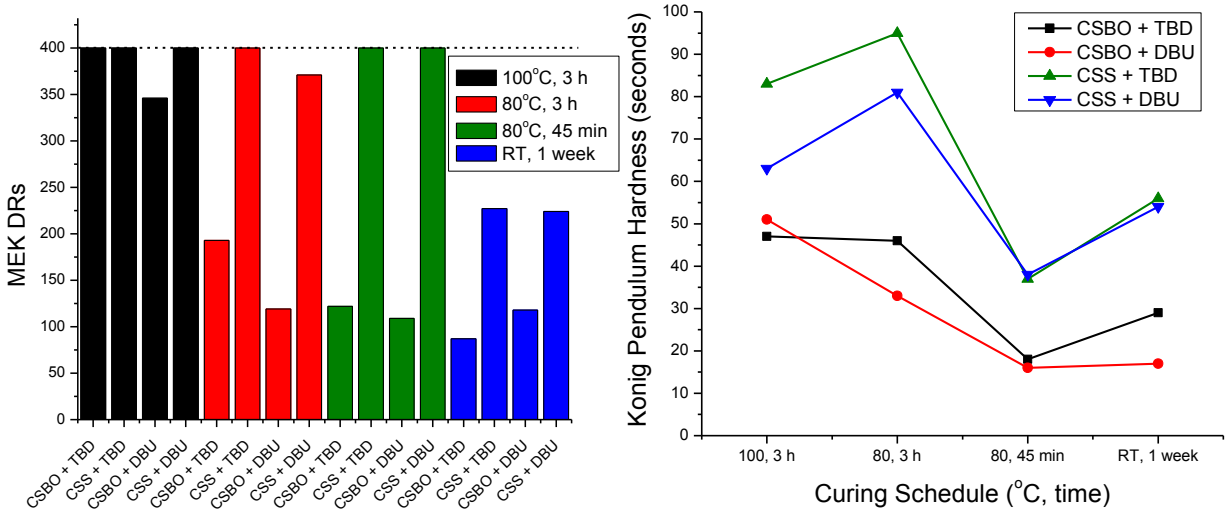

Figure 5.11. Solvent resistance (left) and König pendulum hardness (right) as a function of curing conditions.

5.4.4.4. Effect of solvents

Webster and Crain[38] demonstrated that solvent had little effect on the properties of the NIPU coatings to a large extent. However, Garipov *et al.*[39] showed that protic solvents affect the reaction mechanism by promoting the nucleophilic attack of the amine. Cornille *et al.*[37] performed a kinetic study supporting the hypothesis of Garipov. It also compared how protic deuterated solvents break apart the intramolecular hydrogen bonding, which promotes the reaction. These concepts proved to be consistent with our results summarized in Table 5.11. In general, CSS-based coatings gave greater solvent resistance than CSBO-based coatings when toluene was used as the solvent (Figure 5.12 left). When toluene was replaced with alcohols (2-methoxy-1-propanol and *t*-butanol), the MEK DRs remained relatively high. When *n*-butyl acetate was used to replace toluene, the MEK DRs decreased. Although toluene does not interact thru hydrogen bonding, the bulky phenyl ring could be large enough to encourage mobility in the system than the linear structure of *n*-butyl acetate. Once more, the König pendulum hardness showed greater influence from the resin than the type of solvent used (Figure 5.12 right).

Table 5.11. Coating properties of formulations with 1:1 catalyst:LiOTf with different solvents cured at 80°C for 45 minutes.

Entry	Resin	1% catalyst	Solvents (1:3)	Thickness (μm)	MEK DRs	König Pendulum Hardness (sec)	Pencil Hardness	Crosshatch Adhesion	Reverse Impact (in•lbs)	Conical Mandrel (Elongation-at-break)
1	CSBO	TBD	EEP:toluene	44.2	122	18	HB	5B	172	>28%
2	CSS			45.5	>400	37	H	5B	172	>28%
3	CSBO	DBU		47.2	109	16	HB	5B	172	>28%
4	CSS			34.2	>400	38	H	5B	172	>28%
5	CSBO	TBD	EEP:BA (*n*-butyl acetate)	56.1	129	23	H	5B	172	>28%
6	CSS			46.2	139	42	HB	5B	172	>28%
7	CSBO	DBU		53.9	73	21	H	5B	172	>28%
8	CSS			42.2	211	39	H	5B	172	>28%
9	CSBO	TBD	EEP:PM (2-methoxy-1-propanol)	41.1	135	24	F	5B	172	>28%
10	CSS			41.9	391	46	H	5B	172	>28%
11	CSBO	DBU		38.1	130	25	HB	5B	172	>28%
12	CSS			41.1	>400	47	H	5B	172	>28%
13	CSBO	TBD	EEP:TBOH (*t*-butanol)	50.5	115	21	H	5B	172	>28%
14	CSS			41.7	340	43	F	5B	172	>28%
15	CSBO	DBU		36.6	98	18	H	5B	172	>28%
16	CSS			46.4	>400	61	F	5B	172	>28%

Note: Formulations were 65% solids.

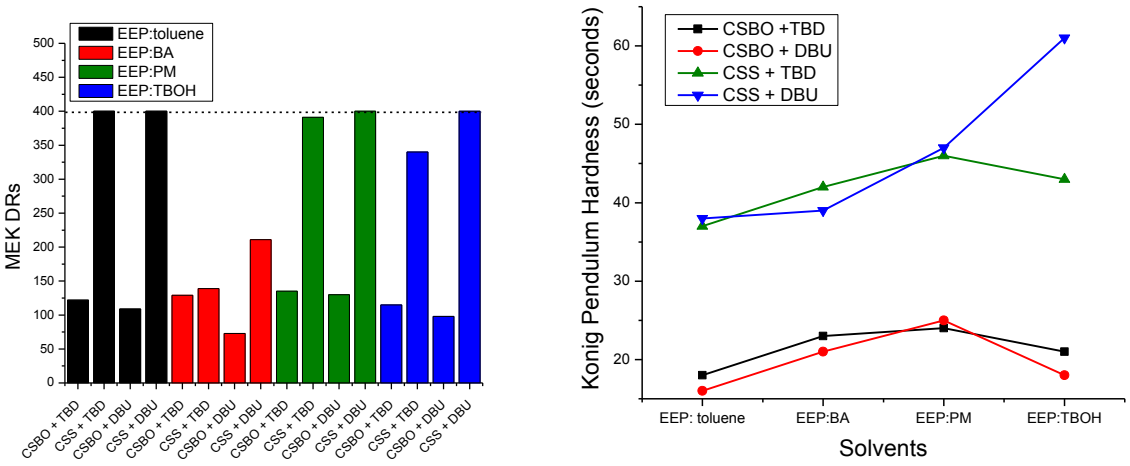

Figure 5.12. Solvent resistance (left) and König pendulum hardness (right) as a function of solvent.

Table 5.12 shows the gloss measurements of the coatings at angles 20°, 60°, and 85°. Generally, polyurethanes have relatively glossy finish. By and large, the values at the gloss angle of 60° gave gloss values >70 gloss units (GU), which correspond to high gloss.

Table 5.12. Gloss measurements of formulations with 1:1 catalyst:LiOTf with different solvents cured at 80°C for 45 minutes.

Entry	Resin	1% catalyst	Solvents (1:3)	Gloss units (GU) 20°	60°	85°
1	CSBO	TBD	EEP:toluene	36.3 ± 1.0	79.0 ± 1.5	86.9 ± 2.2
2	CSS			49.4 ± 1.8	97.5 ± 4.6	94.8 ± 0.9
3	CSBO	DBU		36.9 ± 3.1	72.6 ± 7.5	79.0 ± 10.2
4	CSS			38.3 ± 5.1	88.9 ± 7.6	55.7 ± 4.8
5	CSBO	TBD	EEP:BA (*n*-butyl acetate)	40.0 ± 0.3	90.5 ± 1.8	84.3 ± 1.3
6	CSS			20.8 ± 0.5	98.8 ± 7.2	68.0 ± 6.8
7	CSBO	DBU		36.6 ± 0.7	81.8 ± 1.2	86.4 ± 0.5
8	CSS			21.1 ± 2.7	81.4 ± 4.6	71.4 ± 4.4
9	CSBO	TBD	EEP:PM (2-methoxy-1-propanol)	29.9 ± 0.8	63.1 ± 8.4	23.1 ± 4.9
10	CSS			22.6 ± 3.4	42.1 ± 7.2	15.5 ± 0.9
11	CSBO	DBU		40.5 ± 5.1	87.5 ± 3.1	43.1 ± 5.1
12	CSS			22.8 ± 0.8	34.8 ± 0.9	8.6 ± 1.8
13	CSBO	TBD	EEP:TBOH (*t*-butanol)	31.3 ± 2.3	91.6 ± 0.6	77.3 ± 1.3
14	CSS			28.9 ± 11.6	94.1 ± 3.9	40.2 ± 10.5
15	CSBO	DBU		23.5 ± 0.6	67.9 ± 0.9	57.5 ± 2.3
16	CSS			67.4 ± 5.3	105.0 ± 1.3	76.0 ± 1.1

Note: Formulations were 65% solids.

5.4.4.5. Extent of cure

Coatings were further analyzed using ATR-FTIR. The spectra (Figure 5.13 left) show the presence of a broad peak due to hydroxyl and amino groups that were formed after crosslinking. The formation of a new peak around 1260 cm^{-1} corresponds to the C-N bond due to the carbamate group. There is also a noticeable decrease on the ratio of the cyclic carbonate carbonyl peak to the ester carbonyl peak after crosslinking. Further examination showed that there are at least 4 different types of carbonyl groups present after crosslinking (Figure 5.13 right). The assignment of these carbonyl peaks are as follows: 1800 cm^{-1} cyclic carbonate, 1750 cm^{-1} fatty acid chain esters, 1710 cm^{-1} carbamate, and 1690 cm^{-1} urea side products. The formation of the urea byproducts could have resulted from the transcarbamoylation of the urethane groups when some of the amine crosslinkers attacks the urethane products.

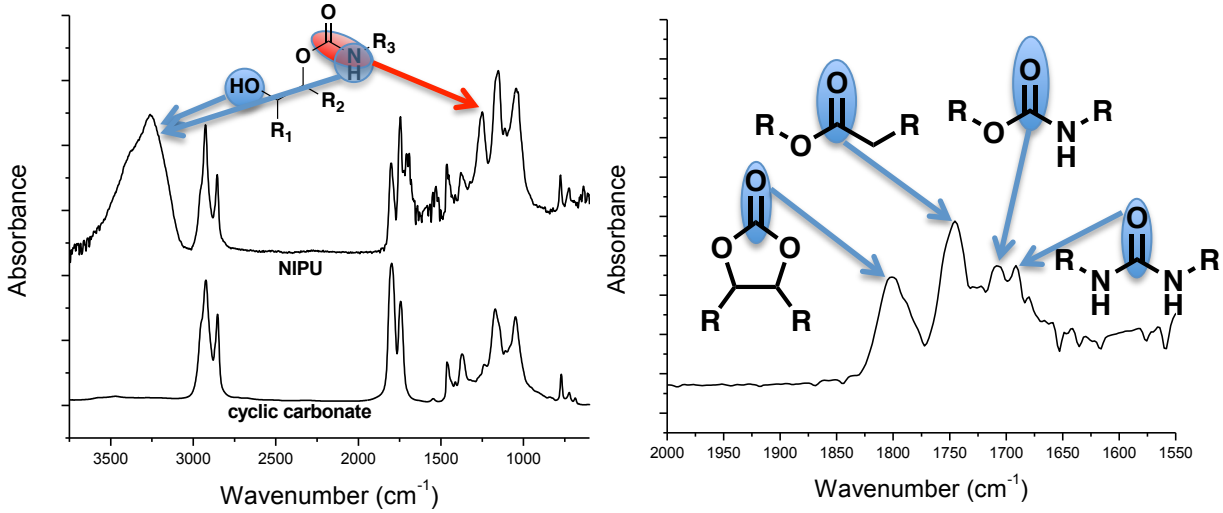

Figure 5.13. Representative ATR-FTIR spectra of a cyclic carbonate and a NIPU (left) and carbonyl region of the NIPU.

5.4.5. Thermal stability and glass transition temperature (T_g)

The thermal stability and T_g of the coatings were also investigated and measured (Table 5.13). Neither varying the solvents nor the type of carbonated resin used seemed to significantly

affect the thermal degradation of the coatings. 5% weight loss were observed at the temperature range of 215-254°C. The thermal degradation behavior of the coatings displayed a single-step decomposition profile. Collectively, the T_g was higher for the coatings made from CSS than their CSBO counterparts. The higher T_gs were expected due to the higher functionality of CSS than CSBO. The T_gs for CSBO-based coatings were in the range of 24-37°C, while that of CSS-based coatings were in the range of 35-58°C. There is a marked T_g improvement when the catalyst was switched from TBD to DBU for the CSS-based coatings but not with the CSBO-based coatings. In each case, the best combination that provides the highest T_g is when CSS and DBU are used together.

Table 5.13. Thermal degradation and glass transition temperatures (T_g) of coatings with 1:1 catalyst:LiOTf in different solvents cured at 80°C for 45 minutes.

Entry	Resin	1% catalyst	Solvents (1:3)	$T_{5\%}$ (°C)	T_g (°C)
1	CSBO	TBD	EEP:toluene	227	24
2	CSS			228	34
3	CSBO	DBU		254	23
4	CSS			248	45
5	CSBO	TBD	EEP:BA	215	37
6	CSS			235	43
7	CSBO	DBU		250	35
8	CSS			241	51
9	CSBO	TBD	EEP:PM	218	39
10	CSS			233	44
11	CSBO	DBU		254	37
12	CSS			238	51
13	CSBO	TBD	EEP:TBOH	218	35
14	CSS			233	49
15	CSBO	DBU		226	37
16	CSS			242	58

Note: Formulations were 65% solids.

5.4.6. Gel point

The main advantage of CSS over CSBO is the higher functionality per molecule. At a given degree of conversion, the crosslink density of CSS will be higher than CSBO. To further

illustrate the difference in crosslink network formation, theoretical gel points (p_c) were calculated using Equation 5.1 derived by Flory and modified by Stockmayer *et al.*[40-46]

$$p_c = \frac{1}{\{r(f_{w,A}-1)(f_{w,B}-1)\}^{1/2}} \quad \text{(Equation 5.1)}$$

where r is the stoichiometric imbalance and $f_{w,A}$ and $f_{w,B}$ are weight-average functionalities of A and B functional groups, respectively. $f_{w,A}$ and $f_{w,A}$ are defined by

$$f_{w,A} = \frac{\sum f_{A_i}^2 N_{A_i}}{\sum f_{A_i} N_{A_i}} \quad \text{(Equation 5.2)}$$

$$f_{w,B} = \frac{\sum f_{B_i}^2 N_{B_i}}{\sum f_{B_i} N_{B_i}} \quad \text{(Equation 5.3)}$$

The summations in Equation 5.2 are for all the molecules containing A functional groups with N_{Ai} representing the number of moles of A_i containing f_{Ai} number of A functional groups per molecule. The same holds true for the B molecules in Equation 5.3. In this case, A corresponds to the cyclic carbonate functionalities while B corresponds to the amino groups. Figure 5.14 was plotted using Equation 1 to calculate for p_c with assumptions of stoichiometrically balanced reagents (r = 1) and multifunctional amines ($f_{w,B} = 2, 3, and\ 4$), taken at f = 2 to 16. Nelson *et al.*[47] calculated the percent weight distribution (Figure 5.15) of the double bonds per molecule of soybean oil and sucrose soyate. These could be translated to the same functionality for the carbonate groups with the assumption that each double bond undergoes complete conversion to the corresponding cyclic carbonate. Using the same distribution (Figure 5.15), the gel points for CSBO and CSS are 0.35 and 0.21, respectively, when crosslinking with trifunctional amines. Using their respective functionalities from Table 1, the gel points are 0.40 (CSBO) and 0.28 (CSS). In both cases, the gel point was reached much sooner by CSS than CSBO, which was typically indicated by the large difference in their solvent

resistance of the coatings they produced. Increasing the functionality of the amine crosslinkers will result in shorter cure times and higher crosslink density (Figure 5.14 vertical dashed lines).

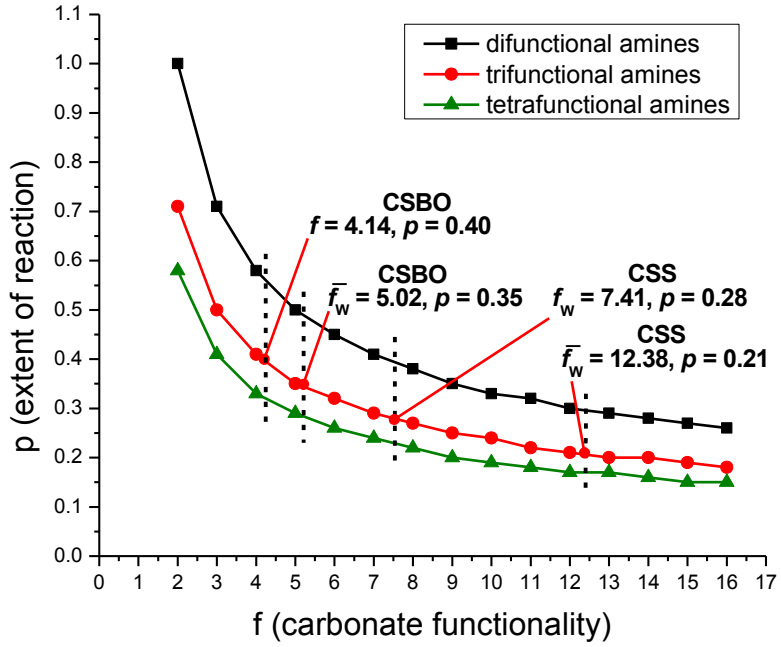

Figure 5.14. Theoretical plot of gel point as a function of cyclic carbonate.

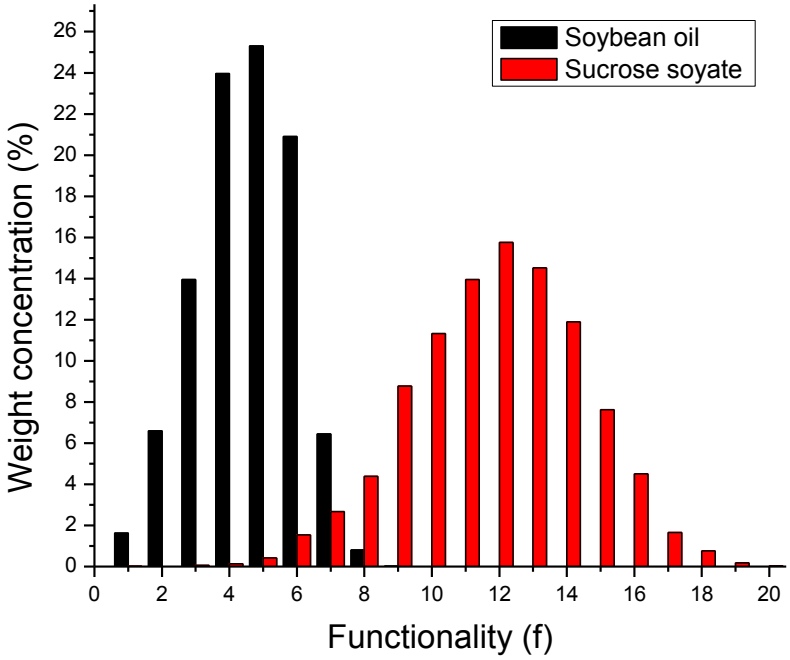

Figure 5.15. Number of double bonds on soybean oil and sucrose soyate. [Reproduced from literature][47]

5.5. Conclusions

Bio-based cyclic carbonates were synthesized under supercritical conditions and reacted with multifunctional amine crosslinkers to develop bio-based non-isocyanate polyurethane coatings. The study optimized the solvents, temperature, and catalyst(s) to establish the best curing conditions. Utilization of EEP as a tailing solvent improved coating appearance and properties. The choice of catalyst is vital since it balances vitrification and coating properties. The addition of a secondary catalyst, namely a Lewis acid (LiOTf), significantly improves the solvent resistance of the coatings. Literature shows that a dual catalyst system consisting of a Lewis acid/Lewis base pair facilitates a cooperative mechanism. Formulations containing the dual catalyst system showed improvement in the coating properties. These coatings also gave promising solvent resistance when allowed to cure at ambient conditions for a week. The formation of hydroxyl groups when cyclic carbonates react with amines introduces hydrogen bonding interactions in the system. Bulky and protic solvents were found to effectively break apart these interactions, thus allowing greater mobility for the polymeric chains. As a result, increased crosslinking gave high solvent resistant coatings. Surface analysis with ATR-FTIR suggests side reactions occurring either due to the transcarbamoylation reaction or the reaction of the unreacted epoxy groups with the amine crosslinkers. Overall, the higher functionality of the carbonated sucrose soyate greatly influenced the improved coating property, effective crosslinking, and glass transition temperatures of the coatings. The difference in crosslinked network was further supported by the calculated gel points for both CSBO and CSS.

5.6. Acknowledgements

This work was supported by the National Science Foundation EPSCoR Award under Grant No. IIA-1355466.

5.7. References

1. Demharter, A., Polyurethane rigid foam, a proven thermal insulating material for applications between+ 130 C and− 196 C. *Cryogenics* **1998,** *38* (1), 113-117.

2. Krol, P., Synthesis methods, chemical structures and phase structures of linear polyurethanes. Properties and applications of linear polyurethanes in polyurethane elastomers, copolymers and ionomers. *Progress in Materials Science* **2007,** *52* (6), 915-1015.

3. Santerre, J. P.; Woodhouse, K.; Laroche, G.; Labow, R. S., Understanding the biodegradation of polyurethanes: from classical implants to tissue engineering materials. *Biomaterials* **2005,** *26* (35), 7457-7470.

4. Zdrahala, R. J.; Zdrahala, I. J., Biomedical applications of polyurethanes: a review of past promises, present realities, and a vibrant future. *Journal of Biomaterials Applications* **1999,** *14* (1), 67-90.

5. Verschoor, L.; Verschoor, A. H., Nonoccupational and occupational exposure to isocyanates. *Current Opinion in Pulmonary Medicine* **2014,** *20* (2), 199-204.

6. Lockey, J. E.; Redlich, C. A.; Streicher, R.; Pfahles-Hutchens, A.; Hakkinen, P. J.; Ellison, G. L.; Harber, P.; Utell, M.; Holland, J.; Comai, A., Isocyanates and human health: Multi-stakeholder information needs and research priorities. *Journal of occupational and environmental medicine/American College of Occupational and Environmental Medicine* **2015,** *57* (1), 44.

7. Rokicki, G.; Parzuchowski, P. G.; Mazurek, M., Non-isocyanate polyurethanes: synthesis, properties, and applications. *Polymers for Advanced Technologies* **2015,** *26* (7), 707-761.

8. Figovsky, O. L.; Leykin, A. D.; Shapovalov, L. L., Non-Isocyanate Polyurethanes-Yesterday, Today and Tomorrow. *International Scientific Journal for Alternative Energy and Ecology* **2016,** (3-4), 95-108.

9. Maisonneuve, L.; Lamarzelle, O. a.; Rix, E.; Grau, E.; Cramail, H., Isocyanate-free routes to polyurethanes and poly (hydroxy urethane) s. *Chemical Reviews* **2015,** *115* (22), 12407-12439.

10. Kathalewar, M. S.; Joshi, P. B.; Sabnis, A. S.; Malshe, V. C., Non-isocyanate polyurethanes: from chemistry to applications. *RSC Advances* **2013,** *3* (13), 4110-4129.

11. Delebecq, E.; Pascault, J.-P.; Boutevin, B.; Ganachaud, F. o., On the versatility of urethane/urea bonds: reversibility, blocked isocyanate, and non-isocyanate polyurethane. *Chemical Reviews* **2012,** *113* (1), 80-118.

12. Guan, J.; Song, Y.; Lin, Y.; Yin, X.; Zuo, M.; Zhao, Y.; Tao, X.; Zheng, Q., Progress in study of non-isocyanate polyurethane. *Industrial & Engineering Chemistry Research* **2011,** *50* (11), 6517-6527.

13. Farhadian, A.; Afshani, G.; Babapour, M.; Babaei Miyardan, A.; Nabid, M. R.; Safari, N., A Facile and Green Route for Conversion of Bifunctional Epoxide and Vegetable Oils to Cyclic Carbonate: A Green Route to CO2 Fixation. *ChemistrySelect* **2017,** *2* (4), 1431-1435.

14. Büttner, H.; Steinbauer, J.; Wulf, C.; Dindaroglu, M.; Schmalz, H. G.; Werner, T., Organocatalyzed synthesis of oleochemical carbonates from CO2 and renewables. *ChemSusChem* **2017,** *10* (6), 1076-1079.

15. Guzmán, A. F.; Echeverri, D. A.; Rios, L. A., Carbonation of epoxidized castor oil: a new bio-based building block for the chemical industry. *Journal of Chemical Technology and Biotechnology* **2017,** *92* (5), 1104-1110.

16. Poussard, L.; Mariage, J.; Grignard, B.; Detrembleur, C.; Jérôme, C.; Calberg, C.; Heinrichs, B.; De Winter, J.; Gerbaux, P.; Raquez, J. M., Non-isocyanate polyurethanes from carbonated soybean oil Using monomeric or oligomeric diamines to achieve thermosets or thermoplastics. *Macromolecules* **2016,** *49* (6), 2162-2171.

17. Javni, I.; Hong, D. P.; Petrović, Z. S., Soy-based polyurethanes by nonisocyanate route. *Journal of Applied Polymer Science* **2008,** *108* (6), 3867-3875.

18. Tamami, B.; Sohn, S.; Wilkes, G. L., Incorporation of carbon dioxide into soybean oil and subsequent preparation and studies of nonisocyanate polyurethane networks. *Journal of Applied Polymer Science* **2004,** *92* (2), 883-891.

19. Howie, J. K.; Schaefer, J. J.; Trout, J. E., Synthesis of polyol medium fatty acid polyesters. U.S. Patent No. 6,995,232: 7 Feb. 2006.

20. Corrigan, P. J., Synthesis of polyol fatty acid polyesters. U.S. Patent No. 6,620,952: 16 Sep. 2003.

21. Schaefer, J. J.; Trout, J. E., Synthesis of purified, partially esterified polyol polyester fatty acid compositions. U.S. Patent No. 6,887,947: 3 May 2005.

22. Webster, D. C.; Sengupta, P. P.; Chen, Z.; Pan, X.; Paramarta, A., Highly functional epoxidized resins and coatings. U.S. Patent No. 9,096,773: 4 Aug 2015.

23. Pan, X.; Webster, D. C., New biobased high functionality polyols and their use in polyurethane coatings. *ChemSusChem* **2012,** *5* (2), 419-429.

24. Paramarta, A.; Pan, X.; Webster, D. C., Highly Functional Acrylated Biobased Resin System. *Radtech Report* **2013,** *1*, 26-32.

25. Nelson, T. J.; Bultema, L.; Eidenschink, N.; Webster, D. C., Bio-based high functionality polyols and their use in 1K polyurethane coatings. *Journal of Renewable Materials* **2013,** *1* (2), 141-153.

26. Kovash, C. S.; Pavlacky, E.; Selvakumar, S.; Sibi, M. P.; Webster, D. C., Thermoset Coatings from Epoxidized Sucrose Soyate and Blocked, Bio-Based Dicarboxylic Acids. *ChemSusChem* **2014,** *7* (8), 2289-2294.

27. Ma, S.; Webster, D. C.; Jabeen, F., Hard and flexible, degradable thermosets from renewable bioresources with the assistance of water and ethanol. *Macromolecules* **2016,** *49* (10), 3780-3788.

28. Ma, S.; Webster, D. C., Naturally occurring acids as cross-linkers to yield VOC-free, high-performance, fully bio-based, degradable thermosets. *Macromolecules* **2015,** *48* (19), 7127-7137.

29. Paramarta, A.; Webster, D. C., The exploration of Michael-addition reaction chemistry to create high performance, ambient cure thermoset coatings based on soybean oil. *Progress in Organic Coatings* **2017,** *108*, 59-67.

30. Paramarta, A.; Webster, D. C., Bio-based high performance epoxy-anhydride thermosets for structural composites: The effect of composition variables. *Reactive and Functional Polymers* **2016,** *105*, 140-149.

31. Pan, X.; Sengupta, P.; Webster, D. C., Novel biobased epoxy compounds: epoxidized sucrose esters of fatty acids. *Green Chemistry* **2011,** *13* (4), 965-975.

32. Monono, E. M.; Webster, D. C.; Wiesenborn, D. P., Pilot scale (10kg) production and characterization of epoxidized sucrose soyate. *Industrial Crops and Products* **2015,** *74*, 987-997.

33. Monono, E. M.; Bahr, J. A.; Pryor, S. W.; Webster, D. C.; Wiesenborn, D. P., Optimizing process parameters of epoxidized sucrose soyate synthesis for industrial scale production. *Organic Process Research & Development* **2015,** *19* (11), 1683-1692.

34. Samanta, S.; Selvakumar, S.; Bahr, J.; Wickramaratne, D. S.; Sibi, M.; Chisholm, B. J., Synthesis and Characterization of Polyurethane Networks Derived from Soybean-Oil-Based Cyclic Carbonates and Bioderivable Diamines. *ACS Sustainable Chemistry & Engineering* **2016,** *4* (12), 6551-6561.

35. Lambeth, R. H.; Henderson, T. J., Organocatalytic synthesis of (poly) hydroxyurethanes from cyclic carbonates and amines. *Polymer* **2013,** *54* (21), 5568-5573.

36. Lombardo, V. M.; Dhulst, E. A.; Leitsch, E. K.; Wilmot, N.; Heath, W. H.; Gies, A. P.; Miller, M. D.; Torkelson, J. M.; Scheidt, K. A., Cooperative Catalysis of Cyclic Carbonate Ring Opening: Application Towards Non-Isocyanate Polyurethane Materials. *European Journal of Organic Chemistry* **2015,** *2015* (13), 2791-2795.

37. Cornille, A.; Blain, M.; Auvergne, R.; Andrioletti, B.; Boutevin, B.; Caillol, S., A study of cyclic carbonate aminolysis at room temperature: effect of cyclic carbonate structures and solvents on polyhydroxyurethane synthesis. *Polymer Chemistry* **2017,** *8* (3), 592-604.

38. Webster, D. C.; Crain, A. L., Synthesis and applications of cyclic carbonate functional polymers in thermosetting coatings. *Progress in Organic Coatings* **2000,** *40* (1), 275-282.

39. Garipov, R. M.; Sysoev, V. A.; Mikheev, V. V.; Zagidullin, A. I.; Deberdeev, R. Y.; Irzhak, V. I.; Berlin, A. A. In *Reactivity of cyclocarbonate groups in modified epoxy–amine compositions*, 2003; Springer: pp 289-292.

40. Stockmayer, W. H., Molecular distribution in condensation polymers. *Journal of Polymer Science Part A: Polymer Chemistry* **1952,** *9* (1), 69-71.

41. Stockmayer, W. H., Molecular distribution in condensation polymers. *Journal of Polymer Science Part A: Polymer Chemistry* **1953,** *11* (5), 424-424.

42. Durand, D.; Bruneau, C. M., Statistics of random macromolecular networks, 2. Stepwise polymerization of polyfunctional monomers bearing A and B coreactive groups. *Macromolecular Chemistry and Physics* **1982,** *183* (4), 1021-1035.

43. Durand, D.; Bruneau, C.-M., Average functionalities of macromolecules in stepwise polyfunctional polymerization. *Polymer* **1982,** *23* (1), 69-72.

44. Miller, D. R.; Macosko, C. W., Average property relations for nonlinear polymerization with unequal reactivity. *Macromolecules* **1978,** *11* (4), 656-662.

45. Miller, D. R.; Valles, E. M.; Macosko, C. W., Calculation of molecular parameters for stepwise polyfunctional polymerization. *Polymer Engineering & Science* **1979,** *19* (4), 272-283.

46. Stafford, J. W., Multifunctional polycondensation and gelation: a kinetic approach. *Journal of Polymer Science Part A: Polymer Chemistry* **1981,** *19* (12), 3219-3236.

47. Nelson, T. J.; Masaki, B.; Morseth, Z.; Webster, D. C., Highly functional biobased polyols and their use in melamine–formaldehyde coatings. *Journal of Coatings Technology and Research* **2013,** *10* (6), 757-767.

CHAPTER 6. OVERALL CONCLUSIONS

6.1. Overall highlights

Epoxidized sucrose soyate (ESS) have been explored in its applicability in several crosslinking technologies. The interesting structure of ESS has led to the investigation of its potential as a bio-renewable starting material. In addition to the rigid sucrose core and flexible fatty acid chains, ESS possesses 11-12 epoxide groups that could easily be transformed into different functional groups capable of further reaction. The overall objective of this study was to exploit the high functionality and explore the applicability in producing thermosets via free radical polymerization and step-growth polymerization. Specifically, thermally initiated free-radical polymerizations were intended for structural composite applications while photoinitiated systems were studied for coatings applications and restorative dental materials. Meanwhile, polycondensation of cyclic carbonates with amine crosslinkers was investigated for making non-isocyanate polyurethane (NIPU) coatings.

6.2. Thermally initiated free-radically polymerized thermosets

Thermosets for structural composite applications were produced from the thermally initiated free-radical polymerization of dimethacrylated epoxidized sucrose soyate (DMESS). The synthesis of DMESS was a one-pot, solvent-free process and produced resins with viscosities much lower than the methacrylated epoxidized sucrose soyate (MESS). It is vital to understand the structure-property relationship of the thermosets when factors such as degree of functionality and reagent ratios were varied. The thermosets produced from this study were generally brittle due to the increased crosslinkable moieties. Since DMESS has high functionality, its tunability was explored by incorporating non-functional esters, as well as determining the effect on material flexibility and toughness. The synthesis of these modified

versions of DMESS only required using a blend of anhydrides in order to introduce the non-functional esters. The thermosets produced had slightly lowered glass transition temperatures (T_g) than their DMESS counterparts but significant improved ductility was observed. These results demonstrated the versatility of highly functionalized resins and their applicability in a broad range of applications.

6.3. Photopolymerized thermosets

The versatility of DMESS was further explored via UV-initiated free-radical polymerizations. DMESS was formulated with four different methacrylated reactive diluents and the thermomechanical properties were evaluated. The properties were compared against a conventional methacrylate, BisGMA, which is a bisphenol A derivative. Generally, the thermosets had comparable properties with the control. The DMESS derived thermosets were inferior in terms of hardness and adhesion on steel but were hydrolytically more stable when moisture uptake was measured. Adhesion on wood substrates were much better than steel, which means application would be much suited for wood furniture coatings or wooden laminate floors. Initial studies on visible light-initiated free-radical polymerizations were also performed, specifically intended for restorative dental materials applications. The study showed potential although it is currently at its infancy stage. The curing process needs to be optimized and oxygen inhibition remains a challenge.

6.4. Non-isocyanate polyurethane (NIPU) coatings

The preparation has been the main challenge for polyurethanes due to the concerns arising from polyisocyanate exposure. Non-isocyanate polyurethanes have gained attention because they provide alternative approaches in polyurethane preparation. Specifically, our study focused on the crosslinking reaction of carbonated sucrose soyate (CSS) with a trifunctional

amine. Cyclic carbonates can be prepared by reacting epoxides with carbon dioxide at supercritical conditions. There are commercially available amine crosslinkers that are bio-based. Otherwise, amines may also be synthesized from bio-based precursors. One drawback for cyclic carbonate and amine crosslinking is the elevated reaction temperature requirement. Our system takes advantage of a cooperative catalysis, which allows crosslinking at a lower temperature. Under identical curing conditions, CSS generates highly solvent resistant polyurethane coatings with higher T_gs than CSBO. The resulting CSS-based coatings always form highly crosslinked polyurethanes than carbonated soybean oil (CSBO). This study also demonstrates the advantage of utilizing highly functionalized resins and the gel point for such systems are typically reached earlier than lower functionalized resins as proven by Flory's theory.

CHAPTER 7. FUTURE WORK

7.1. Highly functionalized dimethacrylated epoxidized sucrose soyate (DMESS)

The degree of functionalization of DMESS was varied and confirmed the dependence of thermomechanical properties on the amount of crosslinkable moieties, which are factors of crosslink density. Currently, the system, from the synthesis of the resin up to the production of the thermoset, is not a hundred percent bio-based. Efforts in creating a fully bio-based system are ongoing. A few aspects that would be worthwhile investigating are the usage of bio-based reagents, green catalysts, and bio-based reactive diluents. Proposed compounds as bio-based reactive diluents derived from renewable sources are illustrated in Figure 7.1. These compounds, made by the Sibi group, are structurally analogous to styrene and would be a good study to investigate the thermomechanical properties and effect of the substituents to the reactivity. Upon completion of these collaborative studies, a fully bio-based system would broaden the applicability of DMESS and would render it as the polymer of choice in many applications.

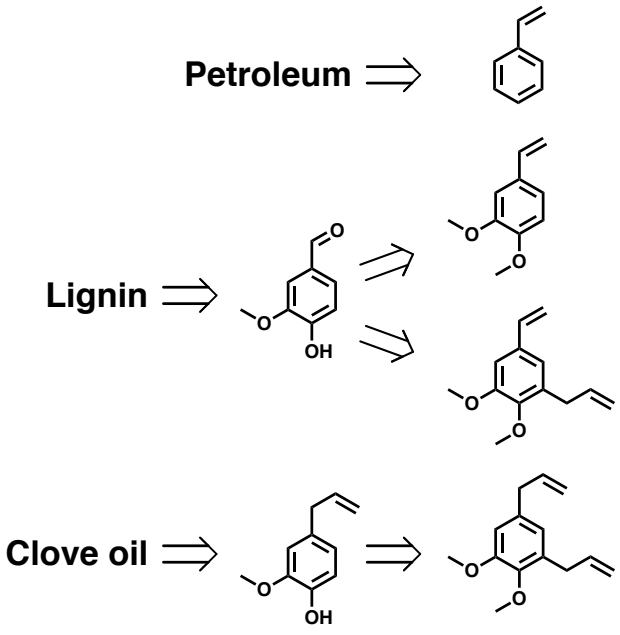

Figure 7.1. Structures of styrene, bio-based reactive diluents, and precursors.

7.2. Tunability of DMESS

The high functionality of DMESS allows for easy tunability with minimal compromise with naturally opposing properties such as glass transition temperature vs. toughness or tensile strength vs. flexibility. DMESS has previously been used as the polymer matrix in producing fiber-reinforced polymer (FRP) composites for aerospace applications. The study showed weak interaction of DMESS with flax fiber due to lower hydroxyl group concentration of DMESS. Increasing the DMESS-flax fiber interaction could be done by either increasing the concentration of the hydroxyl group thereby lowering the amount of the crosslinkable methacrylate groups or introducing functional groups that form new hydroxyl groups. The latter could be accomplished by adding lactide or gamma-valerolactone[1, 2] (Scheme 7.1), both of which are bio-based.

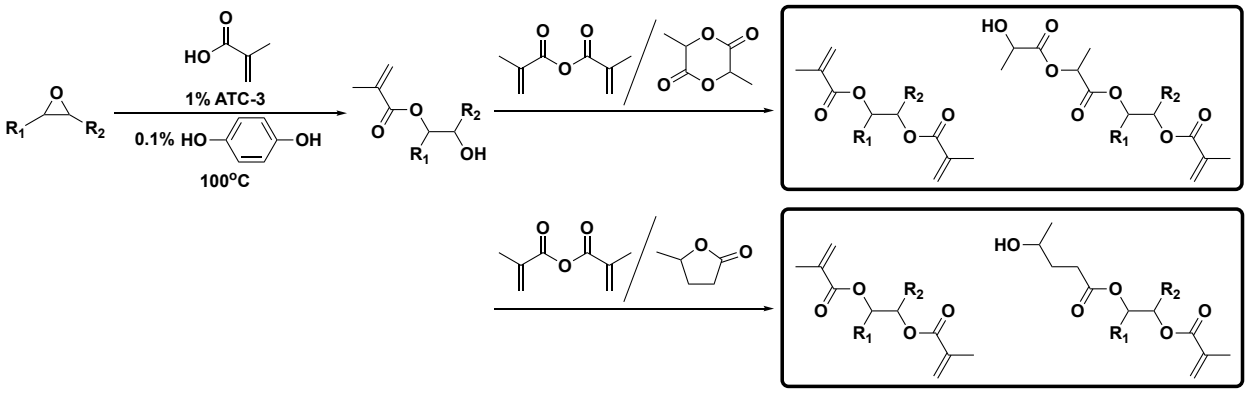

Scheme 7.1. Synthetic route to the modified DMESS resins for aerospace applications.

7.3. Versatility of DMESS: Photopolymerized systems

A UV-curable system was developed for potential application of DMESS as wood coatings. Improvements in the system could be done on increasing the bio-based content by replacing the reactive diluents and photoinitiator. Figure 7.2 shows the structures of possible replacements for the current reactive diluents and photoinitiator. The structure of the proposed bio-based photodegradable methacrylated reactive diluent (Figure 7.2, left) offers the features of

conventional bisphenol A-based monomers such as chemical resistance, flexibility, and reactivity.

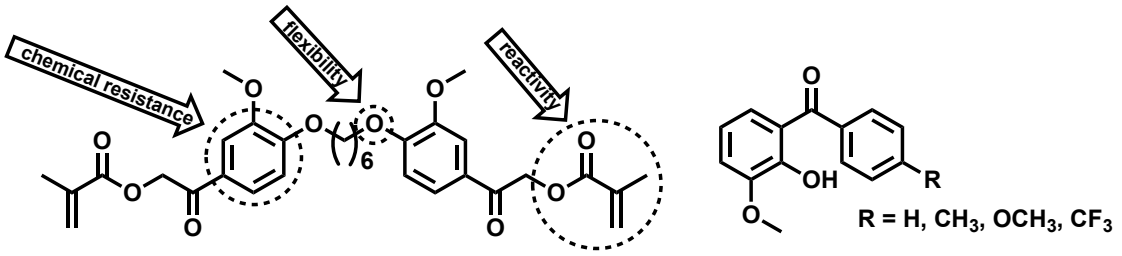

Figure 7.2. Bio-based methacrylated reactive diluent (left) and bio-based photoinitiator (right).

UV-curable coatings displayed good adhesion on wood substrates but poor adhesion on metal substrates. Known adhesion promoters such as catechol-type compounds have been used as building blocks for the design of mussel-inspired synthetic adhesives and coatings.[3, 4] Scheme 7.2 shows the synthetic route that would be approached in forming UV-curable coatings with improved adhesion on metal substrates.

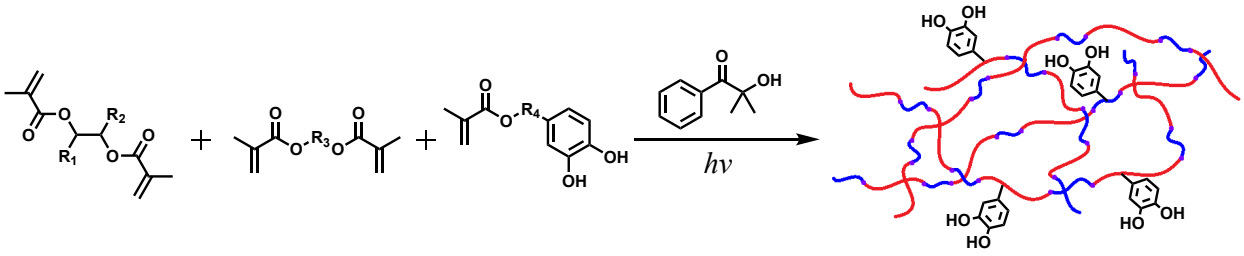

Scheme 7.2. Photopolymerization reaction of DMESS with methacrylated reactive diluents and methacrylated catechol derivatives.

Initial results from the visible-light cured system gave promising results although the parameters for the photopolymerization process need to be optimized to achieve better conversion. It would be worthwhile to screen initiators and study their efficiency. Next steps taken should be investigation of incorporating fillers (Figure 7.3) in the formulation to improve hardness, compressive strength, tensile strength, and elastic modulus while reducing the shrinkage, linear expansion coefficient, and water absorption.[5] Some examples of commonly

used fillers are silica, quartz, ceramic, and hydroxyapatite. Hydroxyapatite is natural mineral that makes up to 70% by weight of human bone. Utilizing it as a filler is advantageous due to its biocompatibility and the ability of fillers to attenuate the irradiation intensity, resulting from light absorption and scattering, penetrating deeper into the composite.[6]

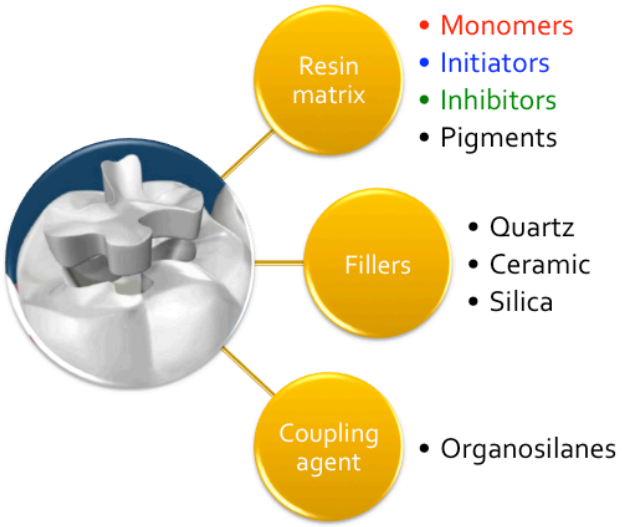

Figure 7.3. Compositions of dental resin formulations.

7.4. Non-isocyanate polyurethanes (NIPUs)

Polyurethanes formed from the reaction of cyclic carbonate and amines offer an alternative approach in synthesizing non-isocyanate polyurethanes (NIPUs). The preparation of the cyclic carbonates required running reactions in supercritical condition, which means operating at high temperatures in pressurized reactors. This process presents a limitation in the optimization of the reaction because monitoring the reaction progress would require intermittent release of the vessel pressure and lowering the temperature. Therefore, optimization of the reaction parameters would establish a protocol and produce consistent results.

Cooperative catalysis gave results that showed potential in producing NIPU coatings cured under ambient conditions. Lithium triflate (LiOTf) was used as the Lewis acid that further promotes crosslinking of the system. Investigation of organocatalysts to replace LiOTf would create a

metal-free system and increase the bio-based content if the said catalyst could be obtained from renewable sources. Exploration of bio-based amine crosslinkers could also increase the overall bio-based content. Lastly, addition of pigments and studying the opacity, color, and dispersion quality could open other avenues for pigmented coating applications.

7.5. References

1. Bababrik, R. M.; Wang, B.; Resasco, D. E., Reaction Mechanism for the Conversion of γ-Valerolactone (GVL) over a Ru Catalyst: A First-Principles Study. *Industrial & Engineering Chemistry Research* **2017,** *56* (12), 3217-3222.

2. Alonso, D. M.; Wettstein, S. G.; Dumesic, J. A., Gamma-valerolactone, a sustainable platform molecule derived from lignocellulosic biomass. *Green Chemistry* **2013,** *15* (3), 584-595.

3. Xu, Z., Mechanics of metal-catecholate complexes: the roles of coordination state and metal types. *Scientific reports* **2013,** *3*.

4. Faure, E.; Falentin-Daudré, C.; Jérôme, C.; Lyskawa, J.; Fournier, D.; Woisel, P.; Detrembleur, C., Catechols as versatile platforms in polymer chemistry. *Progress in polymer science* **2013,** *38* (1), 236-270.

5. Kim, K.-H.; Ong, J. L.; Okuno, O., The effect of filler loading and morphology on the mechanical properties of contemporary composites. *The Journal of prosthetic dentistry* **2002,** *87* (6), 642-649.

6. Stansbury, J. W., Curing dental resins and composites by photopolymerization. *Journal of esthetic and restorative dentistry* **2000,** *12* (6), 300-308.